AD-A065 697 OHIO STATE UNIV COLUMBUS ELECTROSCIENCE LAB F/6 17/9
OPTIMUM FREQUENCIES FOR AIRCRAFT CLASSIFICATION.(U)
JAN 79 L HENG-CHENG , A A KSIENSKI AFOSR-74-2611
UNCLASSIFIED ESL-783815-6 AFOSR-TR-79-0255 NL

1 OF 2
AD A
065697

OSU

OPTIMUM FREQUENCIES FOR AIRCRAFT CLASSIFICATION

Heng-Cheng Lin and A. A. Ksienski

LEVEL II

The Ohio State University

ElectroScience Laboratory

Department of Electrical Engineering
Columbus, Ohio 43212

TECHNICAL REPORT 783815-6

January 1979

Grant No. AFOSR-74-2611

U. S. Air Force
Air Force Office of Scientific Research
1400 Wilson Boulevard
Arlington, Virginia 22209

NOTICES

When Government drawings, specifications, or other data are used for any purpose other than in connection with a definitely related Government procurement operation, the United States Government thereby incurs no responsibility nor any obligation whatsoever, and the fact that the Government may have formulated, furnished, or in any way supplied the said drawings, specifications, or other data, is not to be regarded by implication or otherwise as in any manner licensing the holder or any other person or corporation, or conveying any rights or permission to manufacture, use, or sell any patented invention that may in any way be related thereto.

UNCLASSIFIED

SECURITY CLASSIFICATION OF THIS PAGE (When Data Entered)

REPORT DOCUMENTATION PAGE	READ INSTRUCTIONS BEFORE COMPLETING FORM
1. REPORT NUMBER (18) (19) AFOSR-TR-79-0255	2. GOVT ACCESSION NO. / 3. RECIPIENT'S CATALOG NUMBER
4. TITLE (and Subtitle) (6) OPTIMUM FREQUENCIES FOR AIRCRAFT CLASSIFICATION.	5. TYPE OF REPORT & PERIOD COVERED: Interim 6. PERFORMING ORG. REPORT NUMBER: ELS 783815-6
7. AUTHOR(s): Heng-Cheng Lin and A.A. Ksienski	8. CONTRACT OR GRANT NUMBER(s): (15) AFOSR-74-2611
9. PERFORMING ORGANIZATION NAME AND ADDRESS: Ohio State University, Department of Electrical Engineering, Columbus, Ohio 43212 402 251	10. PROGRAM ELEMENT, PROJECT, TASK AREA & WORK UNIT NUMBERS: (16) 61102F 2304/A2 (17) A2
11. CONTROLLING OFFICE NAME AND ADDRESS: Air Force Office of Scientific Research/NM, Bolling AFB, Washington, DC 20332 (11)	12. REPORT DATE: January 1979 13. NUMBER OF PAGES: 123
14. MONITORING AGENCY NAME & ADDRESS(if different from Controlling Office): (14) ESL-783815-6	15. SECURITY CLASS. (of this report): UNCLASSIFIED 15a. DECLASSIFICATION/DOWNGRADING SCHEDULE

16. DISTRIBUTION STATEMENT (of this Report)

Approved for public release; distribution unlimited.

(12) 124 p.

17. DISTRIBUTION STATEMENT (of the abstract entered in Block 20, if different from Report)

(10) Lin /Heng-Cheng A.A./Ksienski

18. SUPPLEMENTARY NOTES

(9) Technical rept.,

19. KEY WORDS (Continue on reverse side if necessary and identify by block number)

Aircraft classification	Fundamental harmonic	Feature selection
Aircraft scattering returns	Polarization	
Optimum frequency	Comples returns	
Phase information	Monte Carlo simulation	
Amplitude returns	Nearest neighbor classifier	

20. ABSTRACT (Continue on reverse side if necessary and identify by block number)

The results are presented of a search for optimum frequencies to classify eight aircraft types by means of their radar returns. The performance, in terms of misclassification probabilities as a function of SNR, is presented for different feature sets ranging from amplitude returns for a single frequency through amplitude and phase for various frequency pairs.

402 251 all

DD FORM 1 JAN 73 1473

UNCLASSIFIED

CONTENTS

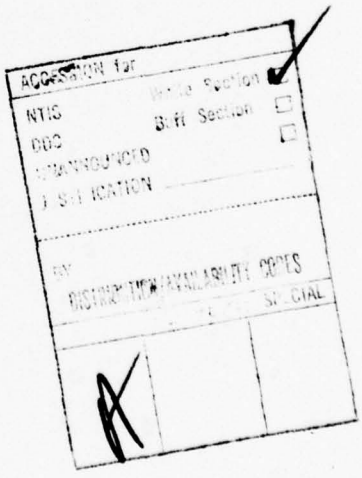

I. INTRODUCTION

The objective of this research effort was to determine the optimum frequencies at which a radar should be operated to obtain reliable aircraft classification. Previous efforts established the range of frequencies which should be utilized to accomplish such classification.[1-5] In previously reported results a set of harmonically related frequencies were used ranging in number from 12 down to 4, where the 4 frequencies were picked in the range most strongly contributing to the reduction of classification errors. The present effort was motivated by the realization that the frequency parameter is the most costly and its use should therefore be minimized. The objective was thus explicitely set, first to find the optimum single frequency of operation if only one frequency were permitted, and determine the minimum classification error achievable when all other scattering parameters associated with that frequency were utilized. Next, a two frequency exhaustive search was performed to obtain the frequency combination that would assure the minimum classification error. It was found that by utilizing two frequencies the error levels were sufficiently low so that the introduction of additional frequencies was not warranted. The range of frequencies used was between 2 MHz and 24 MHz with the lower bound set by the largest airplane, the B1. The search for optimum frequencies was carried out in increments of 2 MHz.

Previously published results dealt with four airplanes of similar size, F104, F4, Mig 19 and Mig 21. To provide a more realistically representative set of airplane classes, four additional airplanes were introduced that substantially increased the range of sizes and shapes, they were, F14, Mig 25, SR 71 and B1.

The classification algorithm used in this work is the Nearest Neighbor-rule. This choice was made due to both its nonparametric nature

and its effectiveness in cases where the different classes are distributed on rather convolved surfaces with relatively close proximity to each other.

Section II discusses decision rules, Section III describes the various features available for the aircraft classification process, Section IV discusses the noise model chosen for contaminating the learning sets to produce test sets, Section V describes the method through which test sets were produced and misclassification probabilities computed. Sections VI through IX present the performance results obtained by utilizing feature vectors of increasing dimensionality ranging from single frequency amplitude returns through two frequency complex returns.

II. DECISION RULES

When the statistical nature of the corrupting noise is known the optimum decision rule is that of Bayes, where the misclassification probability is minimized. The average probability of error associated with returns from class C_k is

$$p_e^{(k)} = \sum_{i=1}^{N_k} P_k(i) \left[1 - \int_{x \in R_k} P(x|a_i^k)dx\right] \qquad (1)$$

where N_k denotes the number of discrete points, a_i^k representing the class C_k, and R_k denotes the region of n-space associated with the decision rule for choosing class C_k given N_k sample vectors a_i^k, $P_k(i)$ denotes the a priori probability of occurrence of a_i^k. The regions R_k are disjoint and jointly occupy the entire x domain.

Let K be the number of classes or objects to be distinguished and $P(C_k)$ denote the a priori probability of each class, the average probability of misclassificaiton of the overall system would be

$$P_e = \sum_{k=1}^{K} p_e^{(k)} P(C_k). \tag{2}$$

Combining (1), (2) and assuming $P_k(i) = \frac{1}{N_k}$, we have

$$P_e = 1 - \sum_{k=1}^{K} P(C_k) \left(\frac{1}{N_k} \sum_{i=1}^{N_k} \int_{x \epsilon R_k} P(x|a_i^k) dx \right) \tag{3}$$

Bayes rule is set up to minimize the above by adjusting R_k such that

$$p_e^B = - \sum_{k=1}^{K} \max P(C_k) \left(\frac{1}{N_k} \sum_{i=1}^{N_k} \int_{x \epsilon R_k} P(x|a_i^k) dx \right), \tag{4}$$

or in another notation

$$p_e^B = 1 - \int \max_k P(C_k) \, \overline{P(x|a^k)} \, dx \tag{5}$$

where the integral is carried out over the entire x domain and

$$\overline{P(x|a^k)} = \frac{1}{N_k} \sum_{i=1}^{N_k} P(x|a_i^k) \tag{6}$$

is the average class-conditional probability density function.

For the following special conditions

(1) $P(C_k) = \frac{1}{K}$, (7)

(2) There is only one point in each class, i.e.,

$N_k = 1$, (8)

one chooses class C_r when $P(x|C_r)$ is the maximum, i.e.,

$$\text{if } P(x|C_r) = \max_i P(x|C_i), \text{ choose } C_r. \tag{9}$$

If the corrupted noise is additive gaussian, the point a^r which is at the minimum distance to the tested vector x yields the maximum $P(x|C_i)$, and Bayes rule becomes equivalent to an N.N. classifier, i.e.,

$$\text{if } ||x-a^r|| = \min_k || x-a^k||, \text{ choose } C_r, \tag{10}$$

where we use the usual notation for the Euclidean distance,

$$||x-a^k|| = \left[(x-a_i^k)^T (x-a_i^k)^*\right]^{\frac{1}{2}} . \tag{11}$$

For the cases where there are more than one point in any one of the classes, the N.N. rule classifies the unknown tested point x as a member of the class C_r to which its nearest neighbor belongs, i.e.,

$$\text{if } ||x-a_j^r|| = \min_{i,k} || x-a_i^k|| \text{ , choose } C_r. \tag{12}$$

The average probability of misclassification of an N.N. rule $P_e^{N.N.}$ is bounded by the Bayes error in the following way[6]

$$P_e^B \leq P_e^{N.N.} \leq P_e^B \left(2 - \frac{K}{K-1} P_e^B\right), \tag{13}$$

where K is the number of classes.

The N.N. rule has a practical advantage over the Bayes rule in that the difficulties of determining the regions R_k are eliminated, and of course, the N.N. rule is nonparametric and consequently is applicable to classification problems where the statistics of the noise are not known.

III. FEATURE SELECTION

The features at our disposal are the scattering matrix parameters of a set of given frequencies. A major objective of a classification effort is to minimize the dimensionality of the feature vector for a given performance level. The "cost" of the various parameters, however, in terms of system complexity and difficulty of extraction is not equal. The most costly parameter is the frequency, since each additional frequency may require an additional radar operating at the specified frequency. It is for this reason that the present study is aimed at finding the optimum frequencies given that either a single frequency or at most two frequencies are available. The other parameters that are available are the amplitude, phase and polarization. Here, too, the associated costs are not the same. Obviously, amplitude is the easiest parameter to obtain, polarization is next, and the most difficult one is the phase parameter. The difficulty is in eliminating the phase introduced by range and doppler. One way of eliminating these effects, discussed in Section VIII, is by reference to the fundamental frequency which is well inside the Rayleigh range and at which the target introduces a very small phase shift. The use of the fundamental thus implies the use of a third frequency if phase is extracted by the above method.

As to polarization we are assuming that two orthogonal polarization components are available.

Polarization

In previous studies[1,3,5] the classification performance was computed and shown for each of two orthogonal polarizations. The two components have different characteristics in that the component parallel to the fuselage in the Rayleigh range of frequencies is much stronger than that perpendicular to it, but it has been found that the perpendicular component provides the best discrimination between classes. Thus the first (parallel to the fuselage) provides good SNR in the presence of noise while the second provides good classification properties,

it is thus advisable to use both components in an actual radar. At frequencies beyond the first resonance which the largest aircraft encounter the above statement does not apply, but since the orientation of the aircraft with respect to the radar is a priori unknown, the horizontal and vertical polarizations as described above cannot be preserved, thus any polarization will on the average contain both components with a changing mix. It was therefore decided not to present performance curves for each polarization but rather assume that the radar utilizes both.

IV. NOISE MODEL

The noise model representing the noise and errors of a radar system should have both additive and multiplicative components. The additive components correspond to corruptive influences such as thermal noise and the multiplicative reflect such effects as measurement errors and clutter. Because of the mathematical complexity introduced by multiplicative noise, the noise model chosen here is additive only but represents the multiplicative components, which are signal level dependent, by normalizing the noise variance to the signal power level. Thus for =0.1 the noise standard deviation is 10% of the average signal level. This normalization of the noise further removes such parameters as range to the target, antenna gains, transmitter power, etc. from affecting the relative strengths of noise vs signal. The statistical nature of the noise model is gaussian due to the assumption that several relatively independent sources of noise and error contribute to the total corruptive influence; invoking the central limit theorem their sum tends to a gaussian distribution.

It should be borne in mind that the precise nature of the noise is less important than its effect on the classification performance. Thus no attempt is made to combat the noise effect by devising schemes taylored to its statistics. The noise serves strictly the purpose of determining the degradation of performance with increasing noise levels,

and the assessment of such performance as the selected feature sets are varied.

The noise components are added to the signal as phasors in the following way. A noisy amplitude return of the jth component of a test vector is

$$\sqrt{(S_j+n_1)^2 + (n_2)^2}$$

where S_j is the jth frequency component of the signal amplitude signal and n_1, n_2 are Gaussian noise components with zero means. When the signals considered are complex, noise is added algebraically to the two orthogonal components of the signal. Therefore, the jth component of a test vector becomes

$$\sqrt{(S_{jr}+n_3)^2 + (S_{ji}+n_4)^2}$$

where S_{jr} and S_{ji} are the real and imaginary components of the jth frequency return at the selected aspect angle, and n_3, n_4 are Gaussian noises whose statistics are the same as that of n_1, n_2. The standard deviations of n_1 through n_4 are normalized to $S_j/\sqrt{2}$, which is off by a factor of $1/\sqrt{2}$ from all the previous work[1,2,3,5] but serves as a better indicator of the noise level in terms of the uncorrupted signals.

V. EXPERIMENTS BY MONTE CARLO SIMULATION

An analytical calculation of the probability of misclassification for the N.N. rule is rather involved because it requires multidimensional integration over extremely complicated boundaries. Therefore Monte Carlo simulation was employed to compute performance. In the following tests, 600 random numbers were generated in each case and added to the noise free signals to form the test vectors. The newly formed vectors

were then classified as belonging to one of the classes according to (13) and the probability of misclassification was computed by counting the number of mistakes out of the total number of tests, which was 600 for each case.

The coordinate system utilized in stating the observation angles and polarization is shown in Figure 1. The geometrical center of the airplane coincides with the origin of the coordinate system. Four aspect angles are chosen in the experiments and their scattering returns, as mentioned before, are numerically computed to provide the noise free "learning" set of vectors.

Some a priori information about the aspect angle (θ,ϕ) of an aircraft is usually available which helps in the identification process. In a practical situation, conventional radar Doppler and range combined with known airplane flight dynamics in fact provide a fairly close estimate of (θ,ϕ). The estimate accuracy was assumed to be within $\pm 5^{o}$ in ϕ and θ. In actuality the estimates are better than the above figure. Assuming that it is known that (θ_o,ϕ_o) is within the above limits, only an angle region of 10^{o} in θ and ϕ centered at (θ_o,ϕ_o) need be considered. Since the data are computed only at discrete values of aspect angle, we have a set of angles each of which may correspond to the actual aspect angle of the aircraft.

Four center aspect angles corresponding to alternate (θ_o,ϕ_o) were chosen as representative of the scattering characteristics of the aircraft. They are,

$(0^{o},0^{o})$ nose on,

$(90^{o},90^{o})$ side view,

$(90^{o},0^{o})$ bottom view,

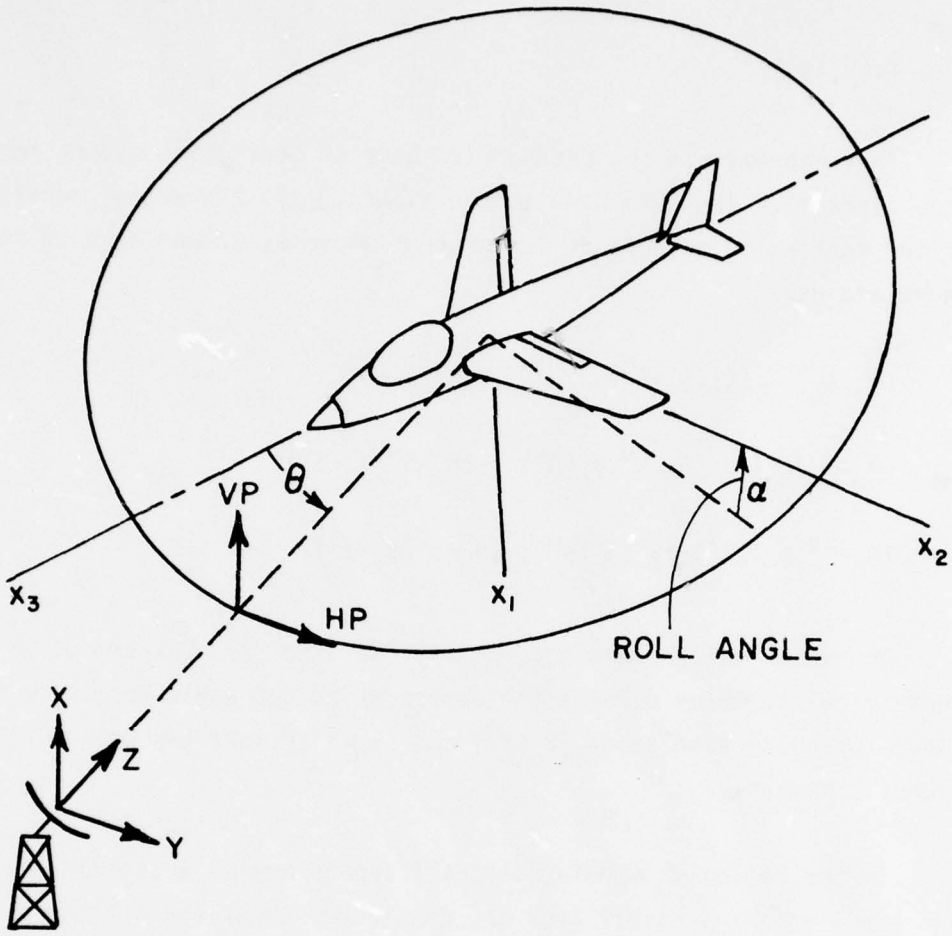

Figure 1. The coordinate system describing aspect angles and polarization.

and

$(45^o, 45^o)$.

They approximate the parametric range of scattering values for each aircraft. The data used in the experiments, therefore, consists of the scattering returns of 9 different aspects, around each of the above angles.

(θ_o, ϕ_o) $(\theta_o, \phi_o + 5^o)$, $(\theta_o, \phi_o - 5^o)$

$(\theta_o - 5_o, \phi_o)$, $(\theta_o - 5^o, \phi_o + 5^o)$, $(\theta_o - 5^o, \phi_o - 5^o)$

$(\theta_o + 5^o, \phi_o)$, $(\theta_o + 5^o, \phi_o + 5^o)$, $(\theta_o + 5^o, \phi_o - 5^o)$

In two of the above cases, namely "nose on" and "bottom view" the geometrical symmetry reduces the number of aspect angle from 9 to 6 since for those situations $(\theta_o + 5^o)$ and $(\theta_o - 5^o)$ yield the same electromagnetic response.

In the following simulations, all aspect angles are equally weighted and the a priori probabilities are considered equal for all the aircraft in evaluating the overall probability of misclassification.

To simplify the notation on the plots the following abbreviations are used.

Class	Aircraft type	Dimensions
C_1:	F 104,	16.69 m x 6.68 m x 4.11 m,
C_2:	Mig 19,	13.49 m x 11.12 m x 2.94 m,
C_3:	F 4,	17.76 m x 11.7 x x 4.96 m,

C_4: Mig 21, 15.76 m x 7.15 m x 4.50 m,

C_5: Mig 25, 21.0 m x 12.2 m x 5.02 m,

C_6: SR 71, 32.74 m x 16.95 m x 5.64 m,

C_7: B 1, 43.58 m x 23.77 m x 10.36 m,

C_8: F 14, 24.36 m x 20.98 m x 7.67 m.

The symbol $f_n = 2n$ MHz is used to represent the frequency, the first harmonic is therefore 2 MHz.

It is clear from the above discussions that

$$P_k(i) = \begin{cases} \frac{1}{6}, & \text{for } (0^o,0^o) \text{ and } (90^o,0^o) \\ \frac{1}{9}, & \text{for } (90^o,90^o) \text{ and } (45^o,45^o) \end{cases}$$

$$\forall \; i,k \qquad (15)$$

The noise standard deviation is normalized with respect to each individual aircraft return. The a priori probabilities here are all set to be 1/8 corresponding to the eight aircraft stipulated.

In the following sections (VI-IX) the cases for single frequency and dual frequency returns will be discussed and the computed classification errors presented.

VI. SINGLE FREQUENCY AMPLITUDE RETURNS

The simplest case considered is classification using a single frequency amplitude return, utilizing two orthogonal polarizations.

Figures 2-6 show the results for the best 5 frequencies out of the 12 frequency data available. The performance is shown for one aspect angle but it is representative of the other angles as well. Since the error rates are unacceptably high, it did not appear to be useful to provide more detailed information on the performance of this feature set. Each curve is computed by Monte Carlo simulation of Equation (1) and the average curve (see Equation (2)) is plotted to show the overall performance at this frequency. Note that the probabilities of misclassification for some aircraft are much larger than those for other aircraft, indicating a bias effect among the targets to be classified. This effect is very large for some aircraft (e.g., $P_e(C_1)$ and $P_e(C_8)$ in Figure 2) and degrades the overall performance quite significantly. The phenomenon is mainly due to the inhomogeneous distribution of data. For instance, the identification of an aircraft with the data surrounded by those of others would be subject to more mistakes than one whose data are only partially in proximity with others. Indeed in a two class case, for example, where the data of one class surround that of the other, the probability of choosing the surrounding class will keep increasing as the noise increases, producing a pronounced bias to the extent that for any large noise variances the probability of selecting the surrounding class will tend to unity and the misclassification probabilities for the two classes will tend to zero and unity respectively. The bias effect may also produce apparently anomalous effects such as, for example, curve $Pe(C_2)$ in Figure 5, where the error probability starts decreasing beyond a certain value of noise variance. To explain this apparently anomalous behaviour we assume a particular distribution for a 2 class classification. Each class has 2 points in one dimensional space as shown in Figure 7. Suppose the 2 C_1 points coincide and 2 C_2 points are not clustered together; instead, they are spread around

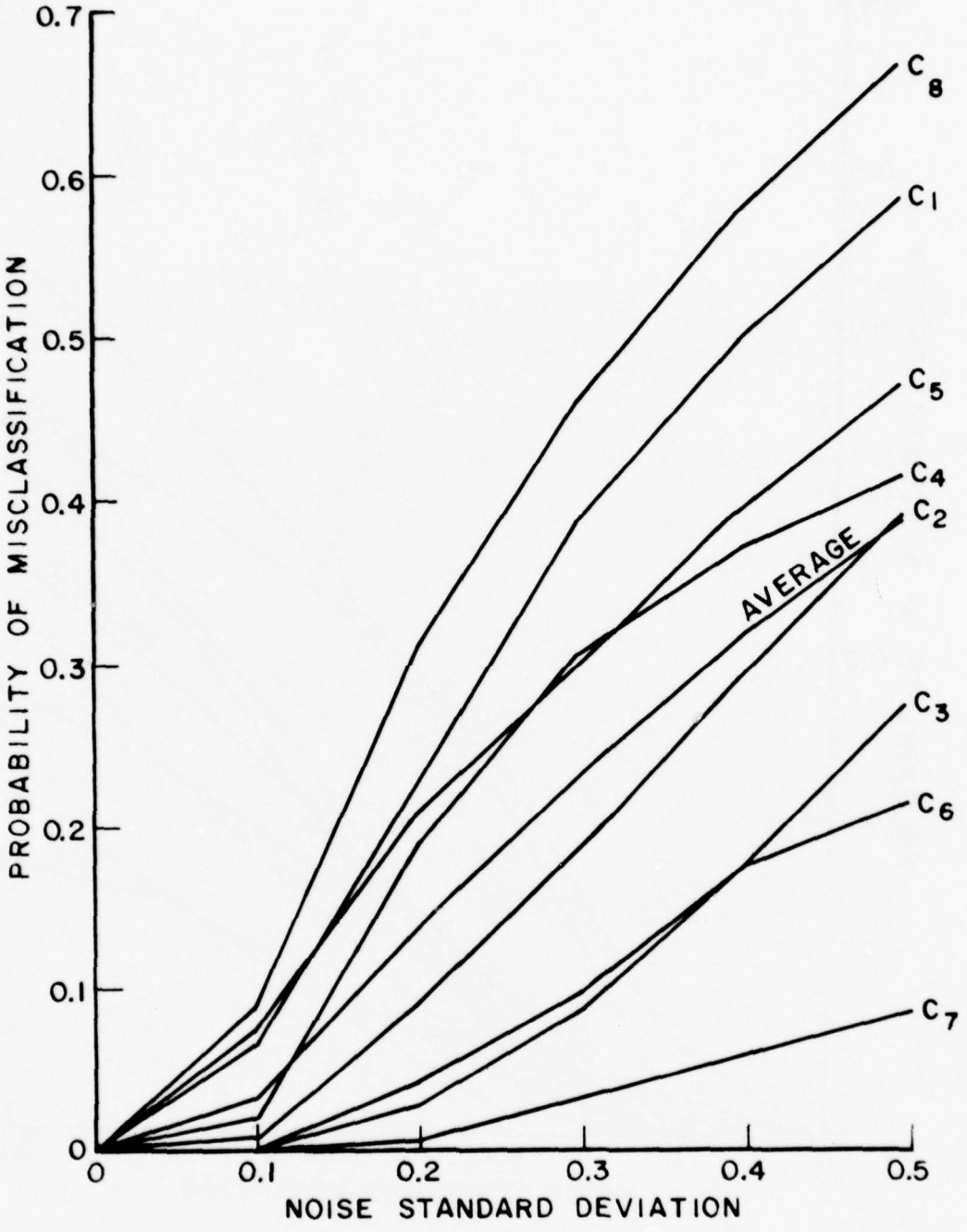

Figure 2. Probability of misclassification for individual aircraft, using amplitude returns at frequency f_1 and $(0^0,0^0)$ aspect angle (nose on).

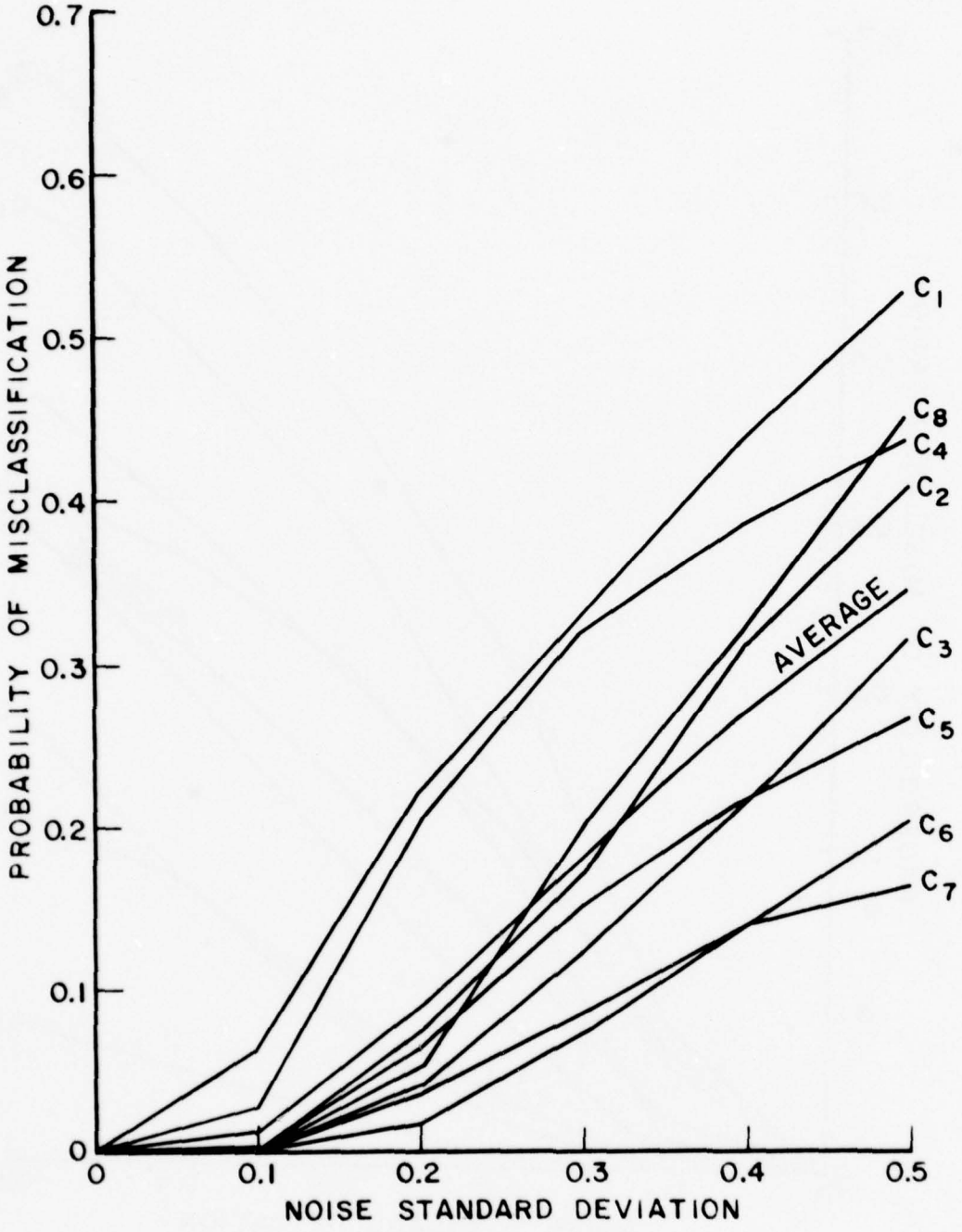

Figure 3. Probability of misclassification for individual aircraft, using amplitude returns at frequency f_2 and $(0^0,0^0)$ aspect angle (nose on).

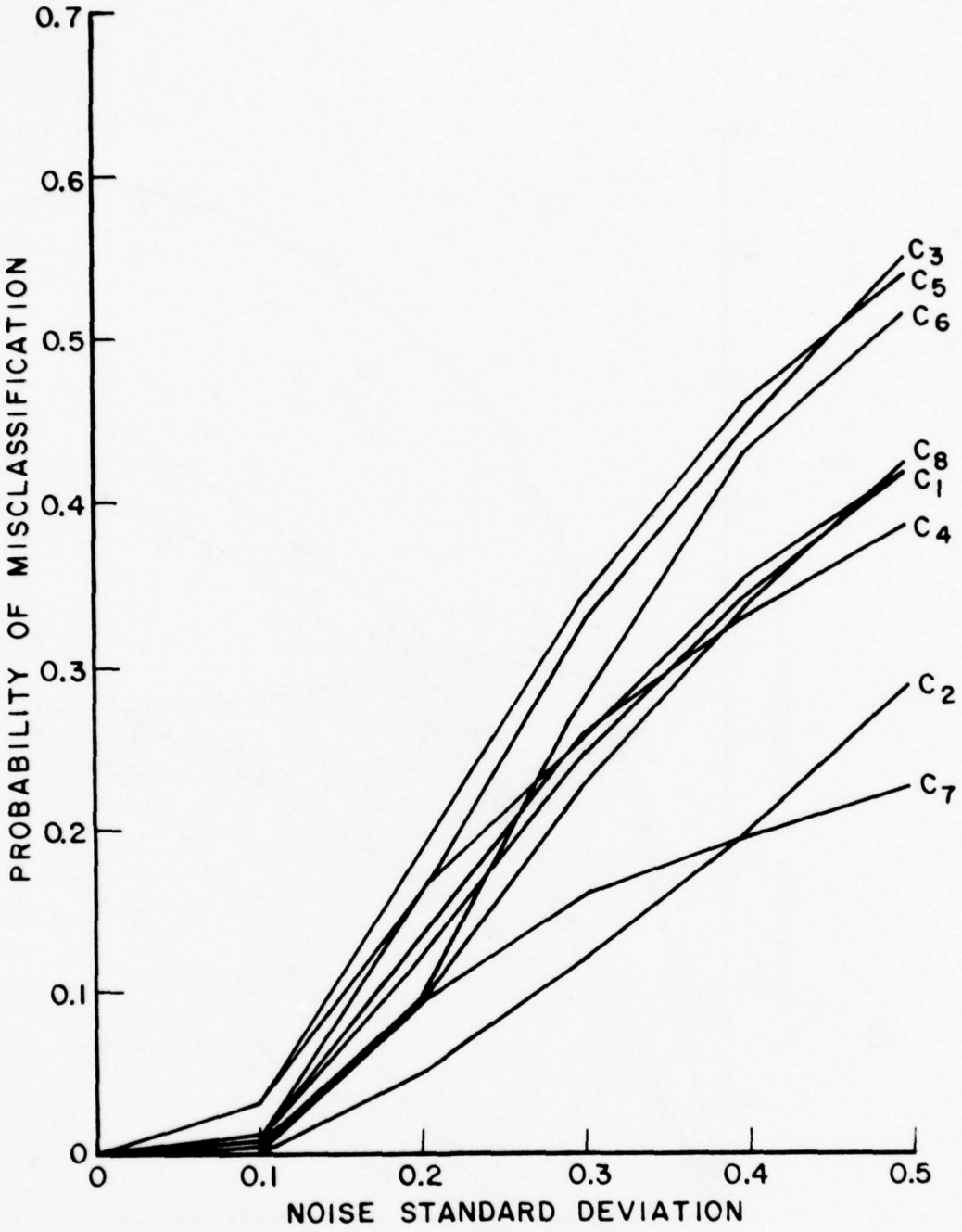

Figure 4. Probability of misclassification for individual aircraft, using amplitude returns at frequency f_3 and $(0^o,0^o)$ aspect angle (nose on).

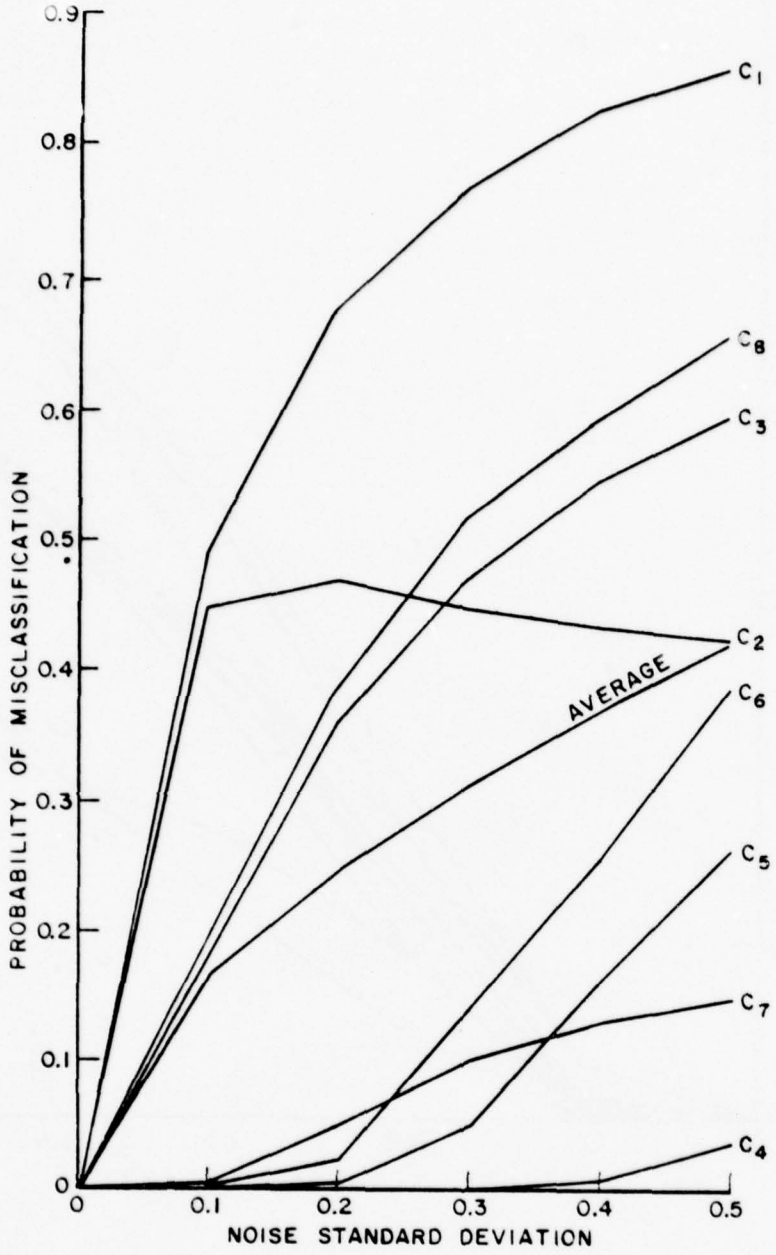

Figure 5. Probability of misclassification for individual aircraft, using amplitude returns at frequency f_7 and $(0^0,0^0)$ aspect angle (nose on).

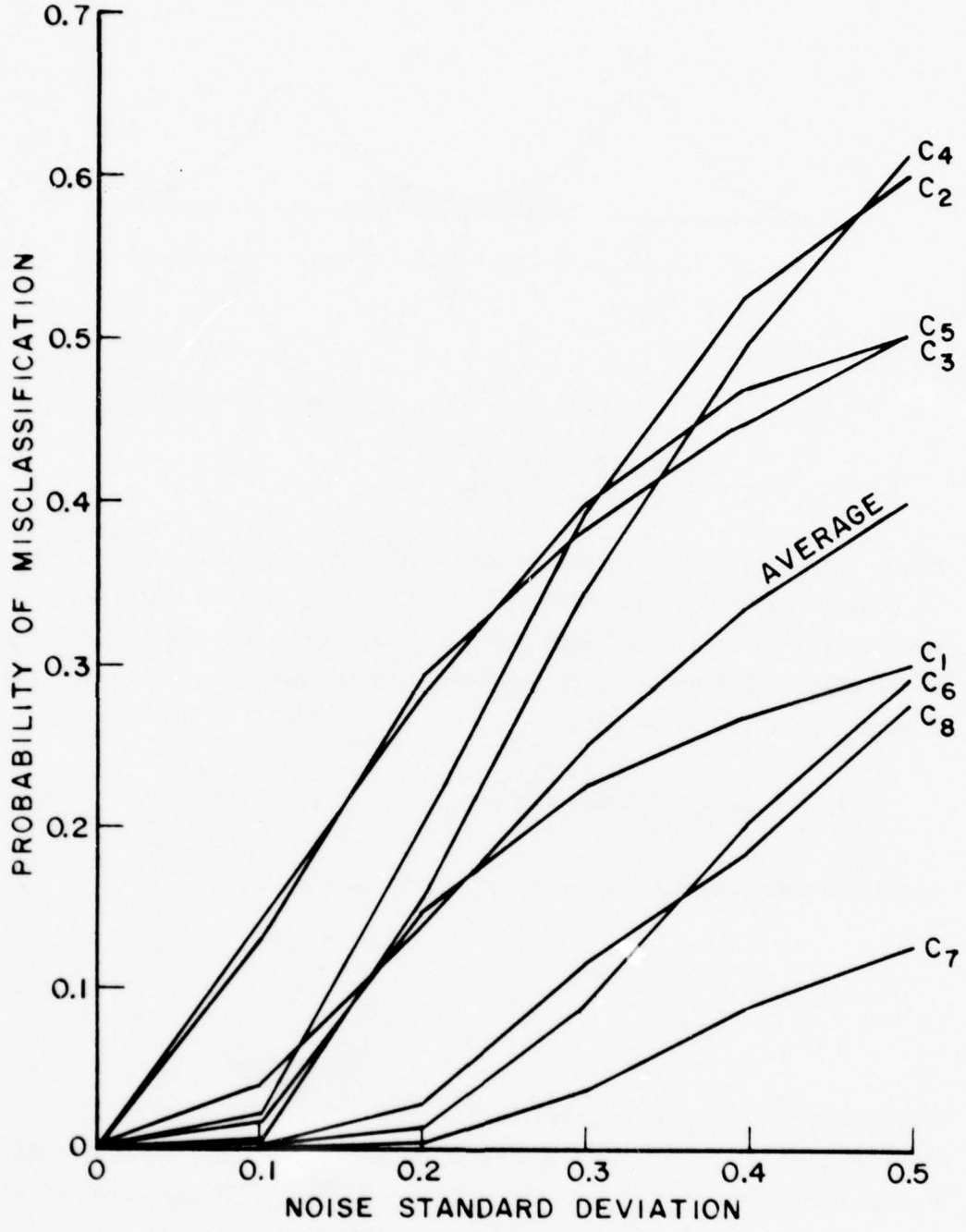

Figure 6. Probability of misclassification for individual aircraft, using amplitude returns at frequency f_{10} and $(0^{o},0^{o})$ aspect angle (nose on).

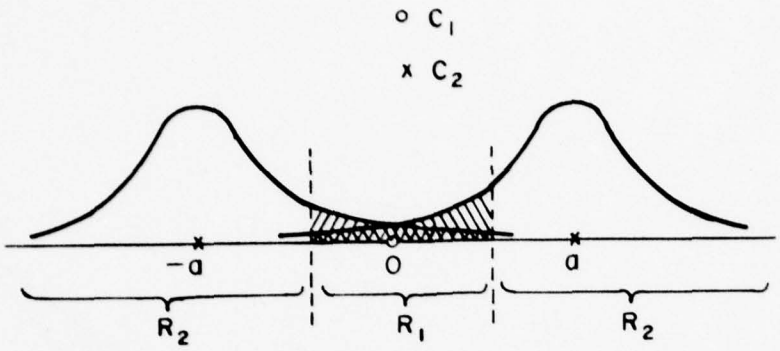

Figure 7. A two class distribution leading to an anomalous classification behavior.
o denotes class C_1
x denotes class C_2

the C_1 points as shown in the figure. The noise added to each class is assumed to be Gaussian with zero mean. It is obvious that an N.N. rule will lead to a fixed boundary for each region and the probability of misclassification of C_2 is just one half of the sum of the two shaded areas. It can be shown that

$$P_e(C_2) = \text{erfc}\left(\frac{a}{2\sigma}\right) - \text{erfc}\left(\frac{3a}{2\sigma}\right) , \tag{15}$$

where the complementary error function is defined as

$$\text{erfc}(x) \triangleq \int_x^\infty \frac{1}{\sqrt{2\pi}} e^{-\frac{y^2}{2}} dy \tag{16}$$

The function $P_e(C_2)$ is plotted in Figure 8. $P_e(C_2)$ increases as a/σ goes up from 0 to 1.05, and decreases as a/σ increases. When a is fixed, $P_e(C_2)$ increases as σ (i.e., the standard deviation of Gaussian noise) goes up till $\sigma = a/1.05$; the shaded areas begin to decrease as σ goes over this point and tend to zero as the noise level goes to infinity. This shows that the probability of misclassification $P_e(C_2)$ does not necessarily increase as the noise level goes up, as was seen for $P_e(C_2)$

in Figure 5. This anomalous behavior is reduced as the dimensionality of the feature vector increases since the likelihood of class enclosure by its neighbor decreases.

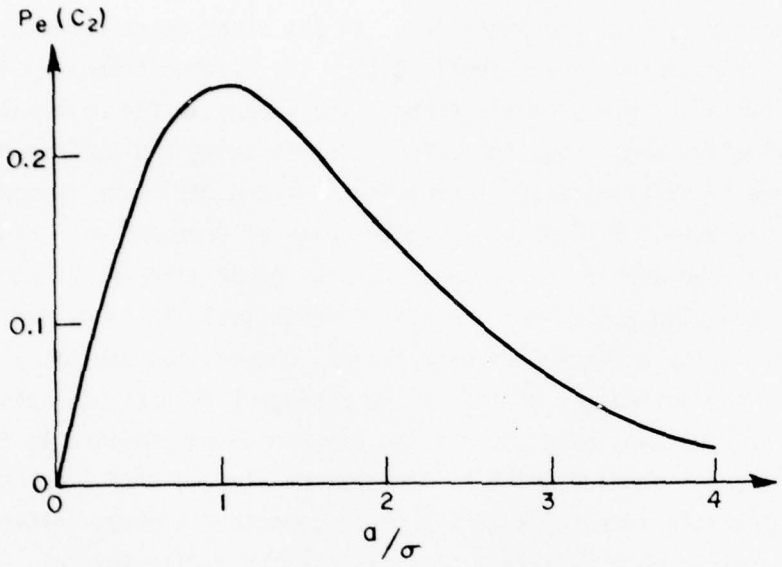

Figure 8. Average probability of misclassification of Class C_2 in Figure 7.

An important characteristic of the classification features is the size of aircraft. Since the electromagnetic amplitude response is approximately proportional to the size of an illuminated scatterer at frequencies below resonance, the targets whose sizes vary significantly from the average would be fairly easy to separate from the main group of targets and hence bear smaller probabilities of error in classification. This is shown by the performance of C_6 and C_7 in Figures 2 and 3. Note that C_7 (B1) is the largest aircraft among all the investigated ones and is distinguished from all others pretty easily in almost all cases since its amplitude returns are much larger than those of others over most of the operating frequency range. This advantage is not present for airplanes of approximately equal size. The discrimination between some airplanes are difficult at certain frequencies

because their scattering returns are very similar. This similarity occurs for different airplanes at different frequencies.

The classification performance shown in Figures 2-6 is for the aspect angle $(0^{o},0^{o})$. The performance at the other three observation angles is represented in in Figures 9-11. The optimum frequency is the same for all angles, namely 4 MHz. The change in the observation and illumination angle does not affect significantly the performance. This is due to relative shape independence of the amplitude response when operating well within the Rayleigh range of frequencies. Figures 12-15 depict the average performance for the eight aircraft at each of the observation angles for the best frequencies. It is evident that f_2 = 4 MHz is the optimum frequency for all observation angles. The reason for the optimality of such a low frequency is that utilizing single frequency amplitude returns the discrimination feature is the scattering cross section which is directly related to size (in the Rayleigh range). The main advantages of higher frequencies is phase information which is ignored when amplitude alone is used as a discriminant.

The relative average performance at the optimum frequency is shown in Figure 16.

VII. SINGLE FREQUENCY COMPLEX RETURNS

A significant improvement over the previous results was achieved by using phase information in addition to amplitude information. With the introduction of phase, the dimensionality of each tested vector increases from two to four. Also the performance at higher frequencies becomes superior to lower frequency performance because the phase variations become more pronounced at the higher frequencies, reflecting shape changes. The size changes are detected by amplitude variation and the combined effect produces a substantially improved performance compared to previous results. The irregularities that appeared in the last section are reduced drastically due to the higher dimensionality.

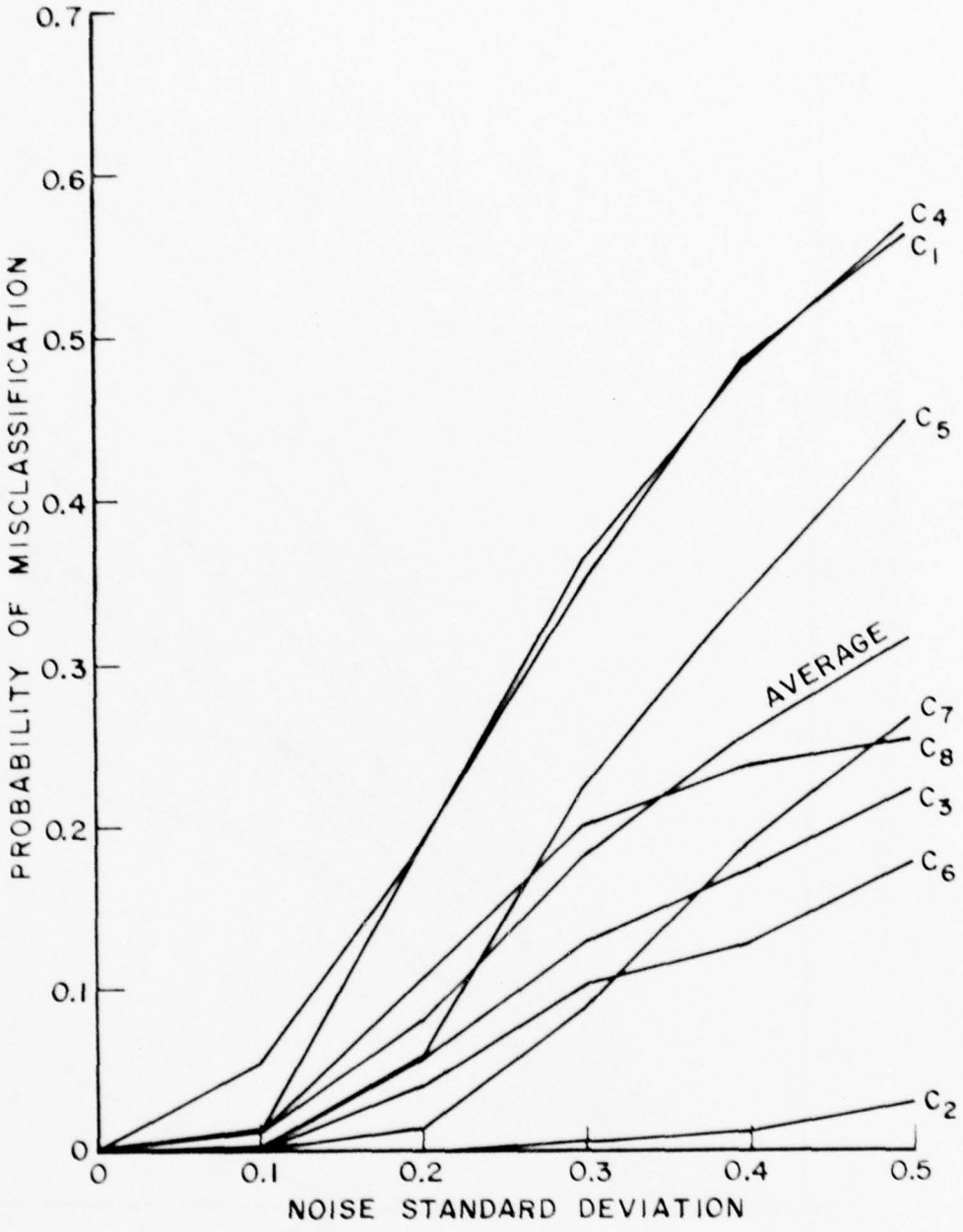

Figure 9. Probability of misclassification for individual aircraft, using amplitude returns at frequency f_2 and $(90^0,0^0)$ aspect angle (bottom view).

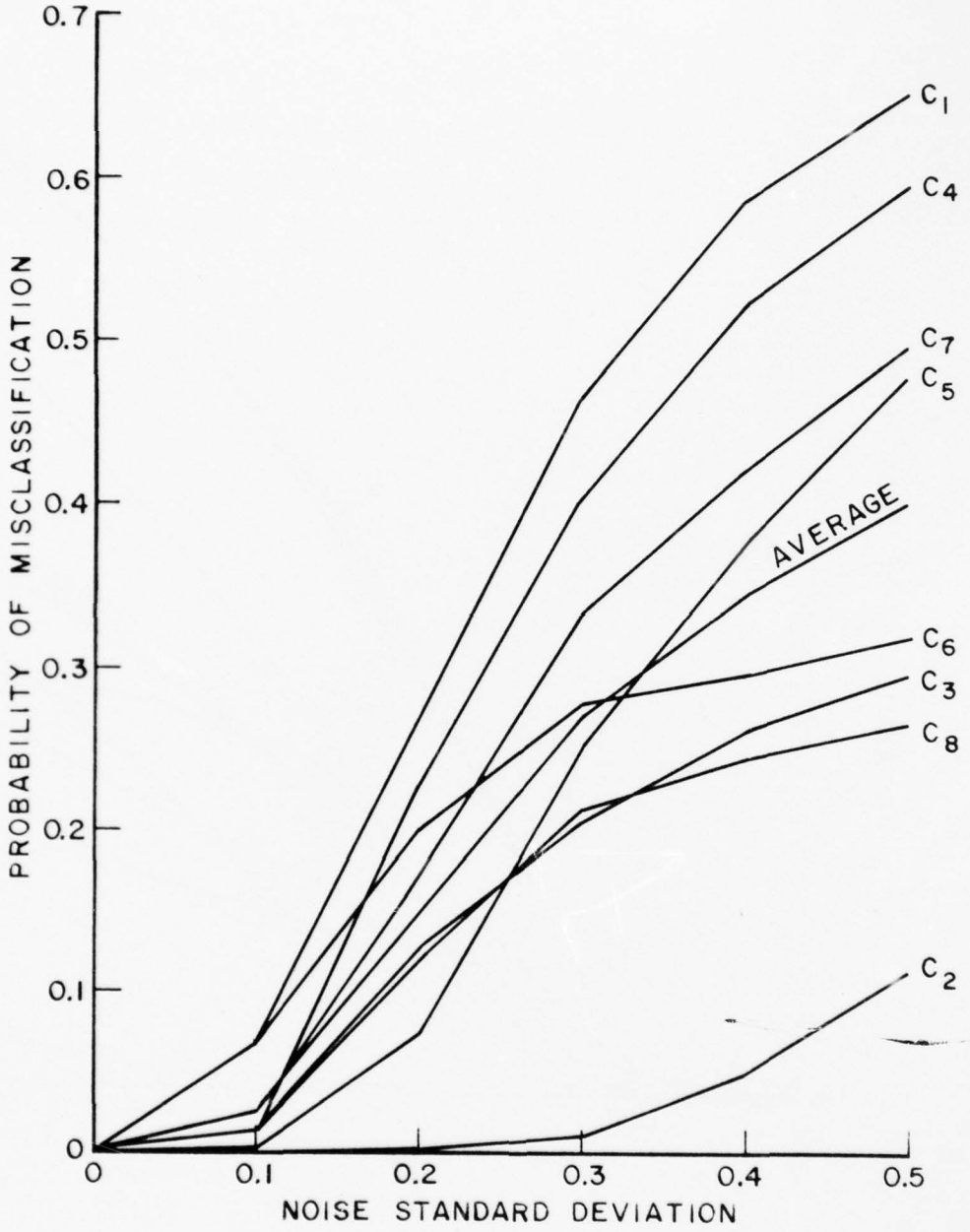

Figure 10. Probability of misclassification for individual aircraft, using amplitude returns at frequency f_2 and $(90^0, 90^0)$ aspect angle (side view).

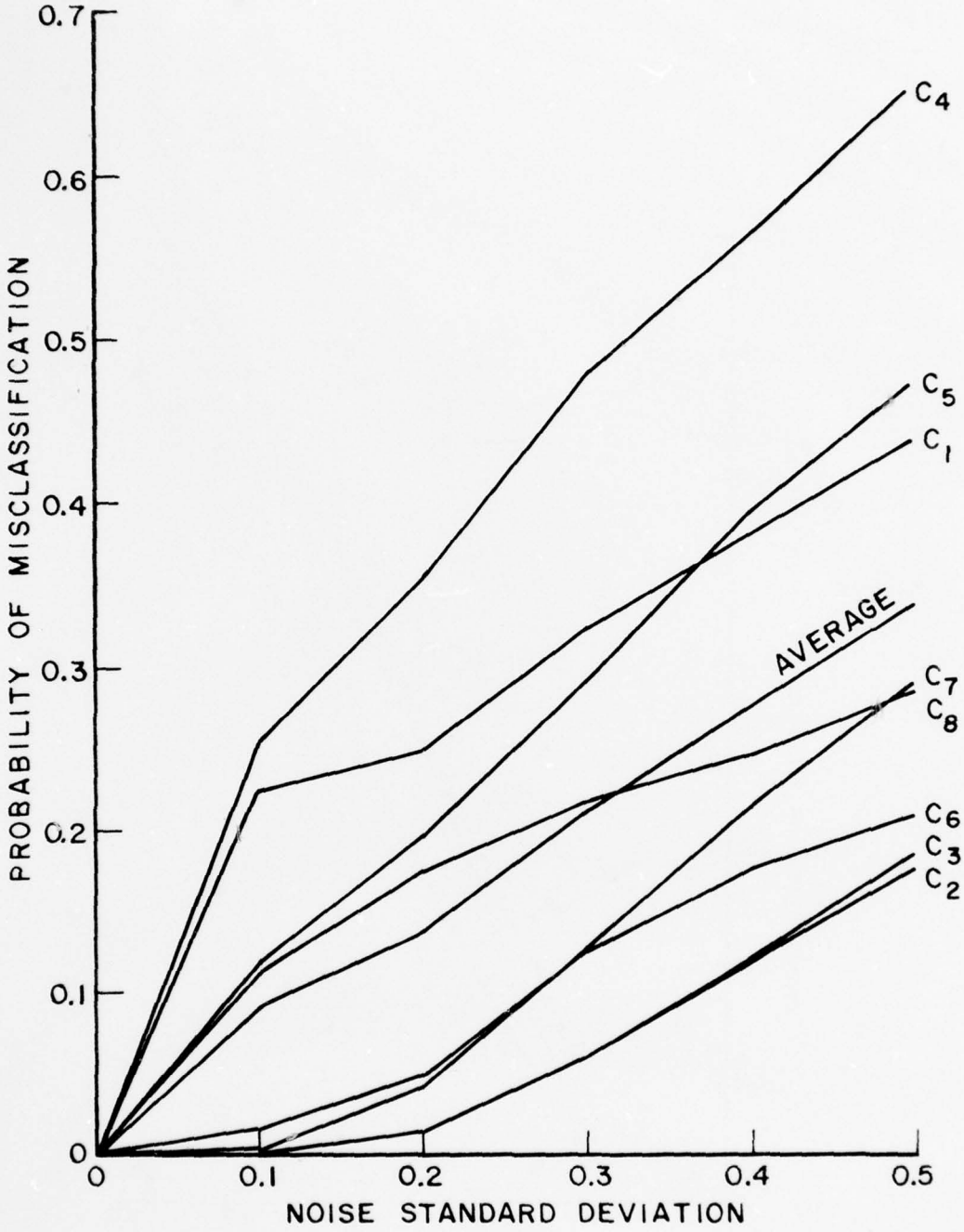

Figure 11. Probability of misclassification for individual aircraft, using amplitude returns at frequency f_2 and $(45^o, 45^o)$ aspect angle.

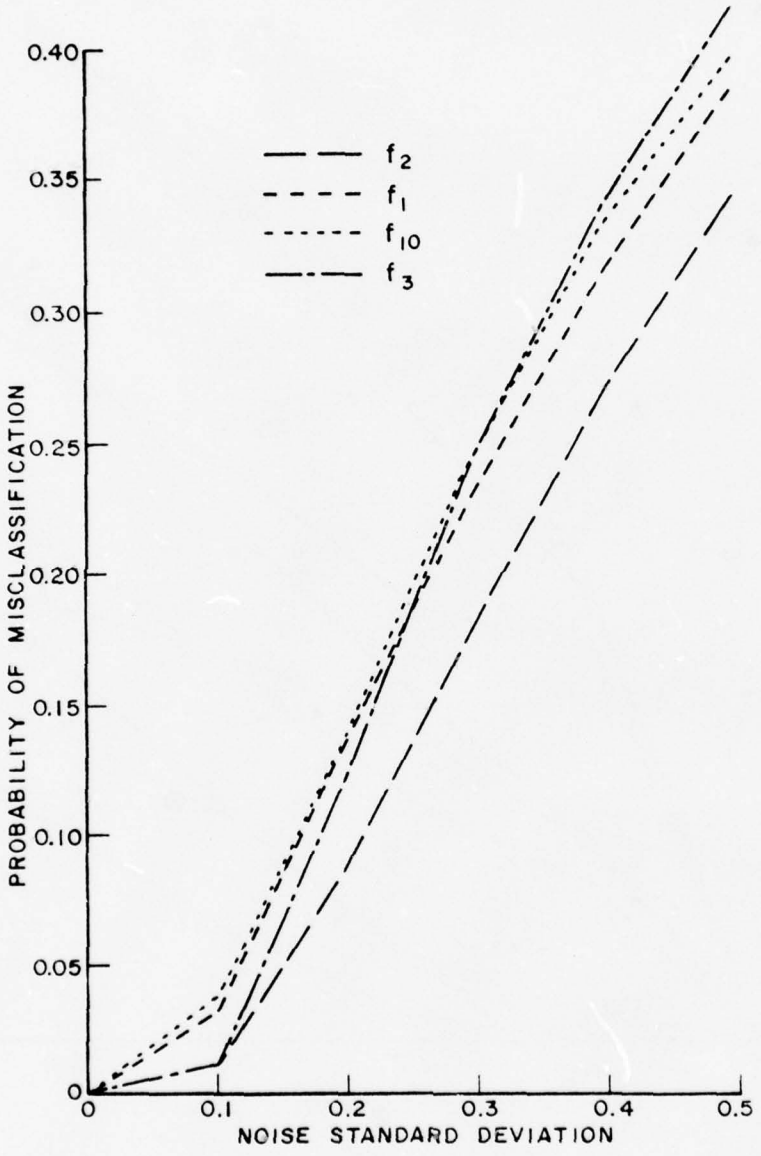

Figure 12. The average performance at different frequencies, using single frequency amplitude returns. The observation angle is $\theta=0°$, $\phi=0°$.

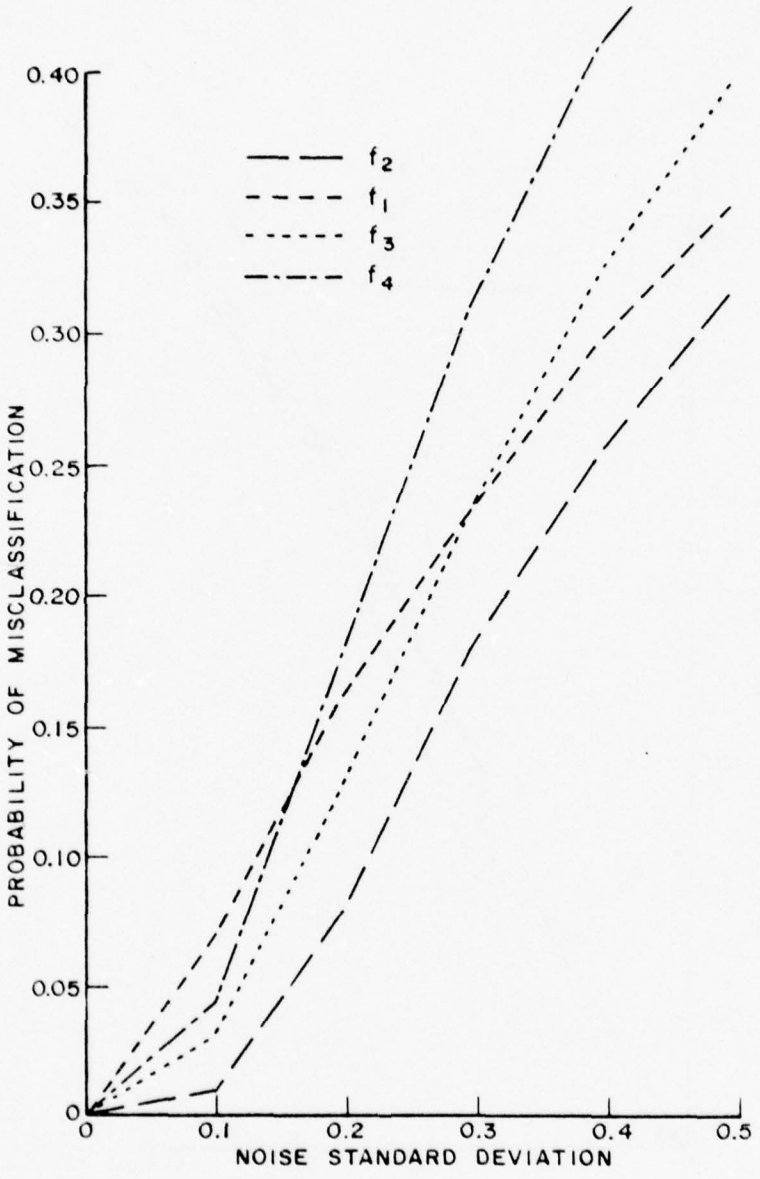

Figure 13. The average performance at different frequencies, using single frequency amplitude returns. The observation angle is $\theta=90^{\circ}$, $\phi=0^{\circ}$.

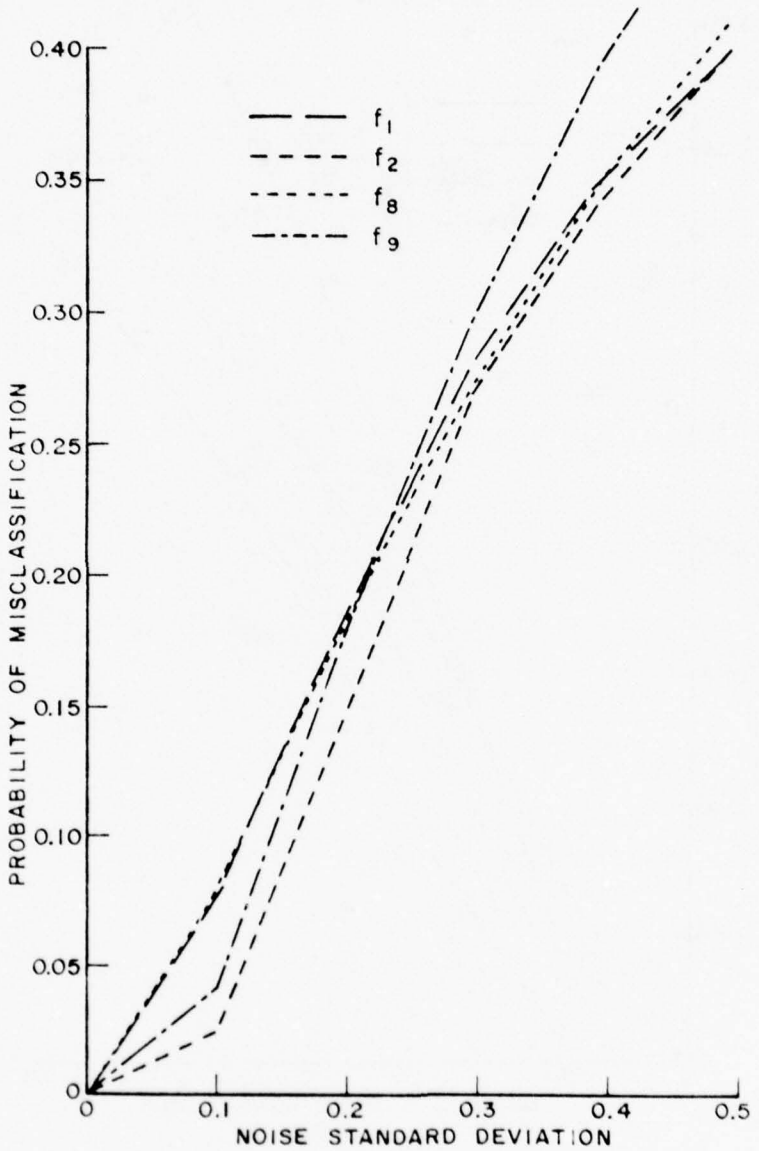

Figure 14. The average performance at different frequencies, using single frequency amplitude returns. The observation angle is $\theta=90^\circ$, $\phi=90^\circ$.

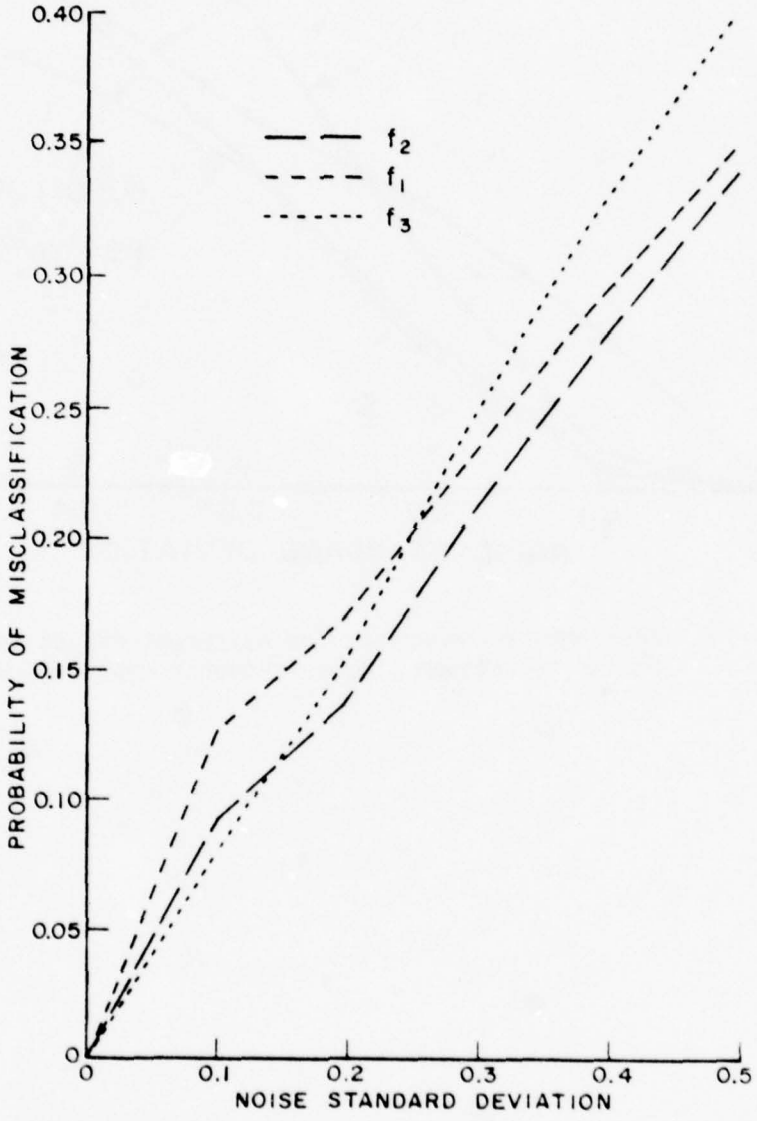

Figure 15. The average performance at different frequencies, using single frequency amplitude returns. The observation angle is $\theta=45°$, $\phi=45°$.

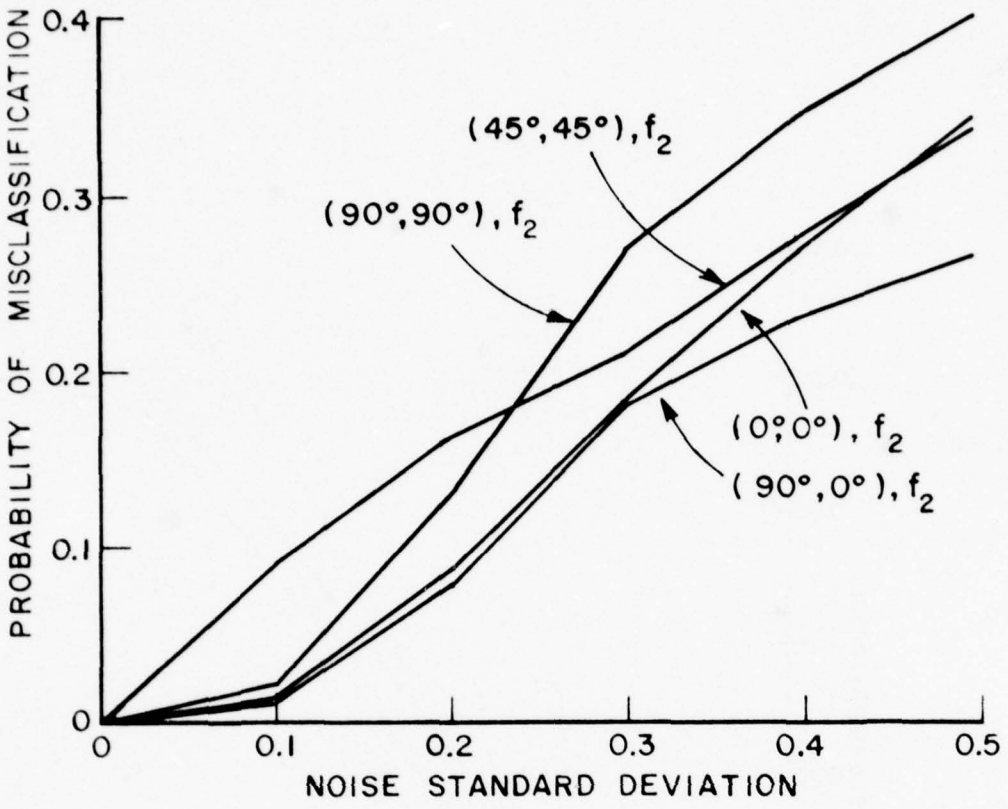

Figure 16. Performance comparison for different aspect angles employing optimum single frequency amplitude returns.

Figures 17-26 show the results for the best frequencies at four aspect angles. The probabilities of misclassification can be seen to be substantially lower than for the amplitude features alone. The errors are negligibly small up to noise levels of 10% of signal level and even for 20% noise level the worst error probability is 0.15 at $(90^{o},90^{o})$ (side view) for targets C_1 and C_4, with other observation angles producing substantially lower errors. In fact when the error is averaged over all classes for each observation angle, the optimum frequencies produce less than .05 probability of misclassification for the $(90^{o},90^{o})$ observation angle, .02 for $(90^{o},0^{o})$ and undetectable errors for $(0^{o},0^{o})$ and $(45^{o},45^{o})$, for a 20% noise level injection (see Figures 27-30).

The bias phenomena described above still exist but are substantially reduced, due to a higher dimensionality of the feature vectors. Some frequencies, however yield significantly better performance than others because the scattering responses of different airplanes at these frequencies are more dissimilar, improving the overall performance (Figures 27-30). This is especially true at the two aspects, $(0^{o},0^{o})$ and $(45^{o},45^{o})$, where the similarity of the data is pretty weak.

The data similarity are exemplified by the bottom view $(90^{o},0^{o})$. The two (vertically and horizontally) polarized waves are exciting the fuselages and the wings of the aircraft. Their dimensions, however, are very close for some aircraft (e.g., for fuselages: C_1 (F 104) - 16.69 m, C_4 (Mig 21) - 16.75 m, C_3 (F 4) - 17.76 m; for wings: C_1 -6.68 m, C_4 - 7.6 m, etc.) At the low frequencies, where overall dimensions dominate, the scattering returns of these aircraft are so close (see Figures 31-32) that to distinguish them becomes rather difficult (see $P_e(C_1)$ and $P_e(C_4)$ in Figures 19 and 20). This kind of data similarity is reduced as the frequency increases ($P_e(C_1)$ and $P_e(C_4)$ in Figures 21 and 22), where the scattering returns are more shape responsive. At f_{12}, we obtain the best performance at this aspect (Figure 22).

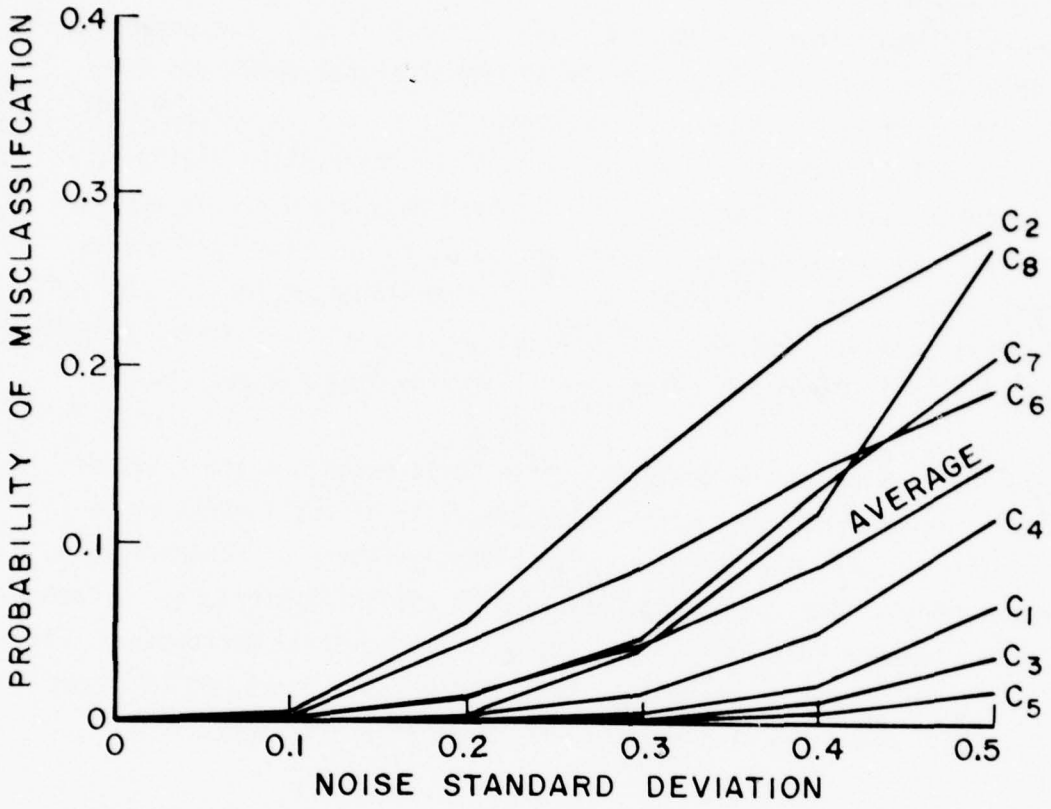

Figure 17. Probability of misclassification for individual aircraft, using complex returns at frequency f_{11} and (0°,0°) aspect angle (nose on).

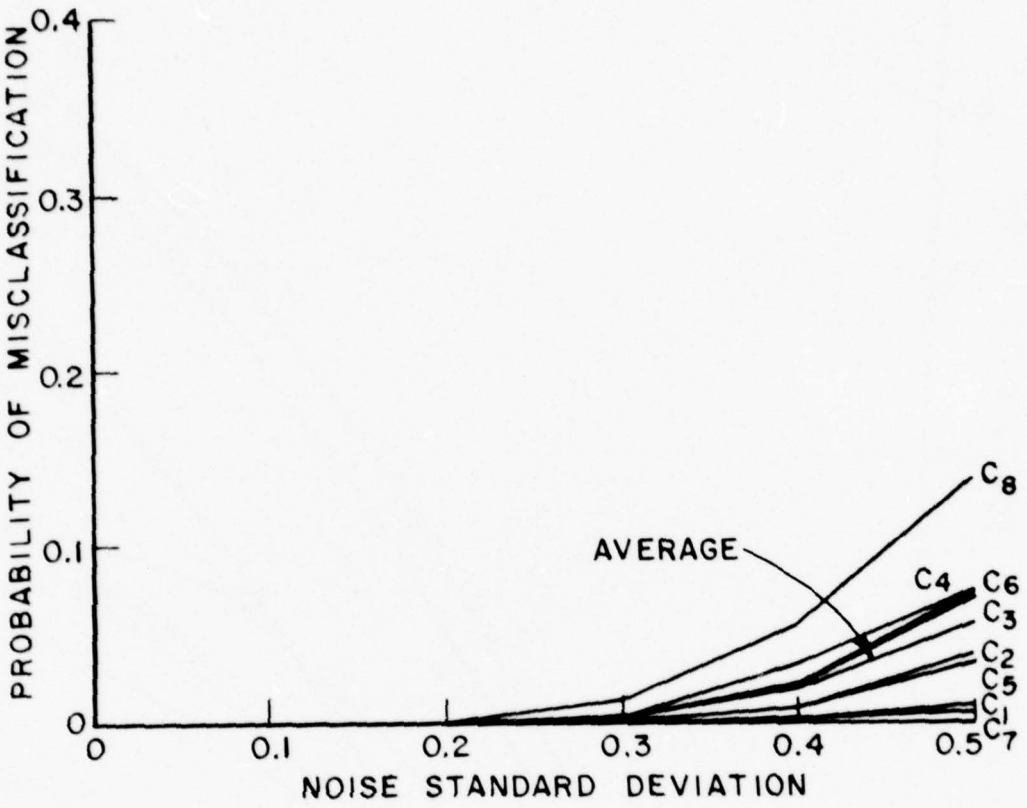

Figure 18. Probability of misclassification for individual aircraft, using complex returns at frequency f_{12} and $(0^0,0^0)$ aspect angle (*nose on*).

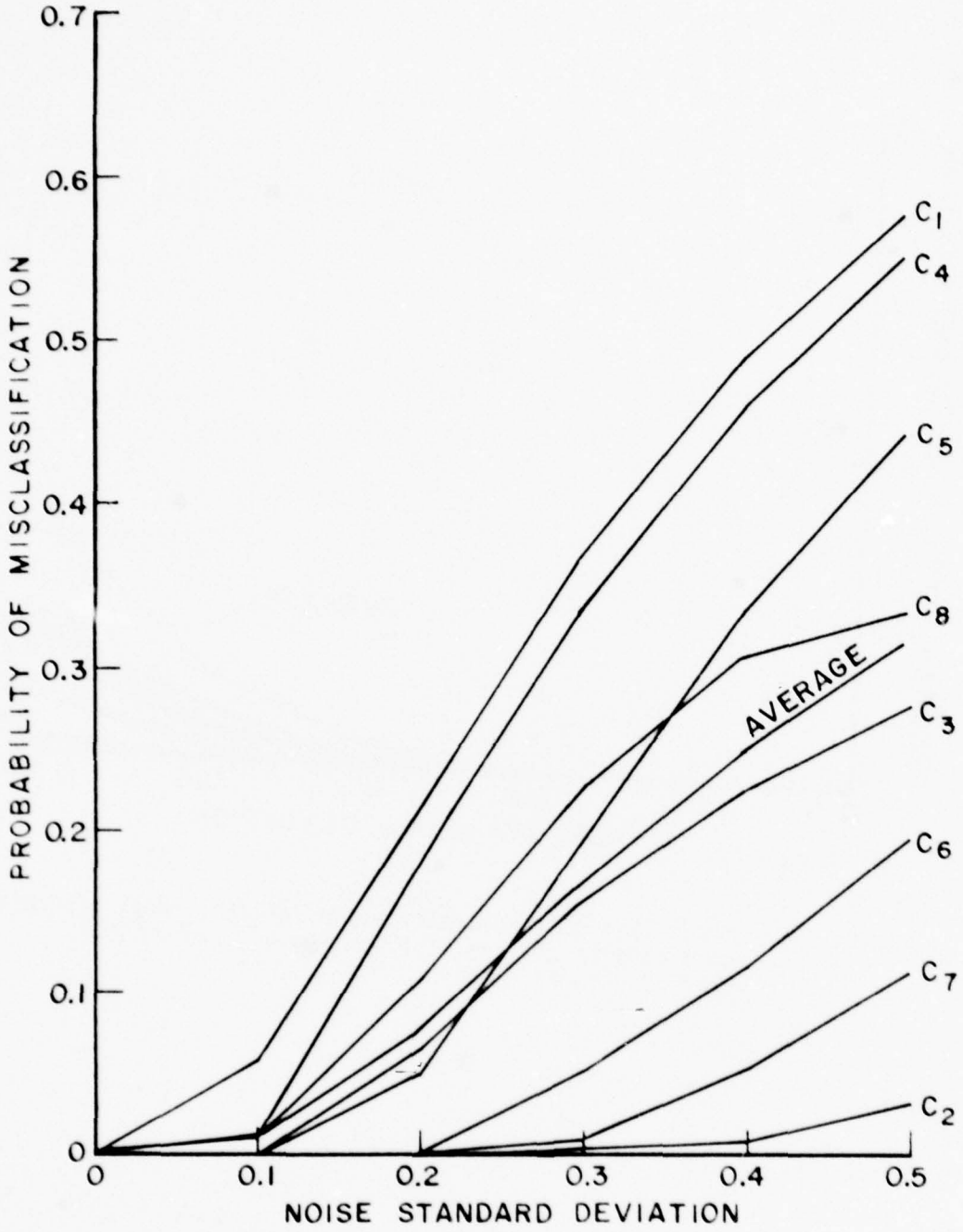

Figure 19. Probability of misclassification for individual aircraft, using complex returns at frequency f_2 and $(90^0, 0^0)$ aspect angle (bottom view).

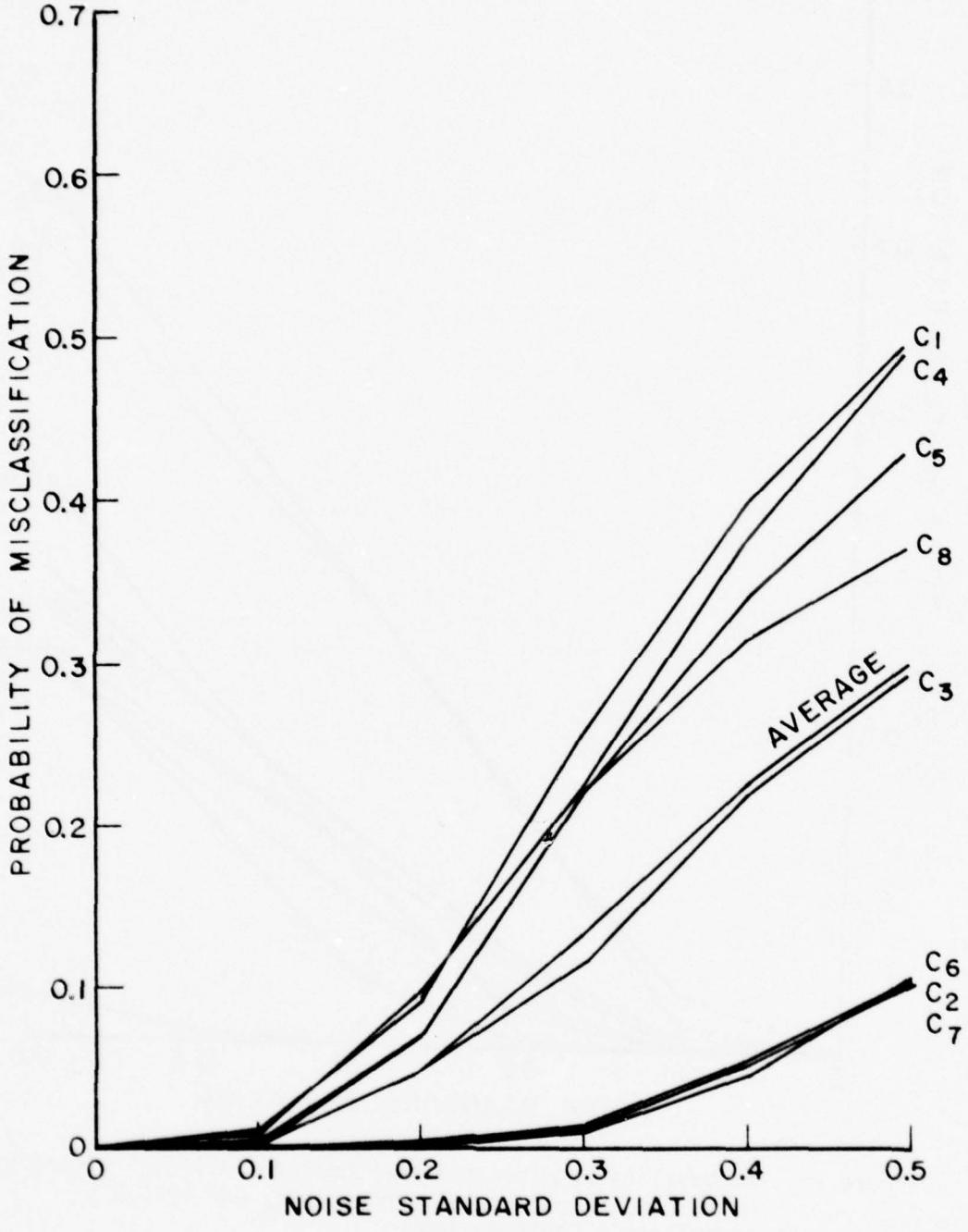

Figure 20. Probability of misclassification for individual aircraft, using complex returns at frequency f_3 and $(90^0, 0^0)$ aspect angle (bottom view).

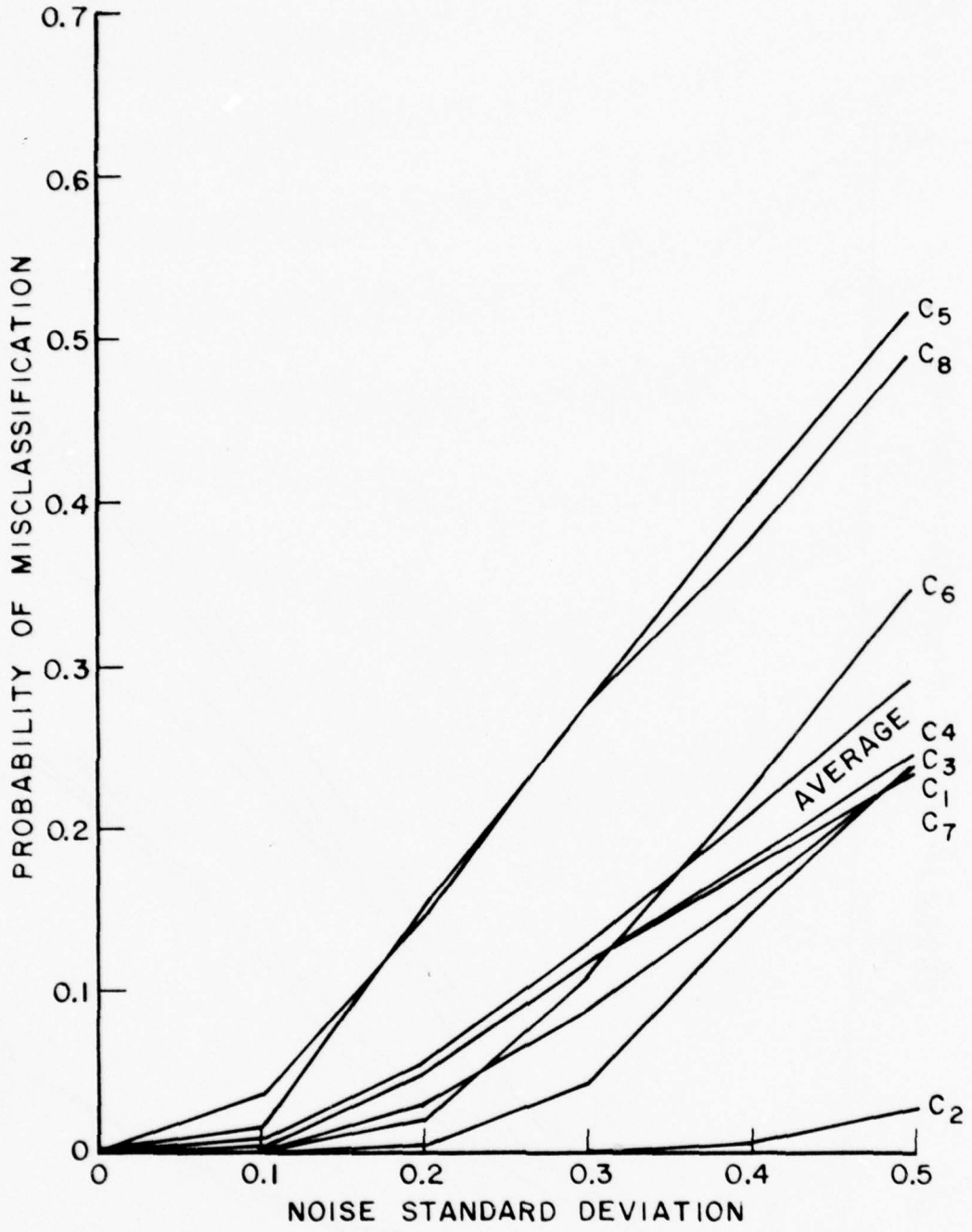

Figure 21. Probability of misclassification for individual aircraft, using complex returns at frequency f_6 and $(90^\delta, 0^\delta)$ aspect angle (bottom view).

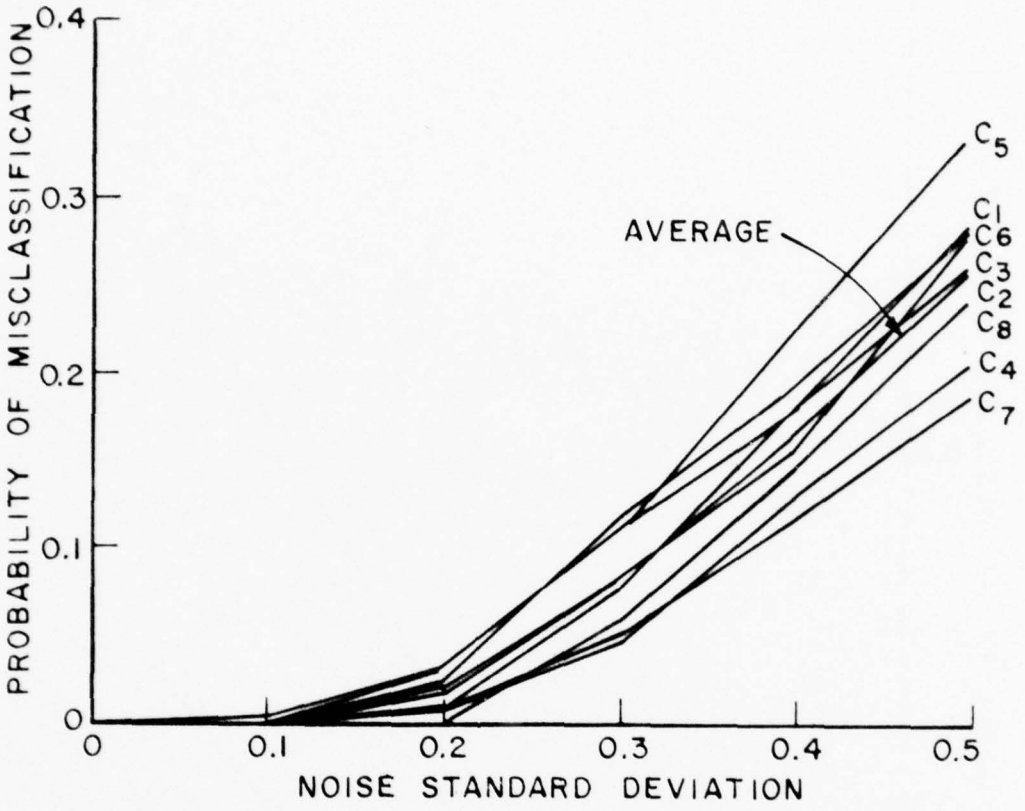

Figure 22. Probability of misclassification for individual aircraft, using complex returns at frequency f_{12} and $(90^0, 0^0)$ aspect angle (bottom view).

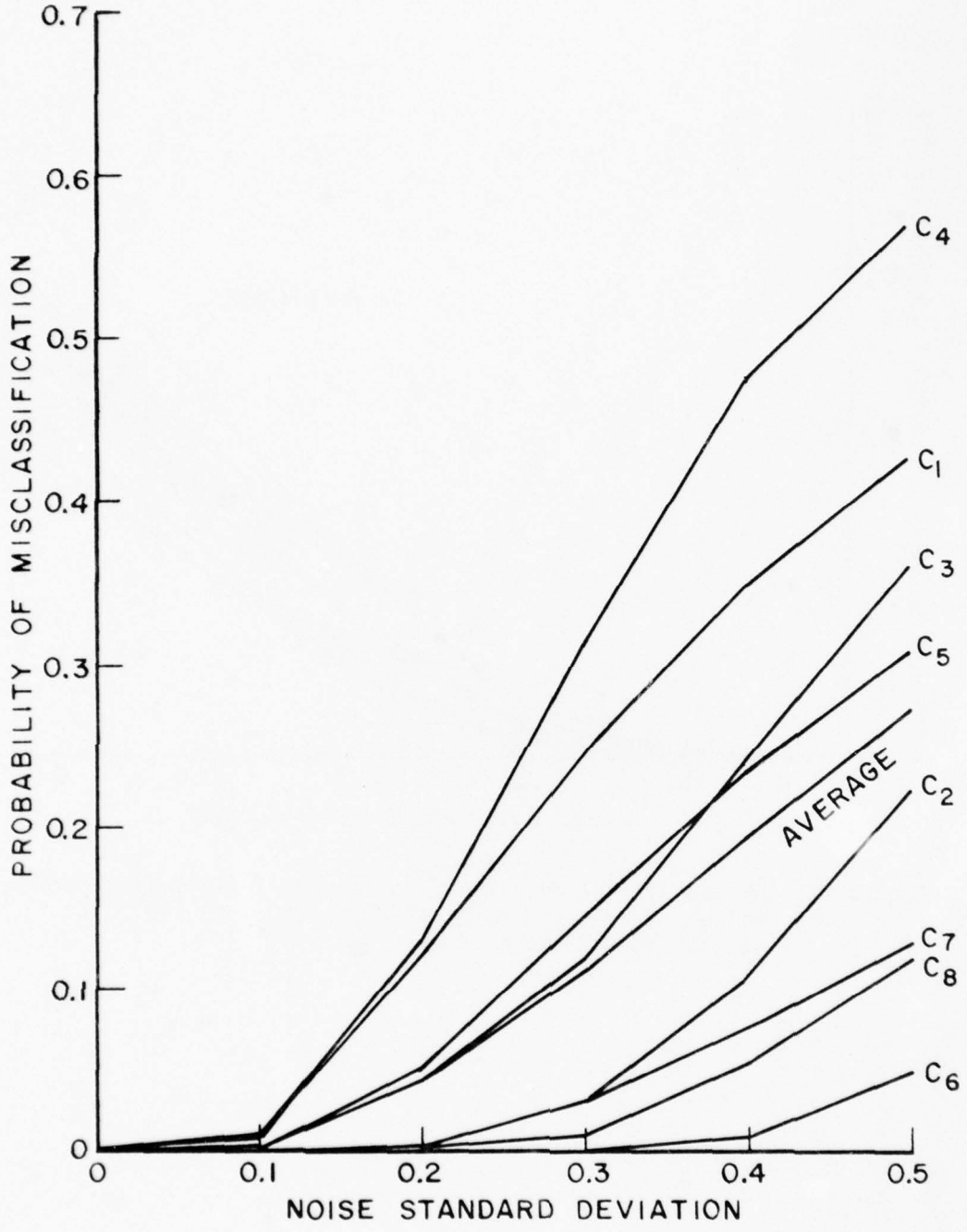

Figure 23. Probability of misclassification for individual aircraft, using complex returns at frequency f_{12} and $(90^{0},90^{0})$ aspect angle (side view).

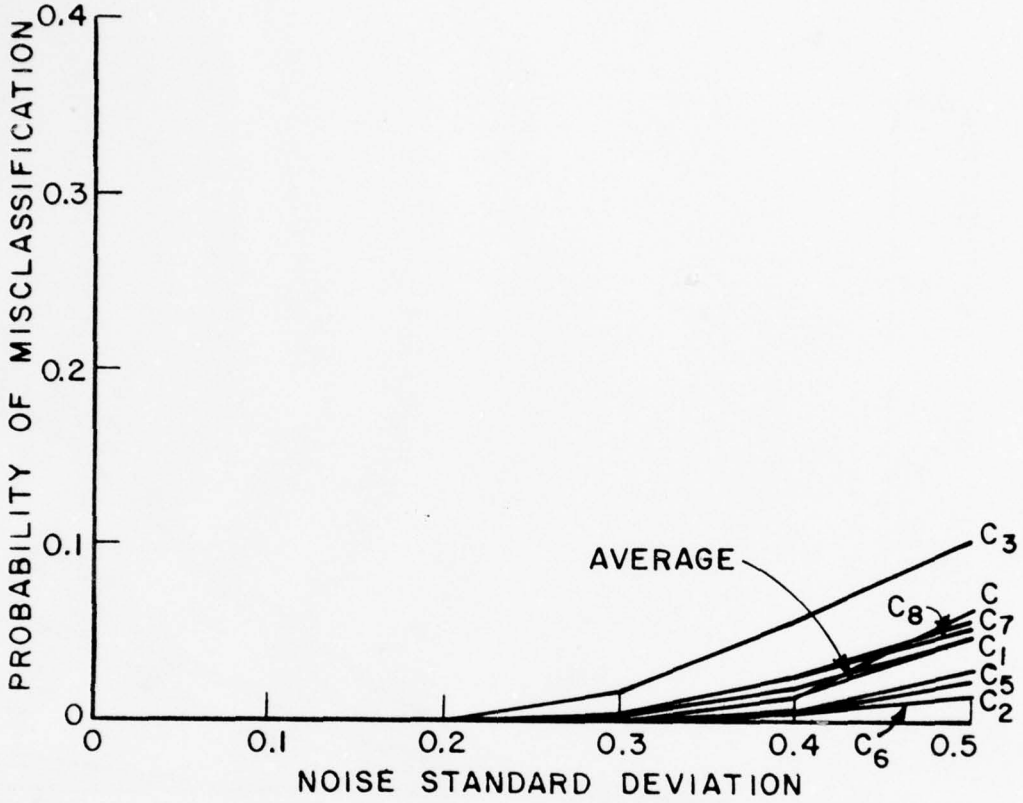

Figure 24. Probability of misclassification for individual aircraft, using complex returns at frequency f_6 and $(45^0, 45^0)$ aspect angle.

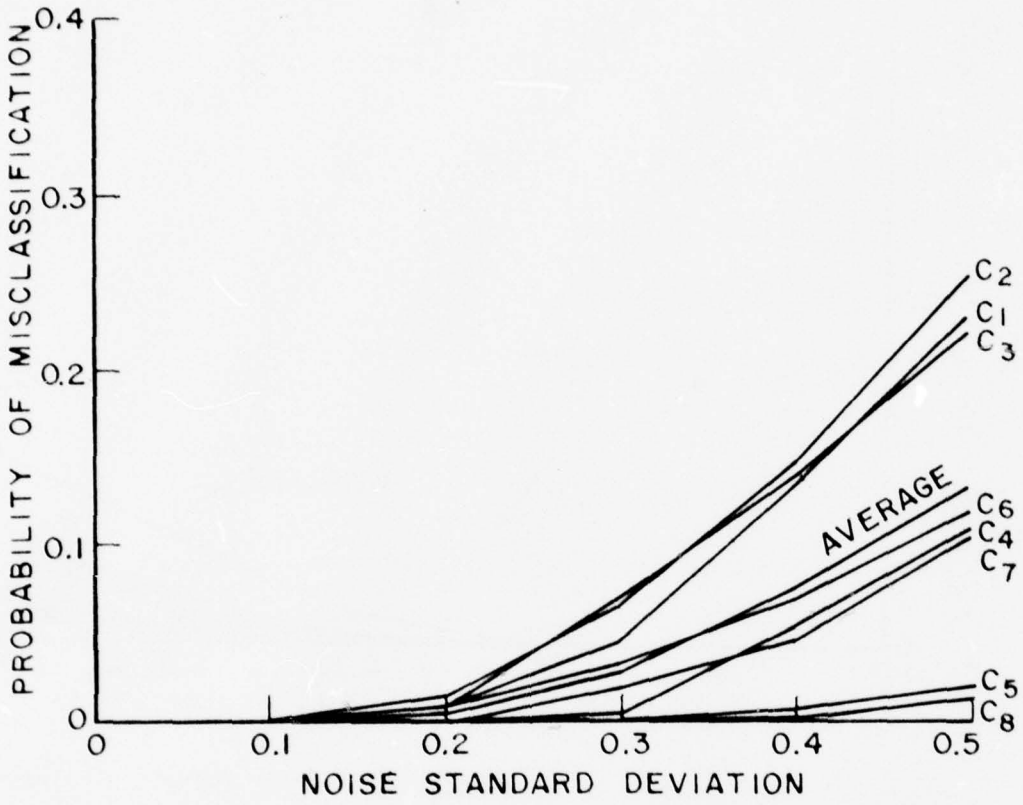

Figure 25. Probability of misclassification for individual aircraft, using complex returns at frequency f_8 and $(45^0,45^0)$ aspect angle.

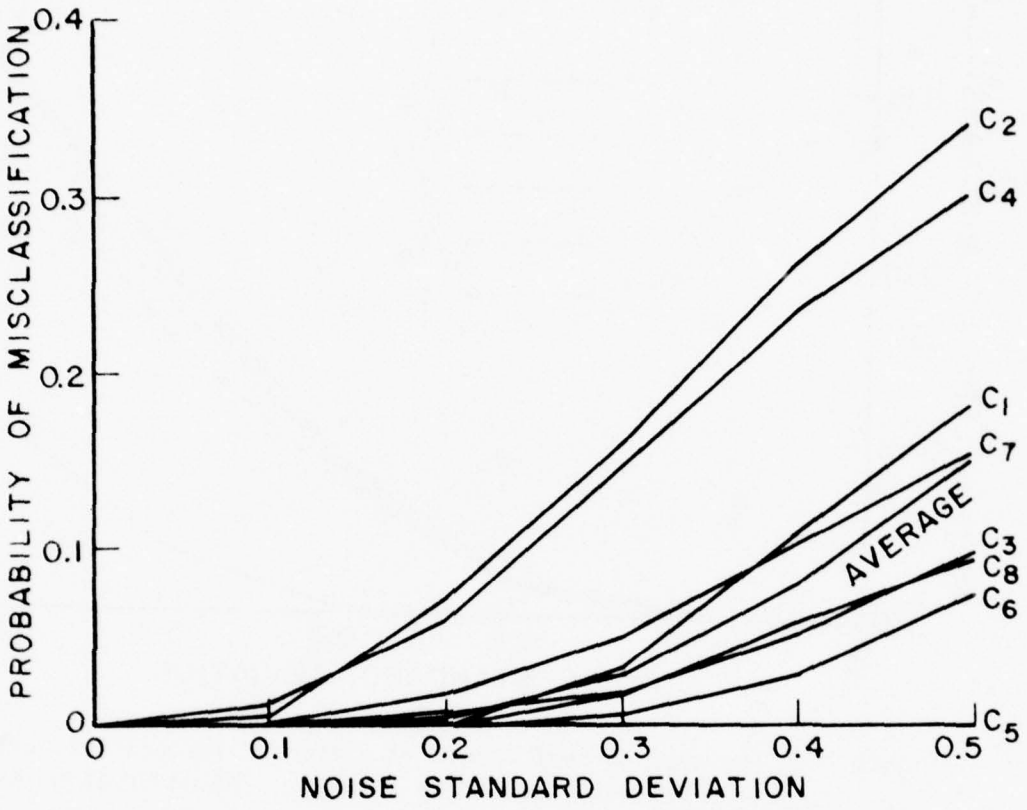

Figure 26. Probability of misclassification for individual aircraft, using complex returns at frequency f_{11} and $(45^{o},45^{o})$ aspect angle.

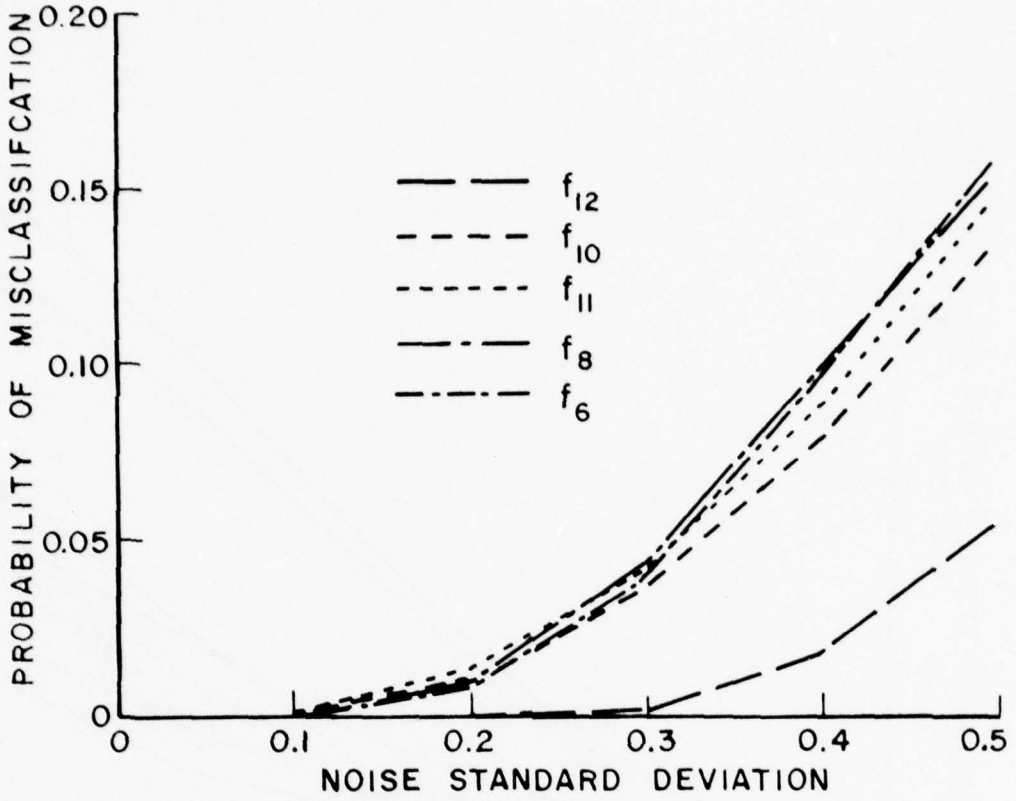

Figure 27 The average performance at different frequencies, using single frequency complex returns. The observation angle is $\theta°=0°$, $\phi=0°$.

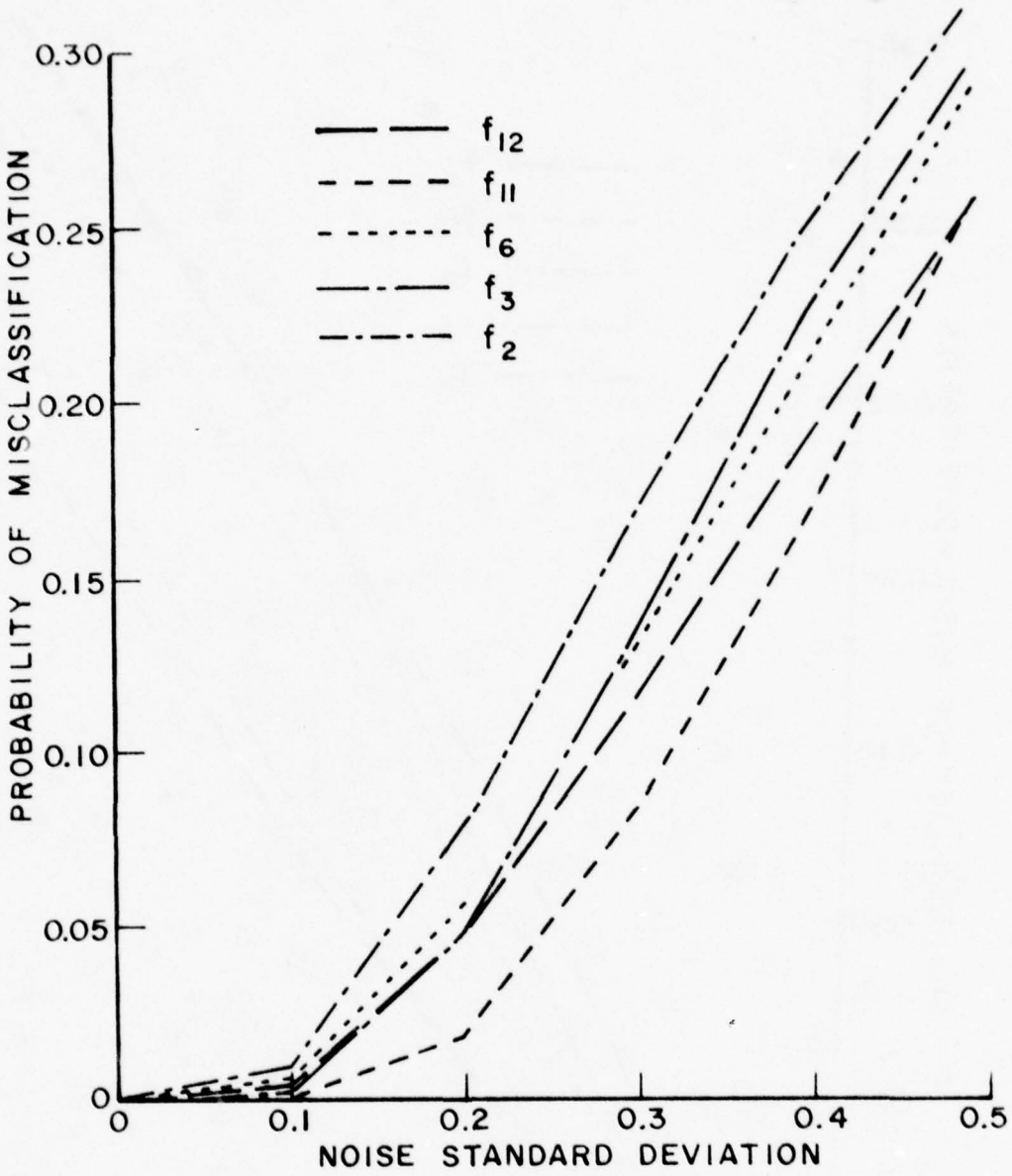

Figure 28. The average performance at different frequencies, using single frequency complex returns. The observation angle is $\theta=90°$, $\phi=0°$.

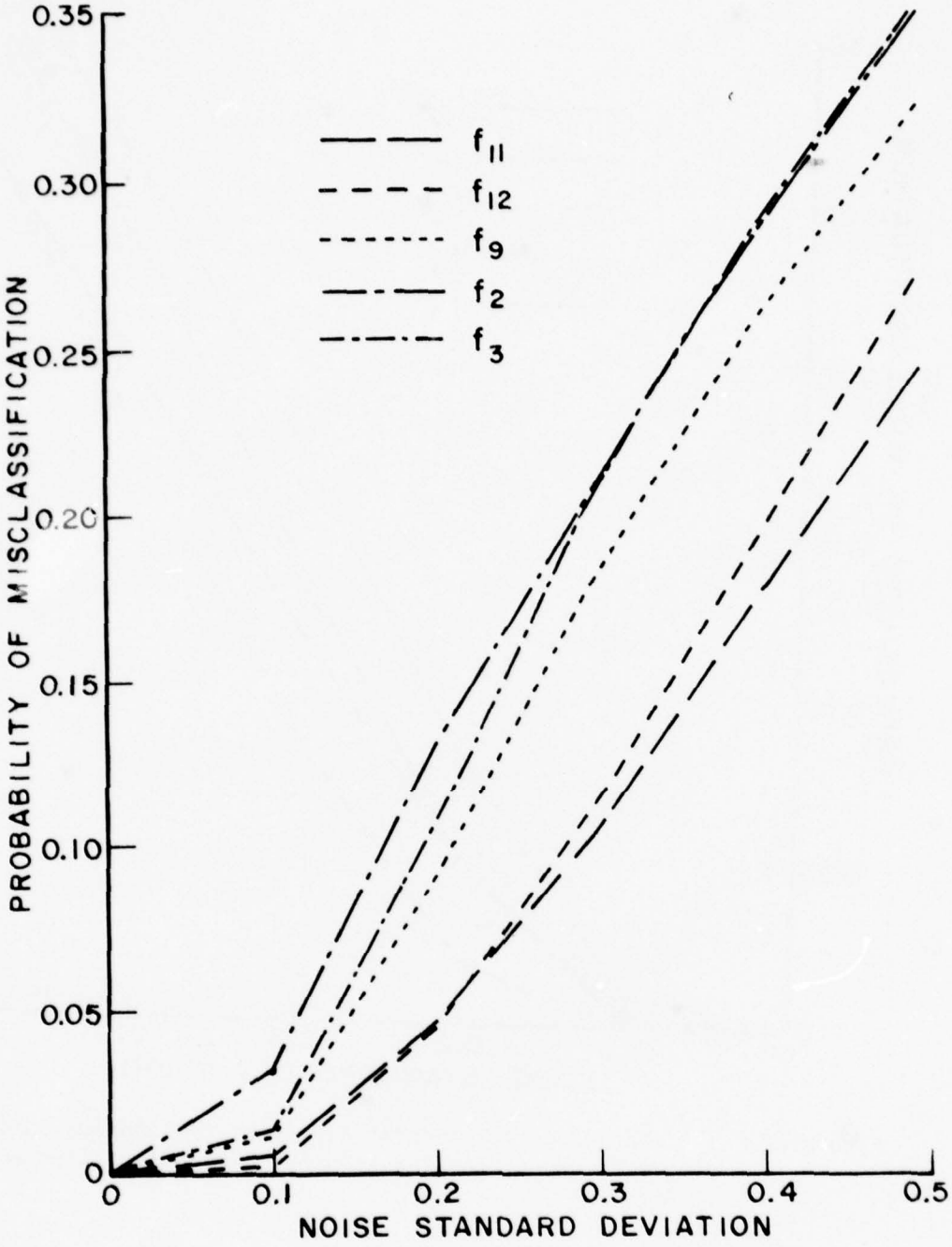

Figure 29. The average performance at different frequencies, using single frequency complex returns. The observation angle is $\theta=90°$, $\phi=90°$.

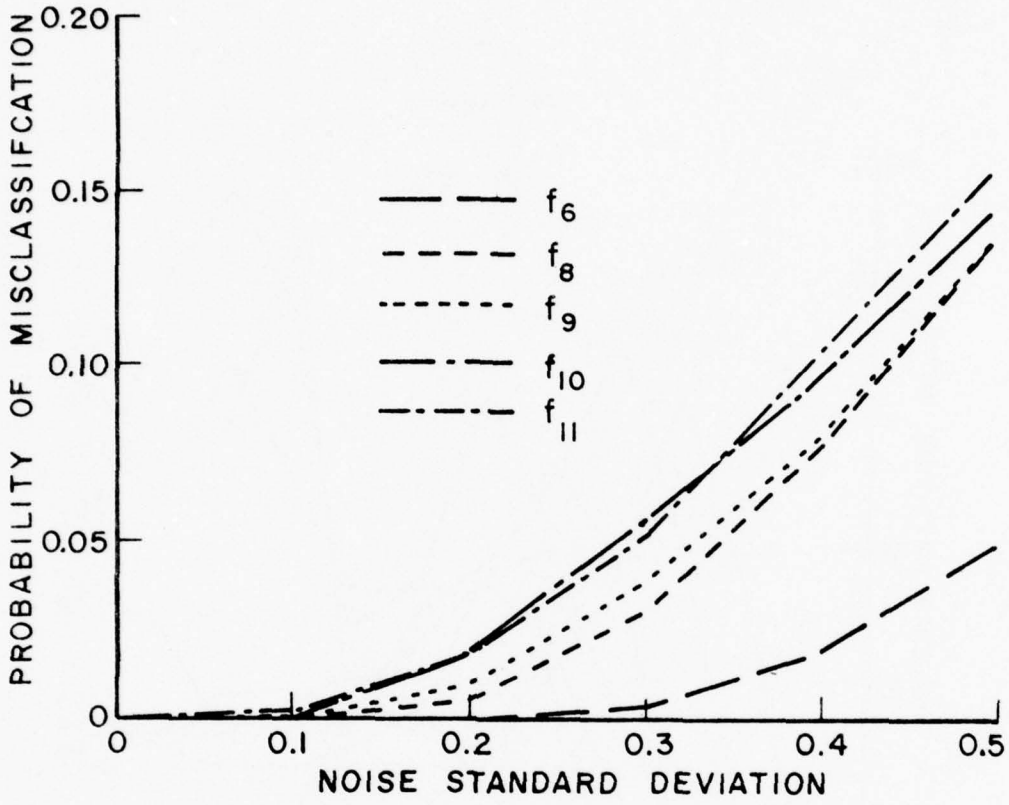

Figure 30. The average performance at different frequencies, using single frequency complex returns. The observation angle is θ=45°,ϕ=45°.

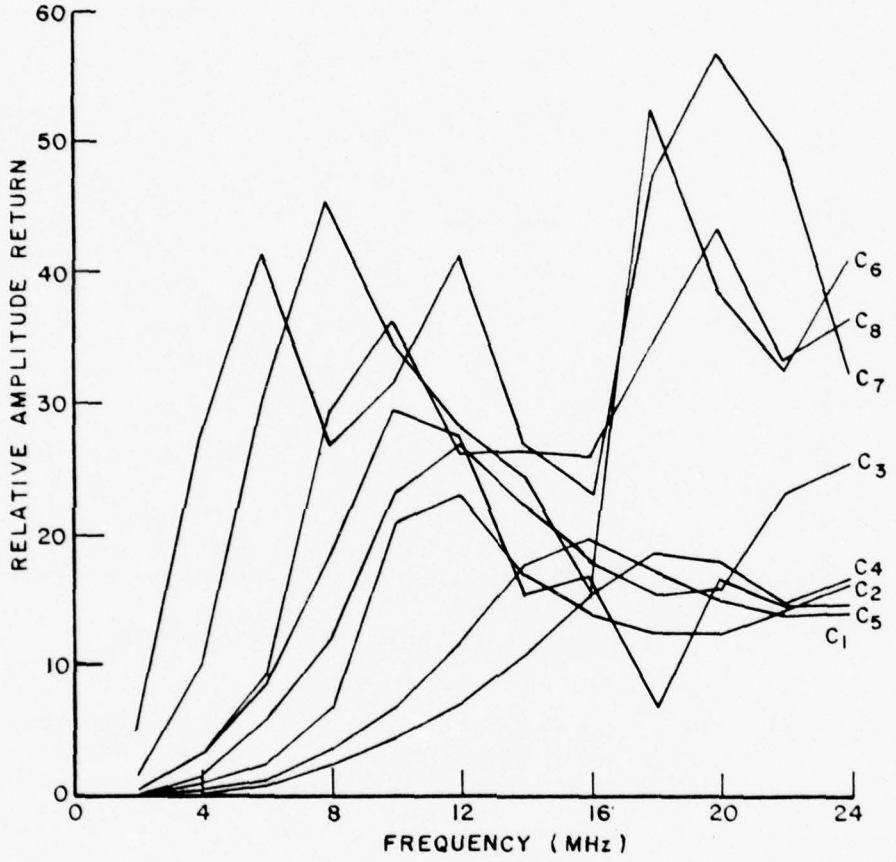

Figure 31. Amplitude returns of horizontally polarized electromagnetic scattering responses for eight aircraft at $\theta=90°$, $\phi=0°$.

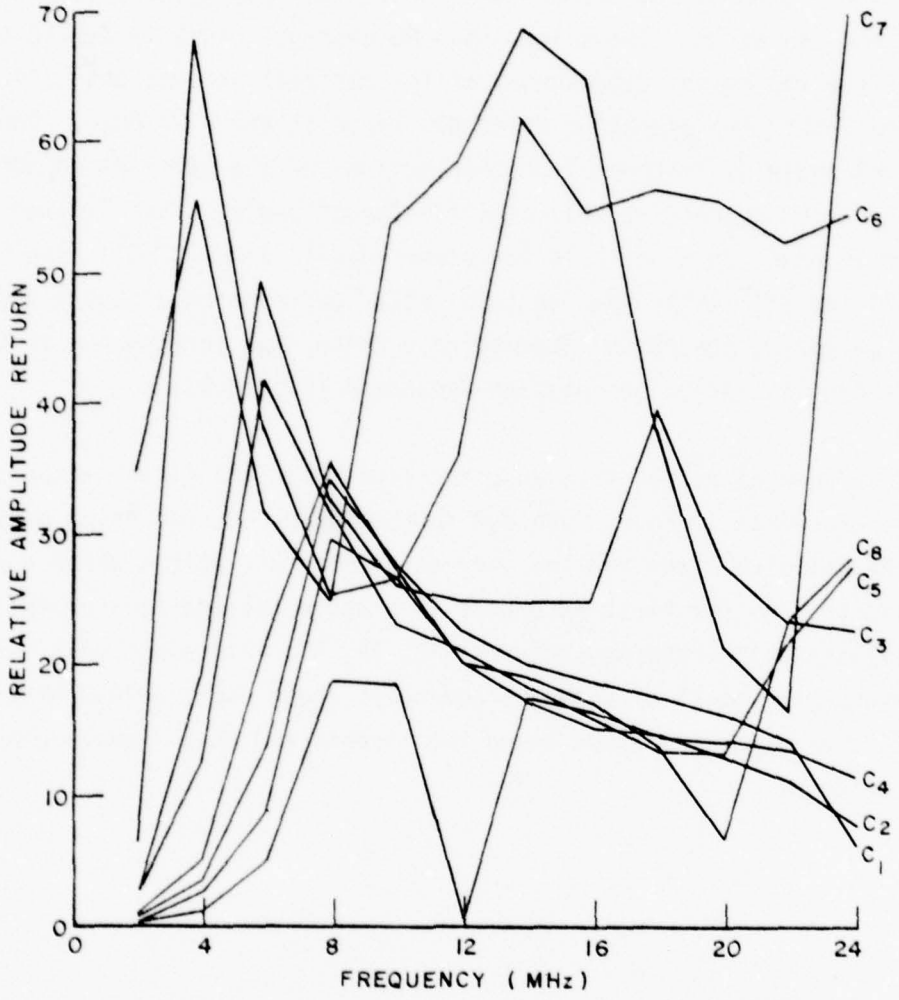

Figure 32. Amplitude returns of vertically polarized electromagnetic scattering responses for eight aircraft at $\theta=90°$, $\phi=0°$.

Comparing the complex responses of the targets (Figures 33-36) to the amplitude responses, we see that employing the phase information not only increases the dimensionality of the features, but also extends the range of each feature from positive values alone to the whole real axis. Note that the imaginary parts of the complex scattering returns of all the aircraft at the bottom view are all positive, indicating that the phases are always less than 90 degrees. This is due to the fact that the height (thickness) of the aircraft is less than 1/4 wavelength within the operating frequency range (2 MHz - 24 MHz). The resultant phase differences from the portions of the aircraft do not vary more than 90 degrees at this specific aspect angle. This limited variation in phase does not hold for other aspects like $(0^{o},0^{o})$ (see Figures 37-42) and $(45^{o},45^{o})$, leading to a better performance at these aspects when utilizing the phase information. Hence, the performance of the classifier is rather orientation dependent (Figure 43).

In general as the frequency increases from the first harmonic up, the performance improves both due to the increased scattering amplitude in the Rayleigh range and the increased phase variations which are shape sensitive. As the first resonance is crossed the scattering amplitude oscillates with frequency (Figures 31, 32, 41, 42), since most targets, however, resonate at different frequencies these oscillations contribute to further data separation among the targets and thus improve overall performance.

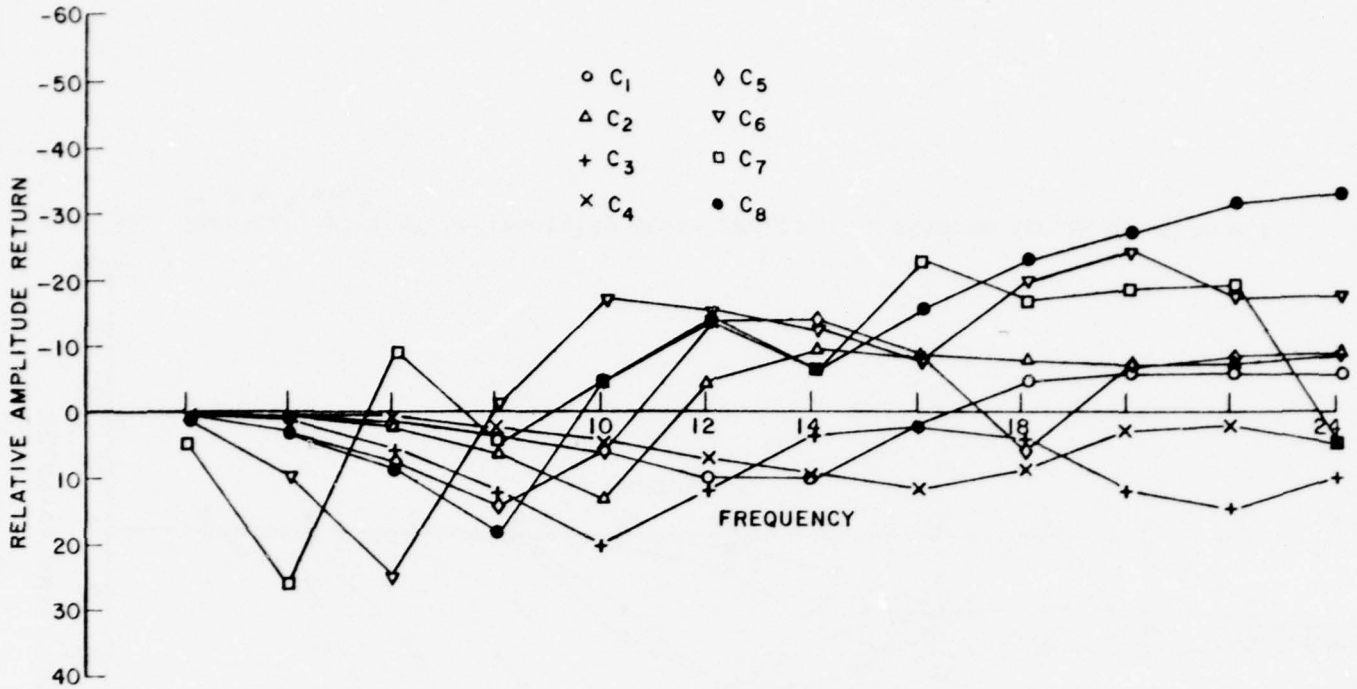

Figure 33. Real part of horizontally polarized returns for eight aircraft at $\theta=90°$, $\phi=0°$. (bottom view).

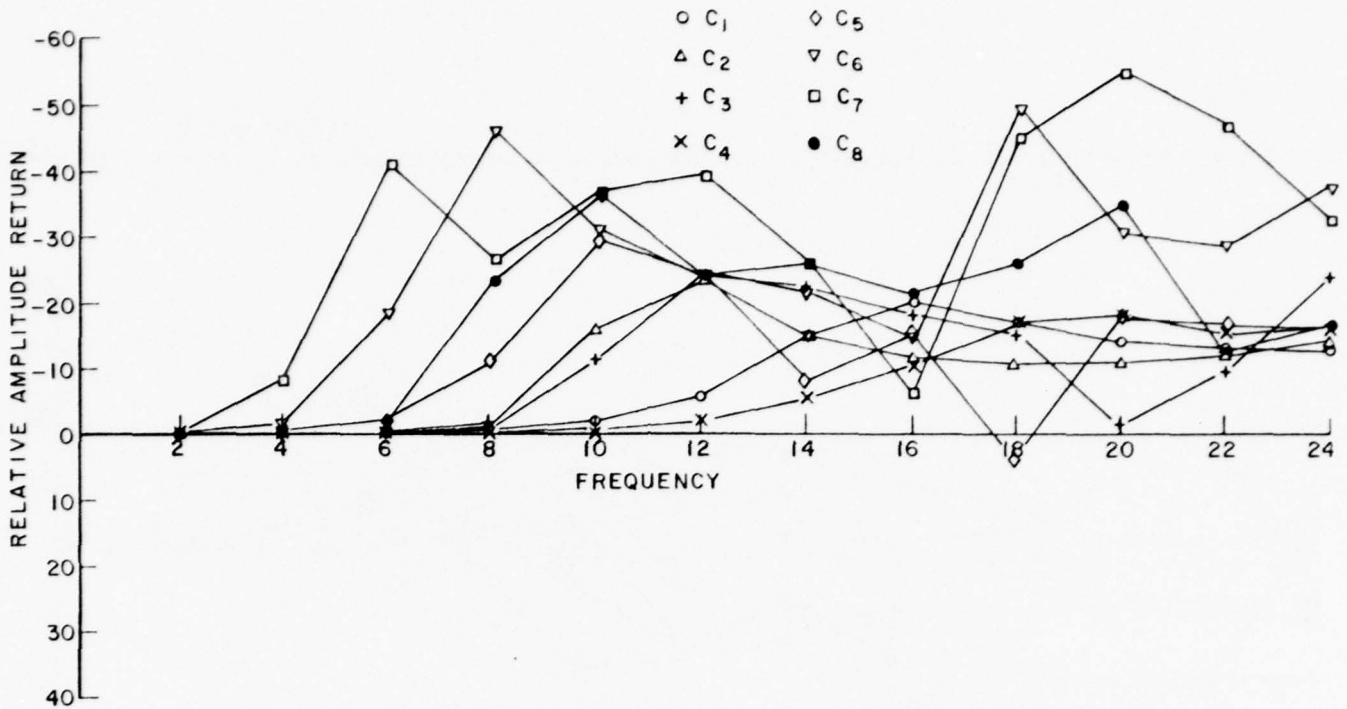

Figure 34. Imaginary part of horizontally polarized complex returns for eight aircraft at $\theta=90°, \phi=0°$.

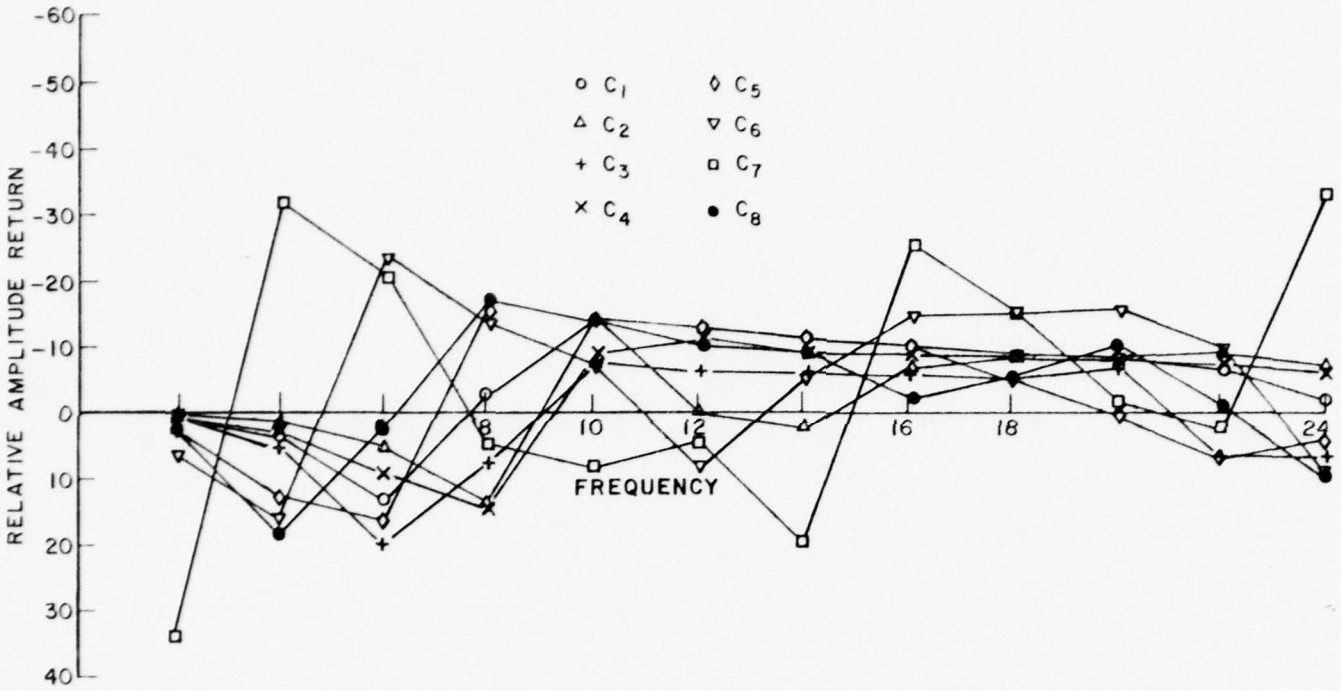

Figure 35. Real part of vertically polarized complex returns for eight aircraft at $\theta=90°$, $\phi=0°$.

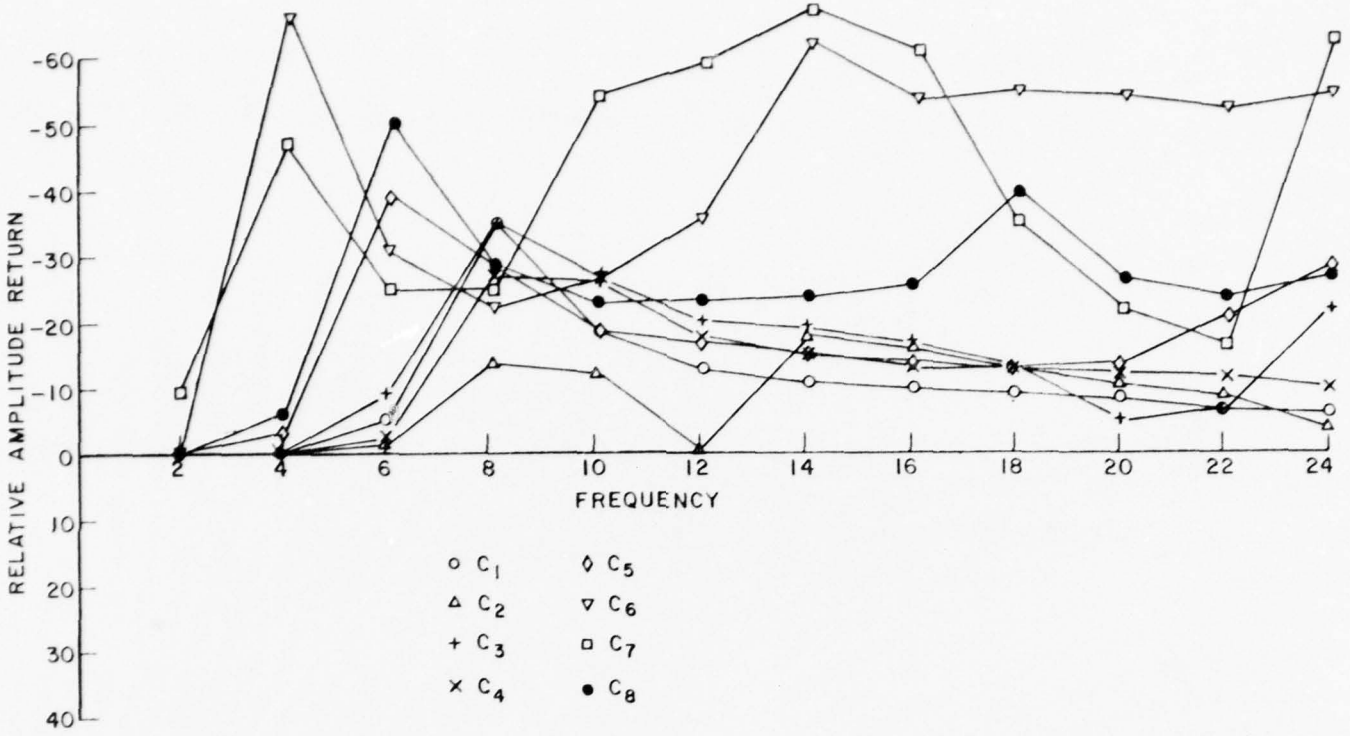

Figure 36. Imaginary part of vertically polarized complex returns for eight aircraft at $\theta=90°, \phi=0°$.

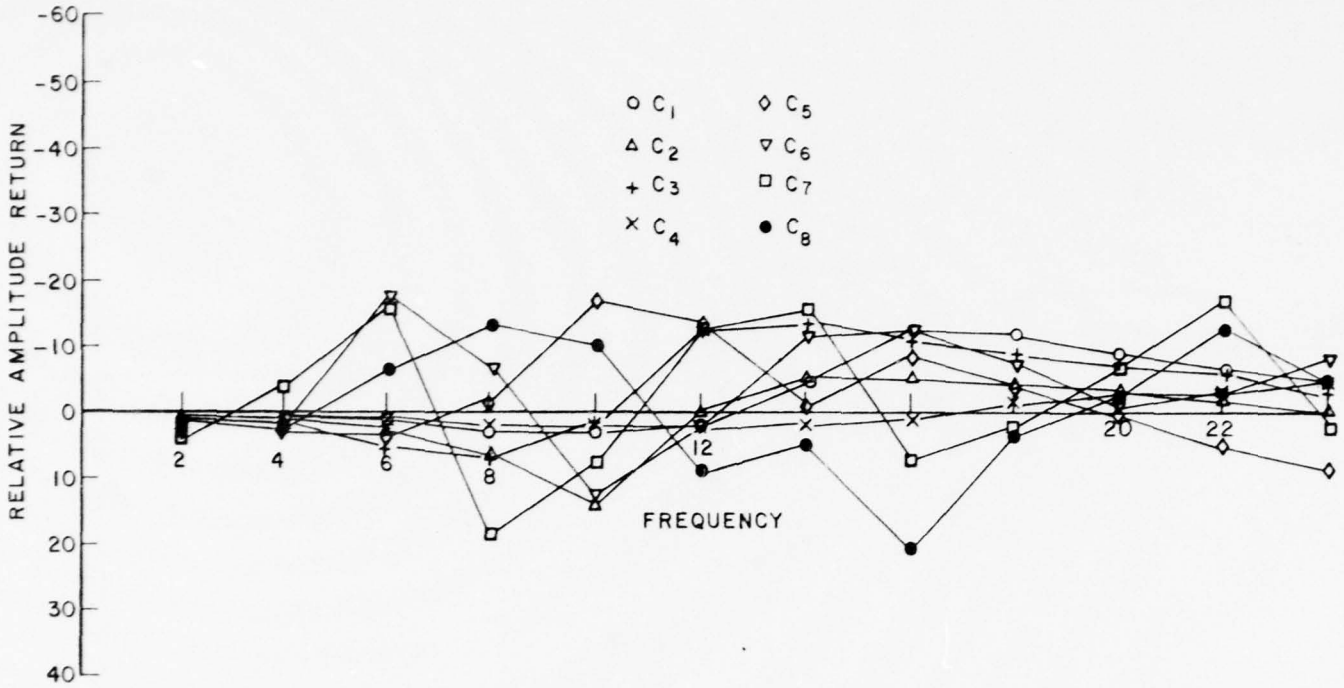

Figure 37. Real part of horizontally polarized complex returns for eight aircraft at $\theta=0°$, $\phi=0°$.

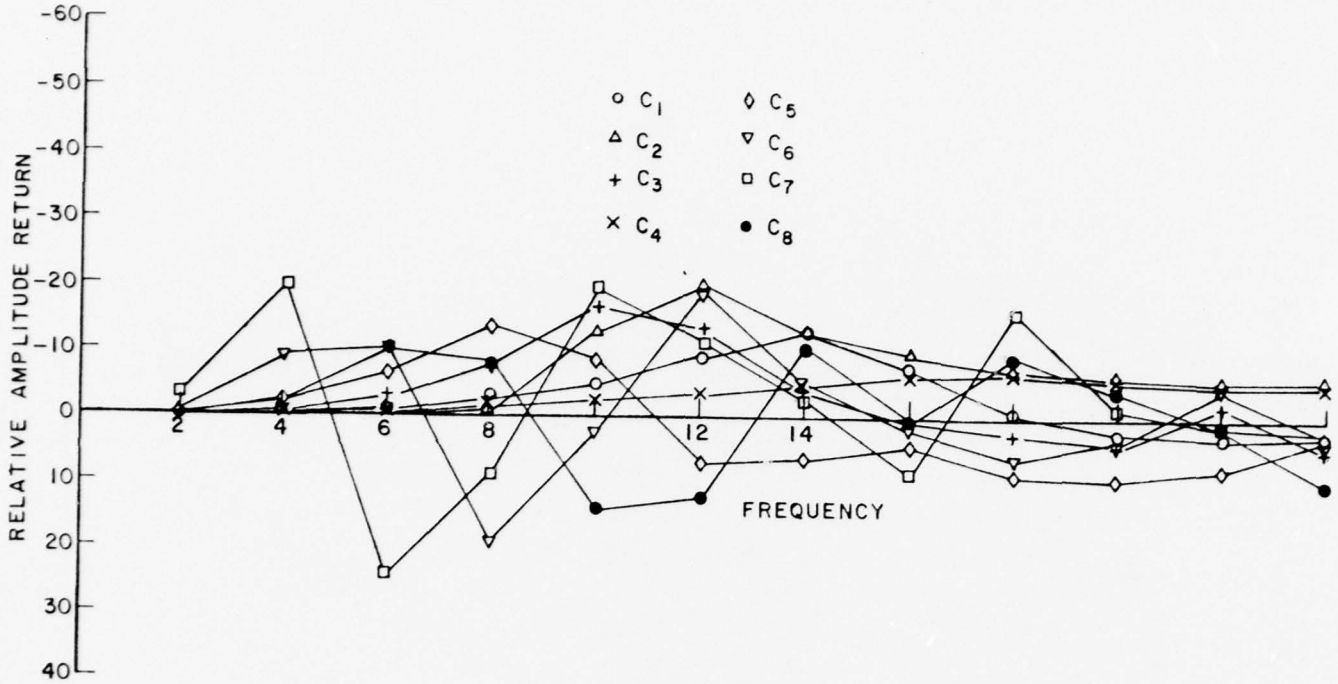

Figure 38. Imaginery part of horizontally polarized wave returns for eight aircraft at $\theta=0°$, $\phi=0°$.

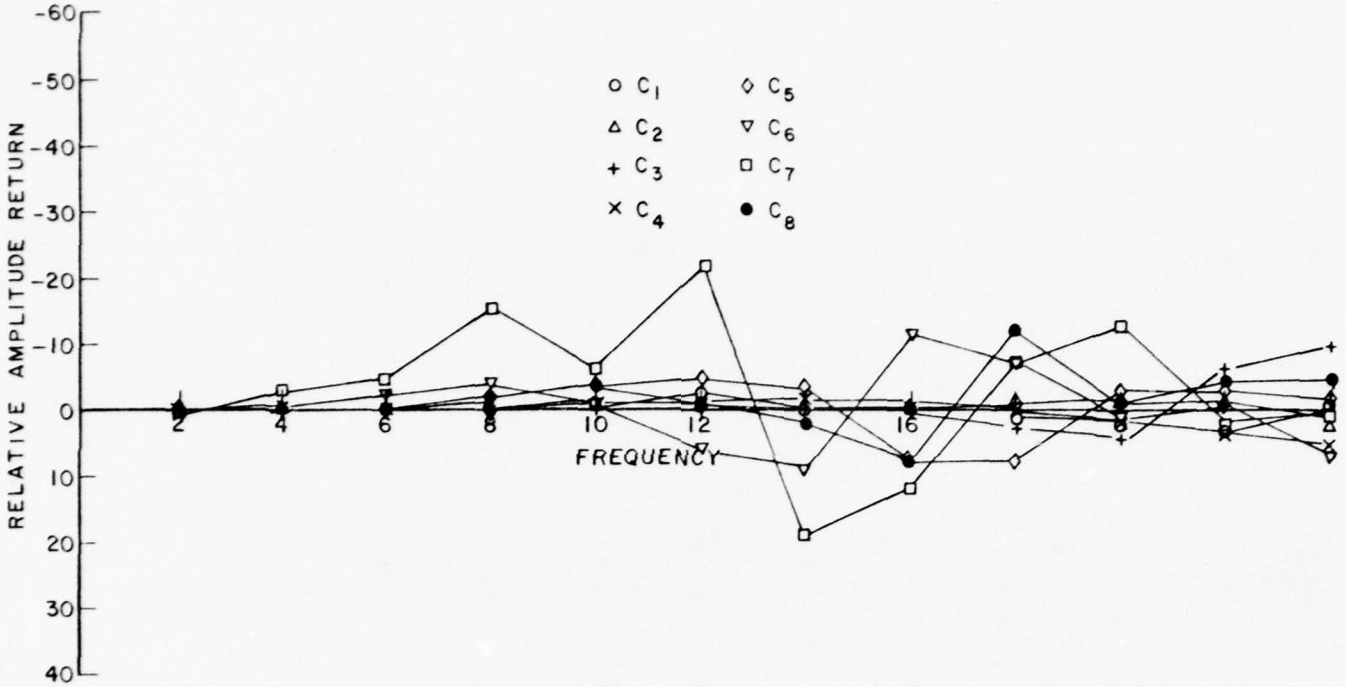

Figure 39. Real part of complex vertically polarized wave returns for eight aircraft at $\theta=0°$, $\phi=0°$.

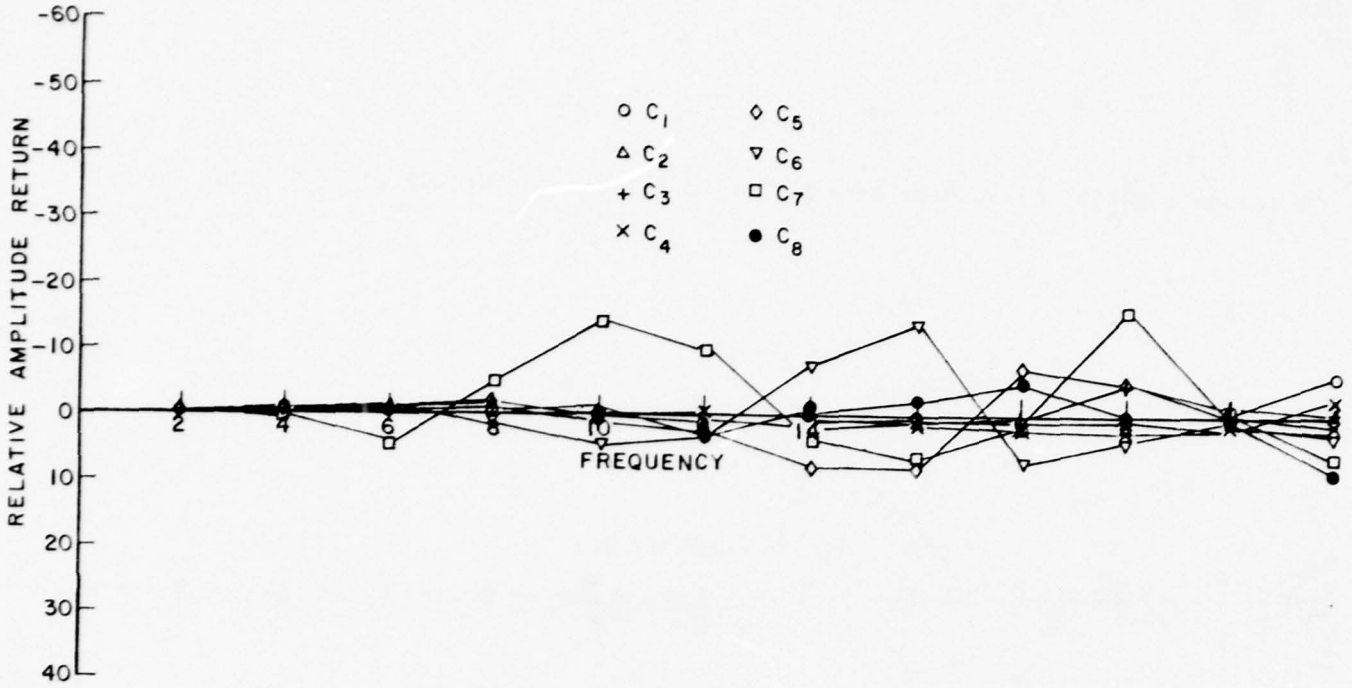

Figure 40. Imaginery part of horizontally polarized complex returns for eight aircraft at θ=0°, φ=0°.

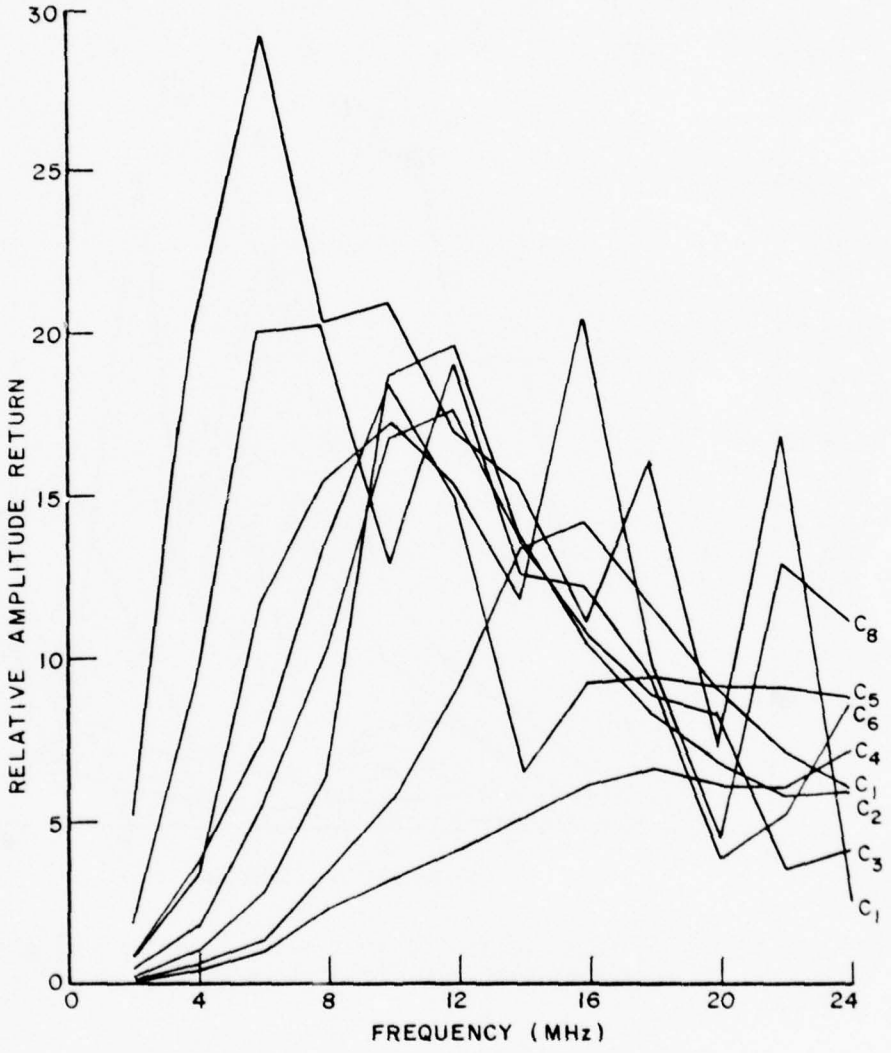

Figure 41. Amplitude returns of horizontally polarized wave for eight aircraft at $\theta=0°$, $\phi=0°$.

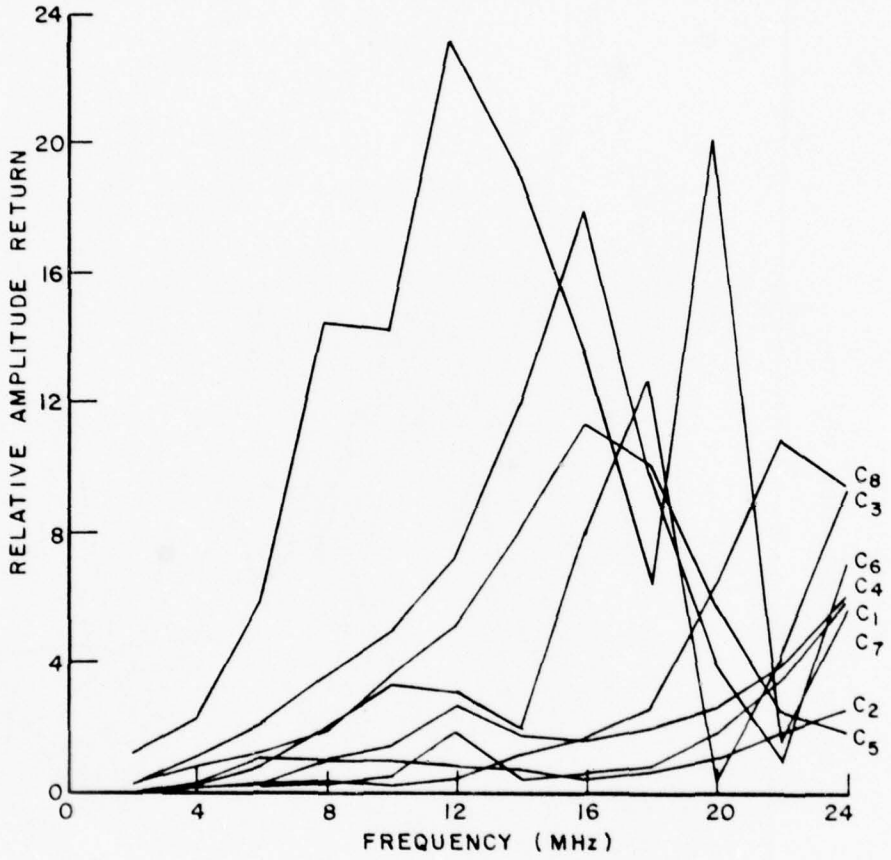

Figure 42. Amplitude returns of vertically polarized electromagnetic scattering response for eight aircraft at $\theta=0°$, $\phi=0°$.

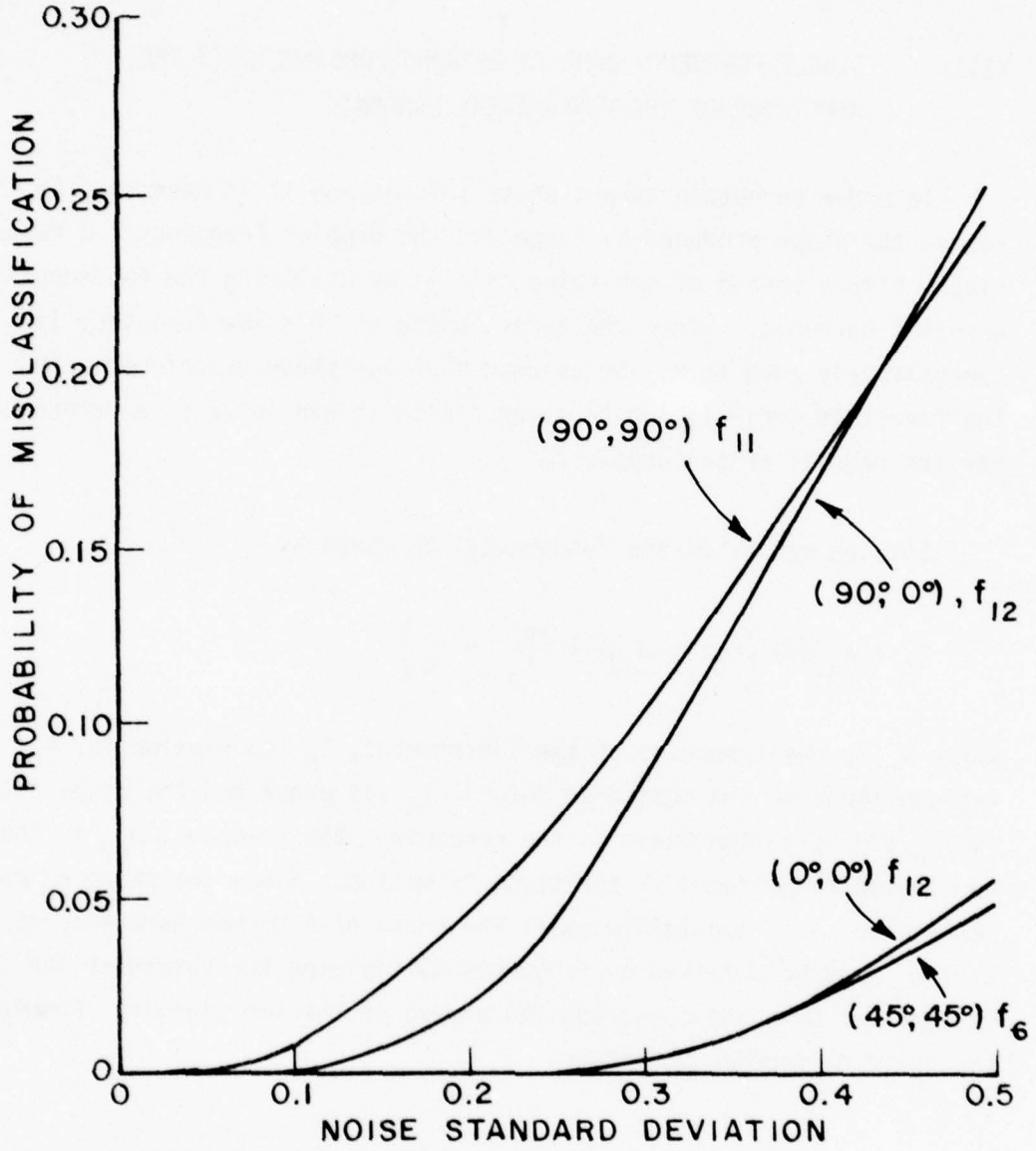

Figure 43. Performance comparison for different aspect angles employing optimum single frequency complex returns.

VIII. SINGLE FREQUENCY COMPLEX RETURNS COMBINED WITH THE AMPLITUDE OF THE FUNDAMENTAL HARMONIC

In order to obtain target phase information it is necessary to remove the phase produced by range and the doppler frequency. A relatively simple method of achieving this is by utilizing the fundamental, or first harmonic. Since the target phase at this low frequency is approximately zero it may be assumed that the phase associated with the target is strictly due to range. Also it can serve as a reference for the removal of the doppler.

Let the return of the fundamental be given by

$$R_o = A_o \cos\left(\omega_o t + \omega_{od} t + \frac{2\pi r}{\lambda_o} + \phi_o\right)$$

where ω_o is the frequency of the fundamental, λ_o its wavelength, A_o the amplitude of the scattered return, ϕ_o its phase and the range delay $2\pi r/\lambda_o$ adding to the phase at the receiver. The frequency ω_{od} is the Doppler shift produced by the target's motion. Since the phase ϕ_o may be assumed to be negligibly small the phase of a higher harmonic, at say $n\omega_o$, may be obtained by frequency multiplying the return of the fundamental by n and comparing the phases of the two signals. Forming the phase difference we obtain

$$\Delta\phi = n\omega_o t + n\omega_{od} t + \frac{2\pi r}{(\lambda_o/n)} + \phi_n - n\omega_o t - n\omega_{od} t$$

$$- \frac{2n\pi r}{\lambda_o} - n\phi_o = \phi_n - n\phi_o \simeq \phi_n.$$

Thus the range effect on phase as well as the Doppler are removed, yielding the phase of the scattered object at the nth harmonic. If this

approach is indeed utilized, one must assume the availability of the first harmonic and it is apparent that it would be advantageous to utilize this additional feature in the classification process. Including the added feature yields the performance shown in Figures 44-55 which indicate somewhat lower error rates than shown in Figures 18-30 that did not use the lowest harmonic. The improvement varies with observation angles and frequencies, in some cases reducing error probabilities by a factor of two and in others just slightly.

A set of curves in Figures 56-59 summarizes the improvements afforded by the successive addition of the features discussed above. The curves show the error probabilities resulting from the use of each of the twelve frequencies f_1 through f_{12}. The comparison is made between the use of A) amplitude alone, B) amplitude and phase, and C) amplitude and phase of each frequency f_2 through f_{12} in conjunction with the first harmonic amplitude.

Comparing the complex (amplitude and phase) to amplitude alone, a very large drop in error probabilities is evident at all but the lowest harmonics where the phase contribution is rather small. Note that the improvement is smallest in the $\theta=90^0$, $\phi=0^0$ case which is the bottom view. The reason for this is the relatively small phase contribution until frequencies reach fairly high levels. As mentioned above the physical distance between the phase center and the geometrical center from this observation angle is very small and consequently the target phase is quite small and increases slowly with rising frequencies. It is in this case where the fundamental harmonic provides a substantial improvement. The same can be seen at all angles for low frequencies where phase is of little help. Curve C reflects substantially reduced error probabilities. As the frequency increases the fundamental provides some improvement but it is not very significant.

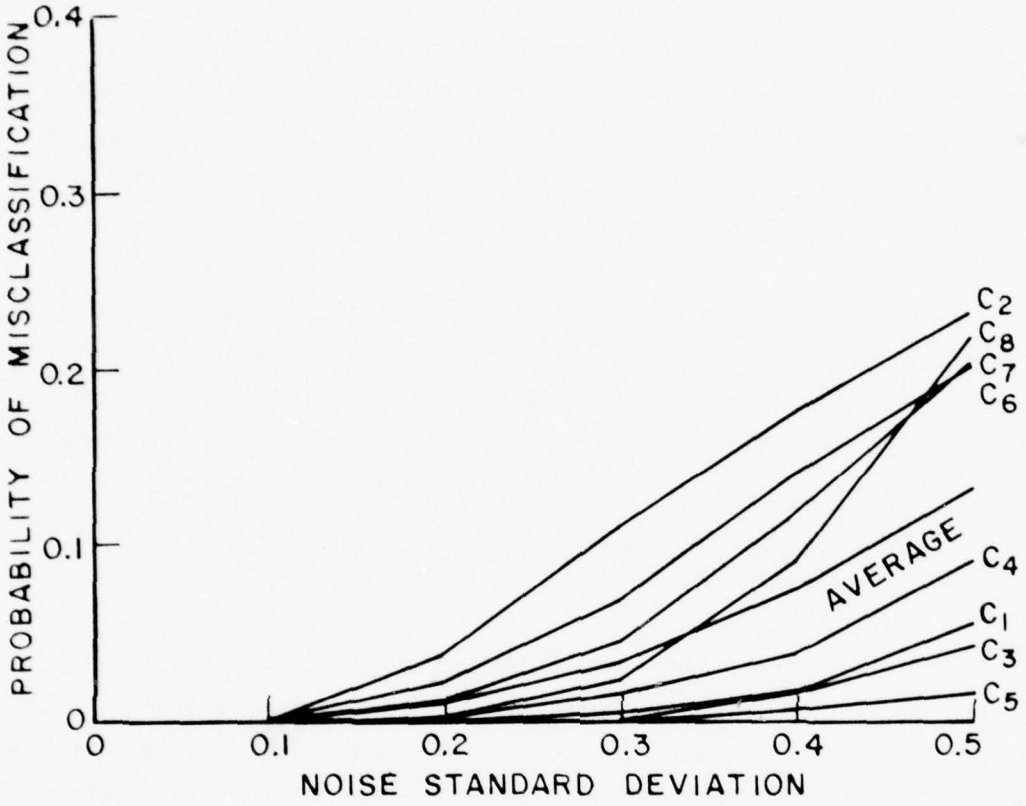

Figure 44. Probability of misclassification for individual aircraft, using complex returns at frequency f_{11} and $(0^0,0^0)$ aspect angle (nose on).

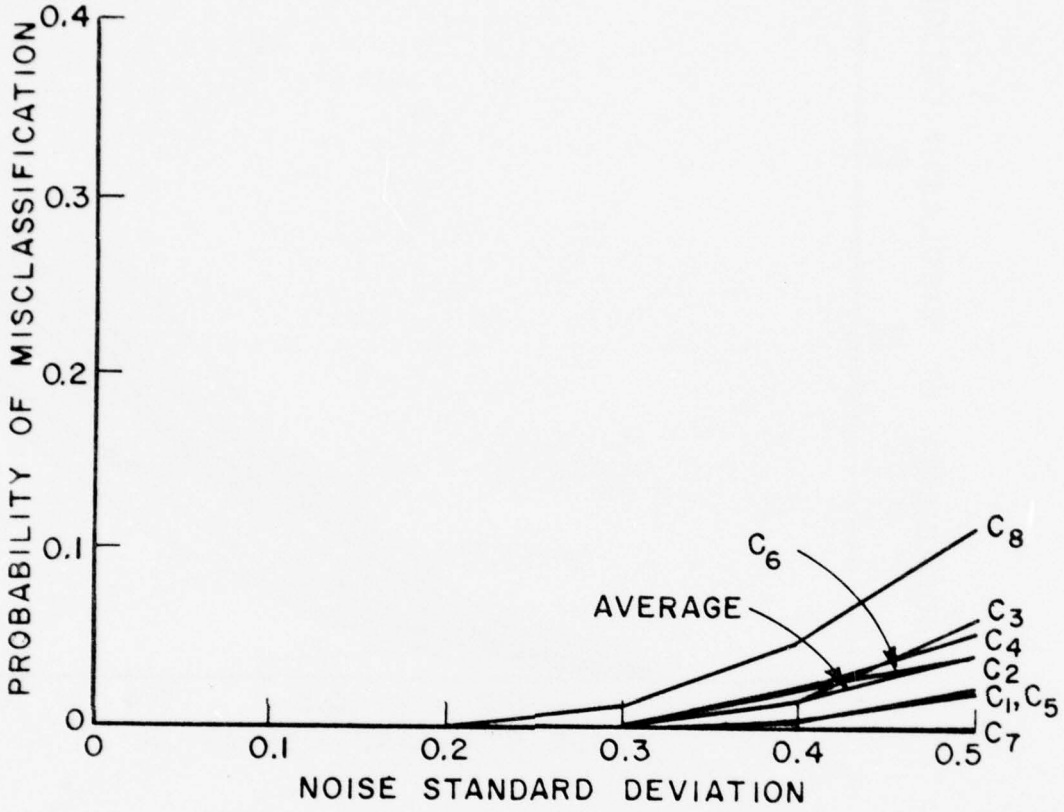

Figure 45. Probability of misclassification for individual aircraft, using complex returns at frequency f_{12} with the fundamental harmonic at $(0^{o},0^{o})$ aspect angle (nose on).

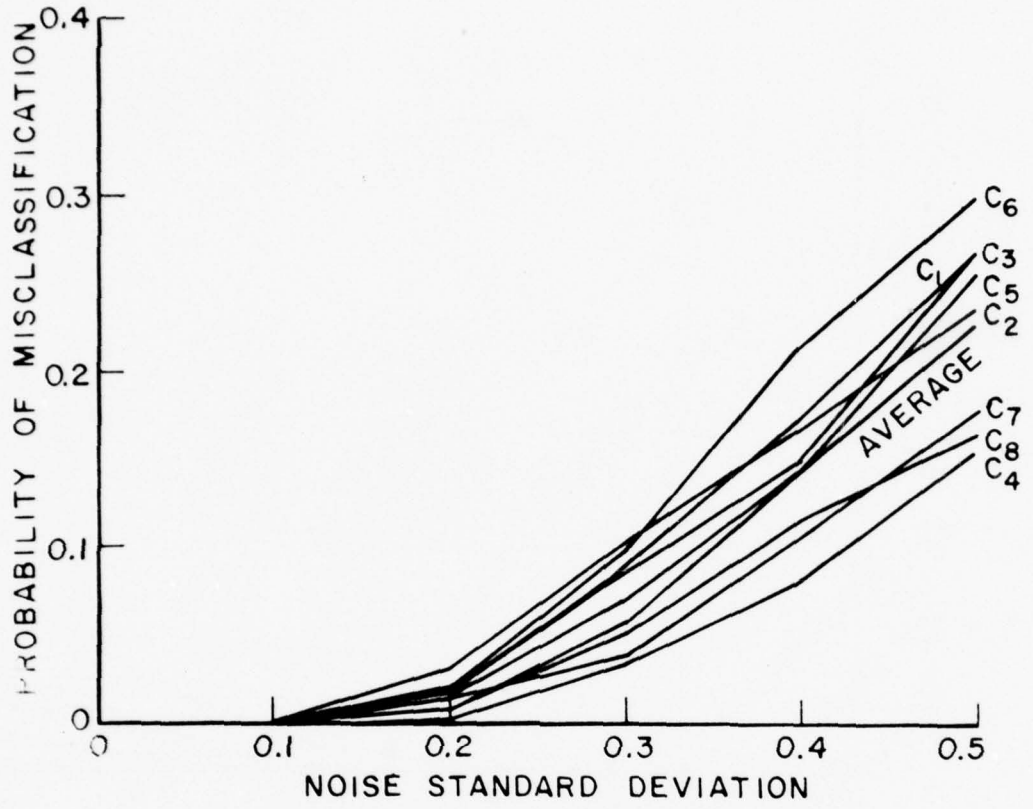

Figure 46. Probability of misclassification for individual aircraft, using complex returns at frequency f_{12} with the fundamental harmonic at $(90^0,0^0)$ aspect angle (bottom view).

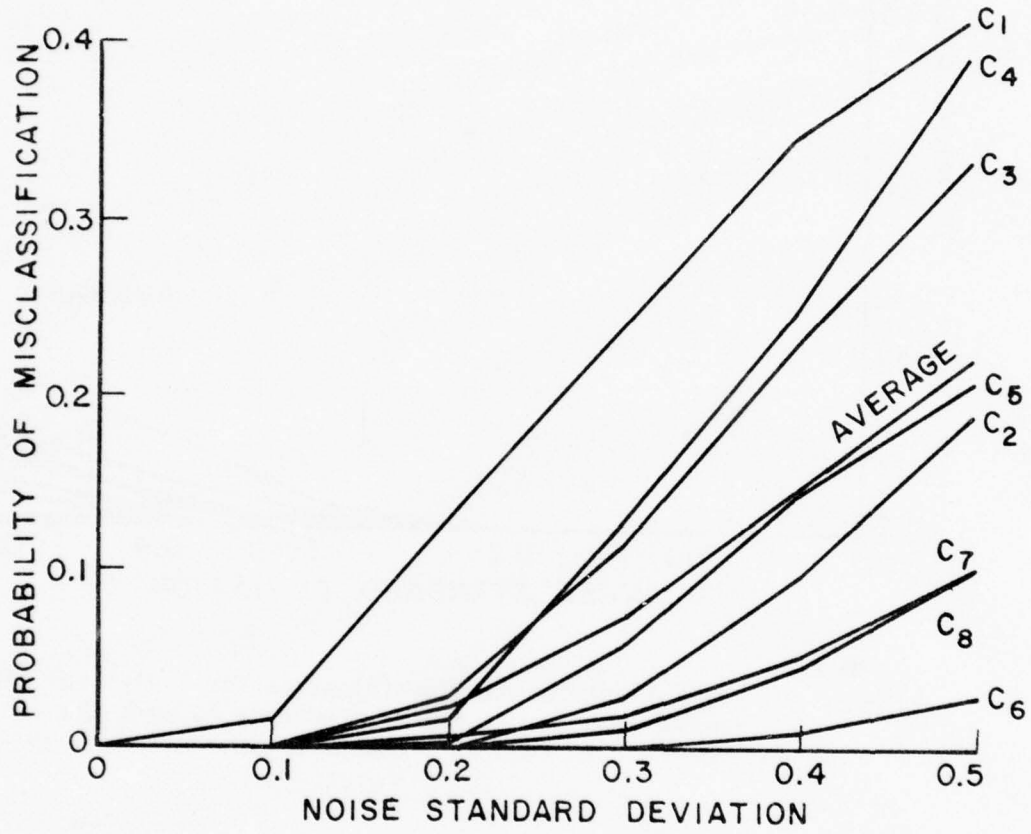

Figure 47. Probability of misclassification for individual aircraft, using complex returns at frequency f_{12} with the fundamental harmonic at $(90^0, 90^0)$ aspect angle (side view).

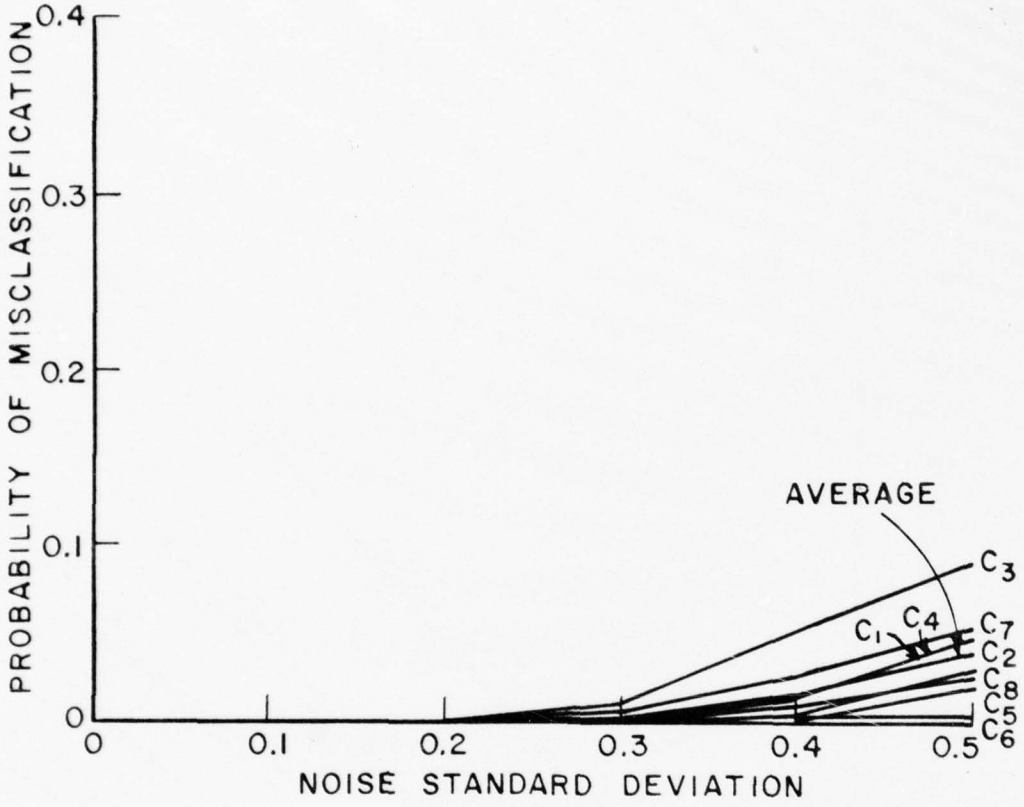

Figure 48. Probability of misclassification for individual aircraft, using complex returns at frequency f_6 with the fundamental harmonic at $(45^{o},45^{o})$ aspect angle.

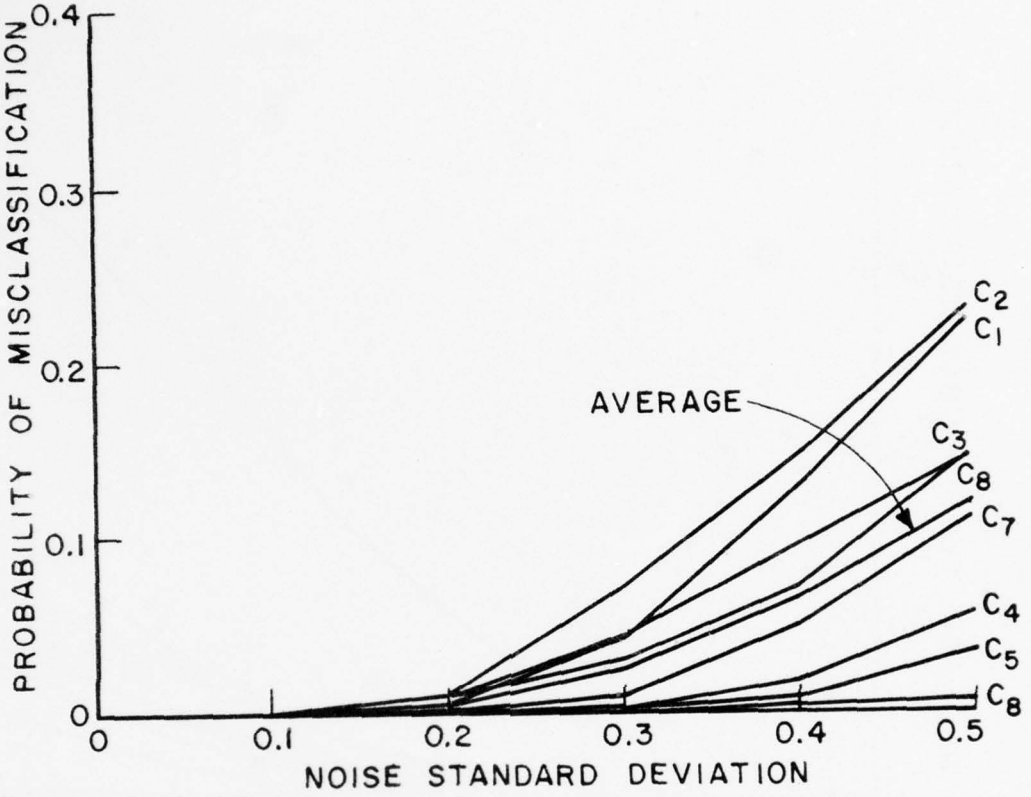

Figure 49. Probability of misclassification for individual aircraft, using complex returns at frequency f_8 with the fundamental harmonic at $(45^0,45^0)$ aspect angle.

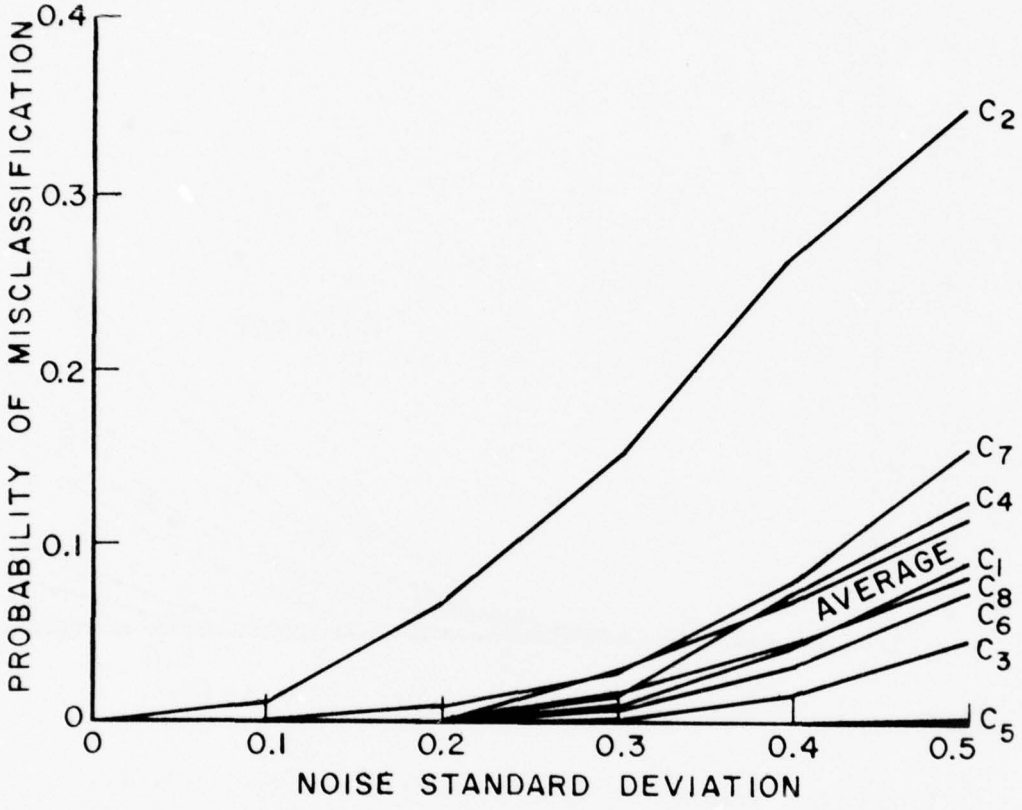

Figure 50. Probability of misclassification for individual aircraft, using complex returns at frequency f_{11} with the fundamental harmonic at $(45^0,45^0)$ aspect angle.

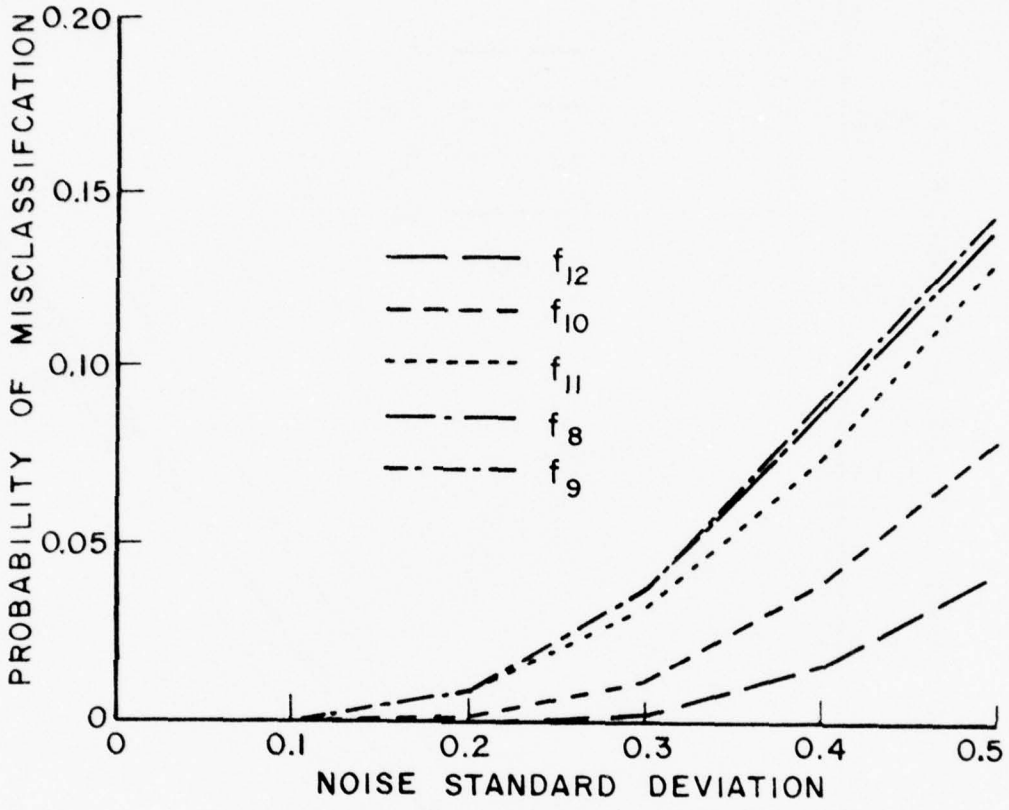

Figure 51. The average performance at different frequencies, using single frequency complex returns and the fundamental harmonic. The observation angle is $\theta=0°$, $\phi=0°$.

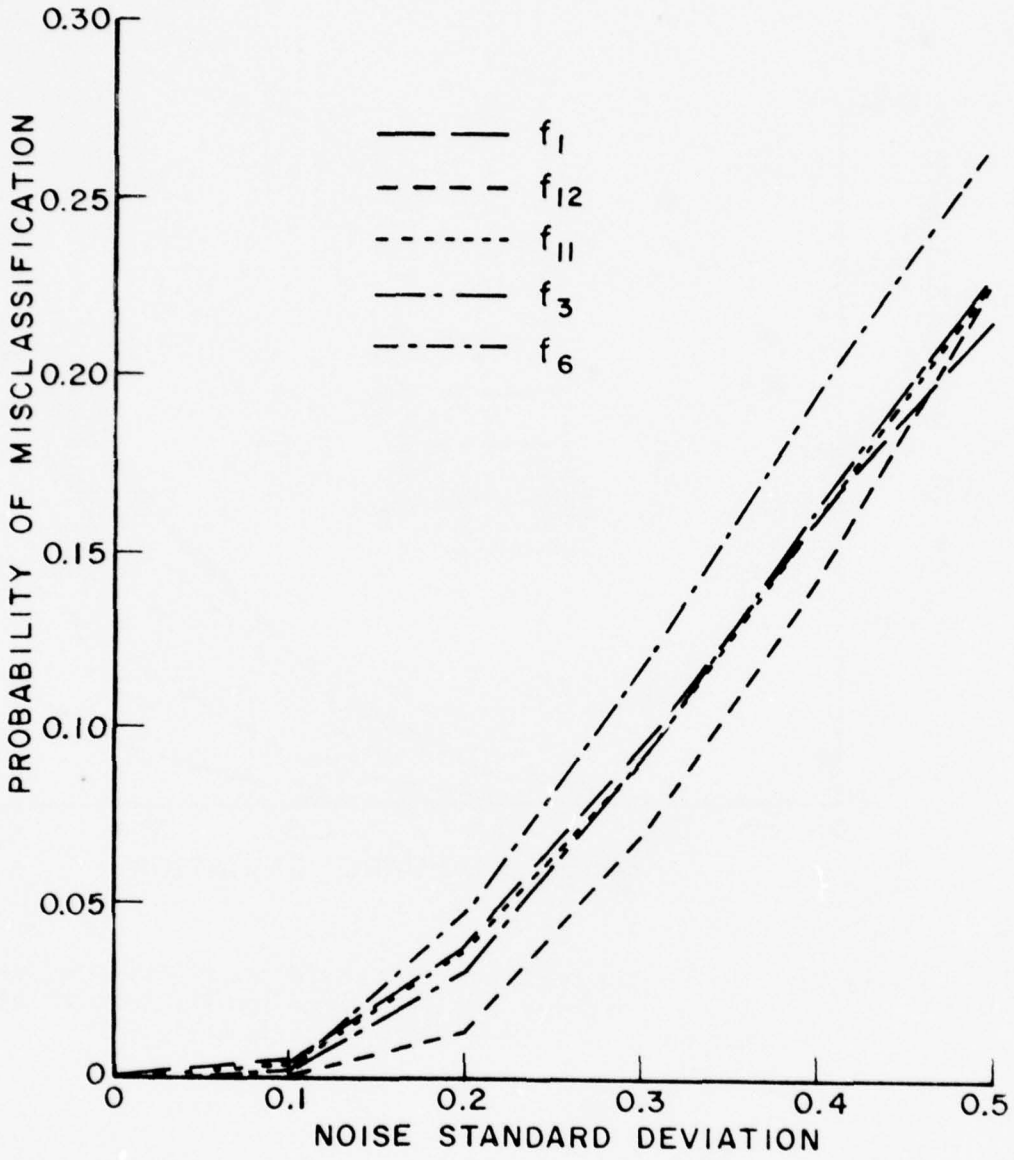

Figure 52. The average performance at different frequencies, using single frequency complex returns and the fundamental harmonic. The observation angle is $\theta=90°$, $\phi=0°$.

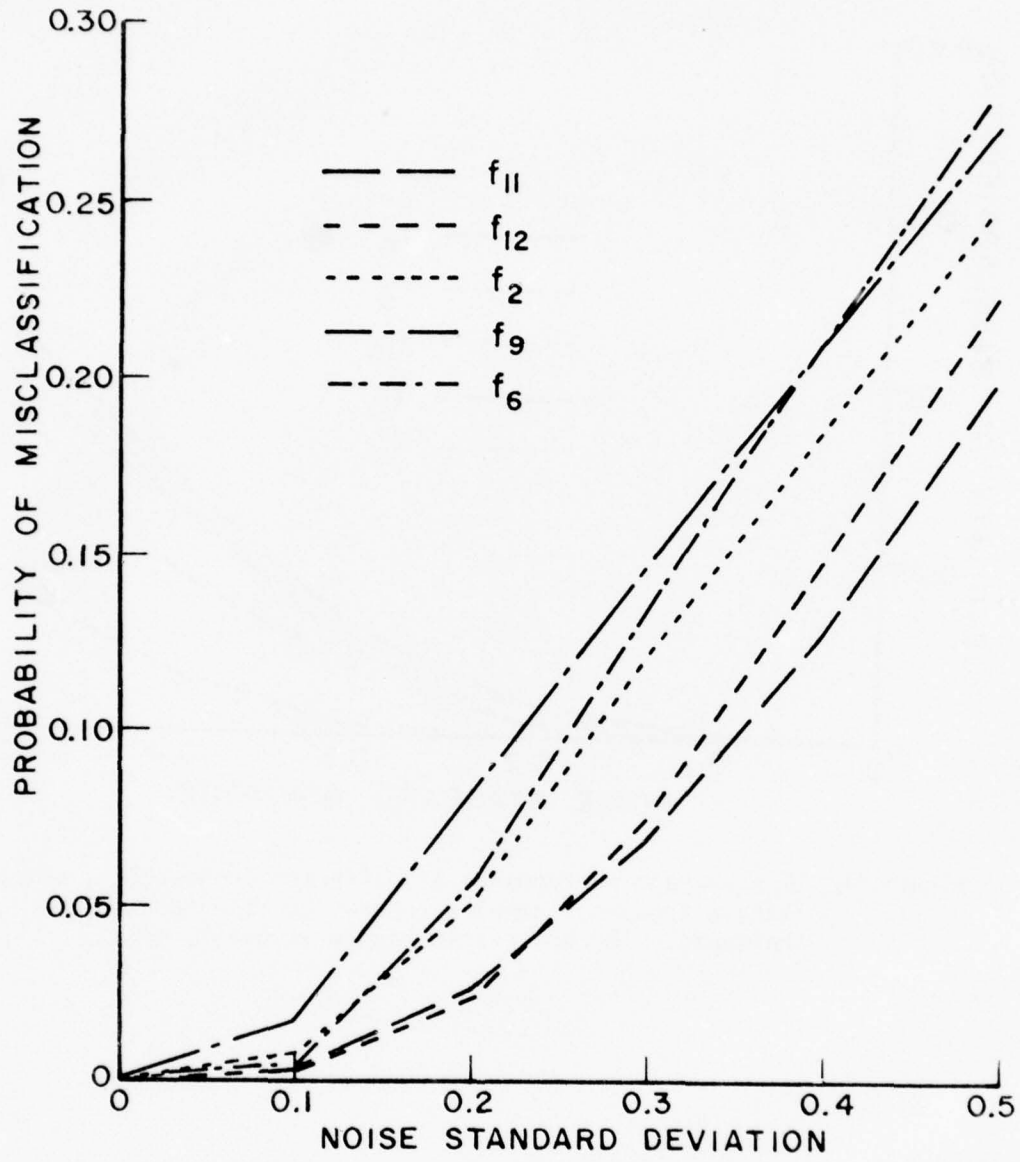

Figure 53. The average performance at different frequencies, using single frequency complex returns and the fundamental harmonic. The observation angle is $\theta=90°$, $\phi=90°$.

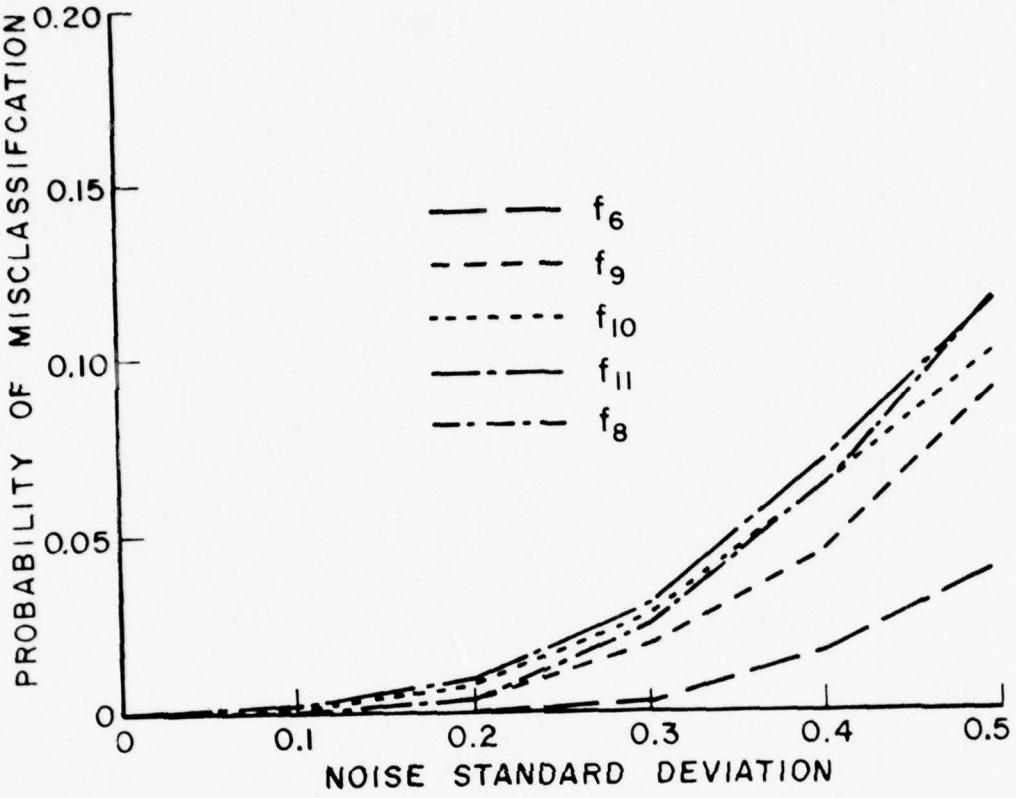

Figure 54. The average performance at different frequencies, using single frequency complex returns and the fundamental harmonic. The observation angle is $\theta=45°$, $\phi=45°$.

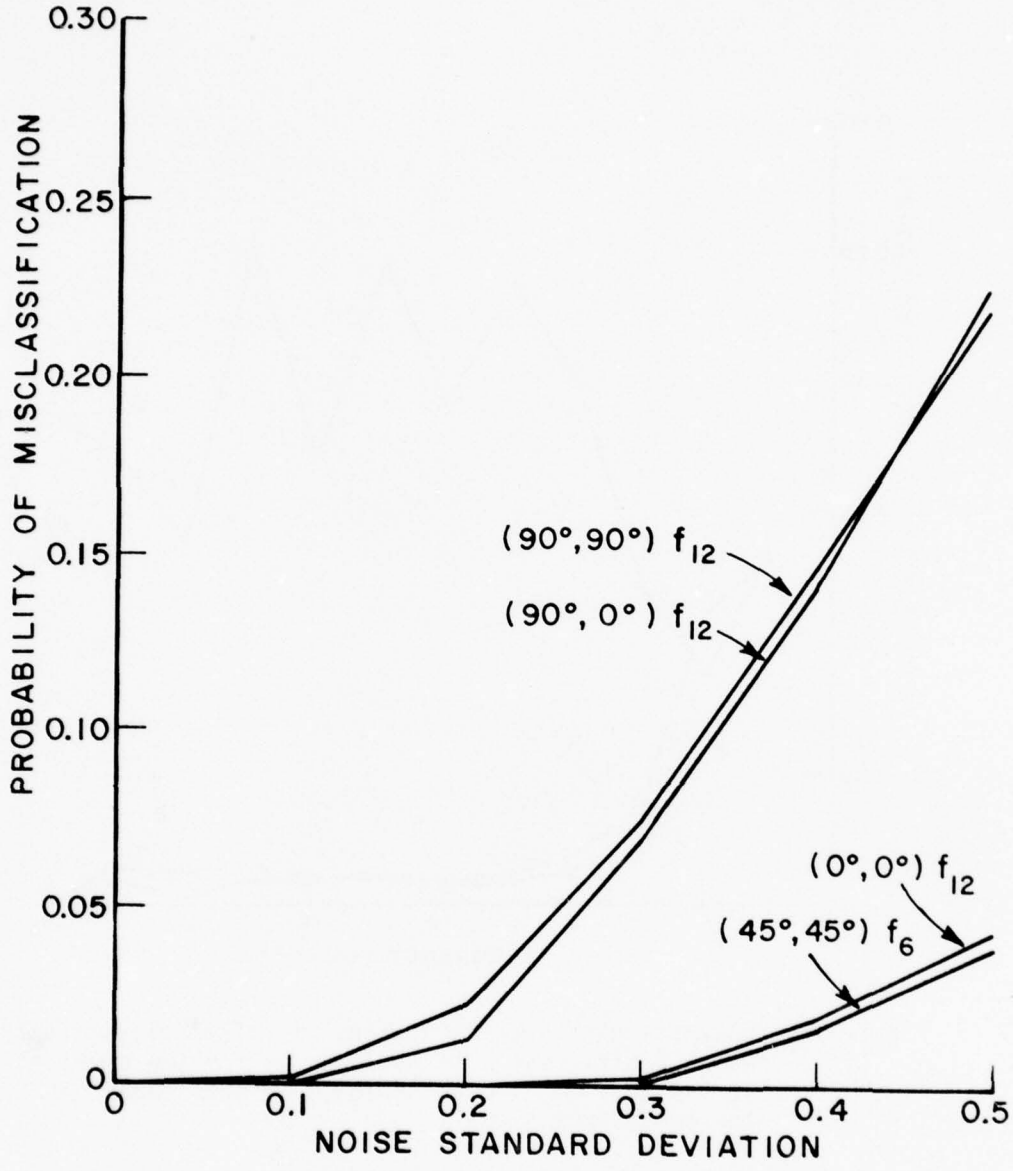

Figure 55. Performance comparison for different aspect angles employing optimum single frequency and the fundamental harmonic returns.

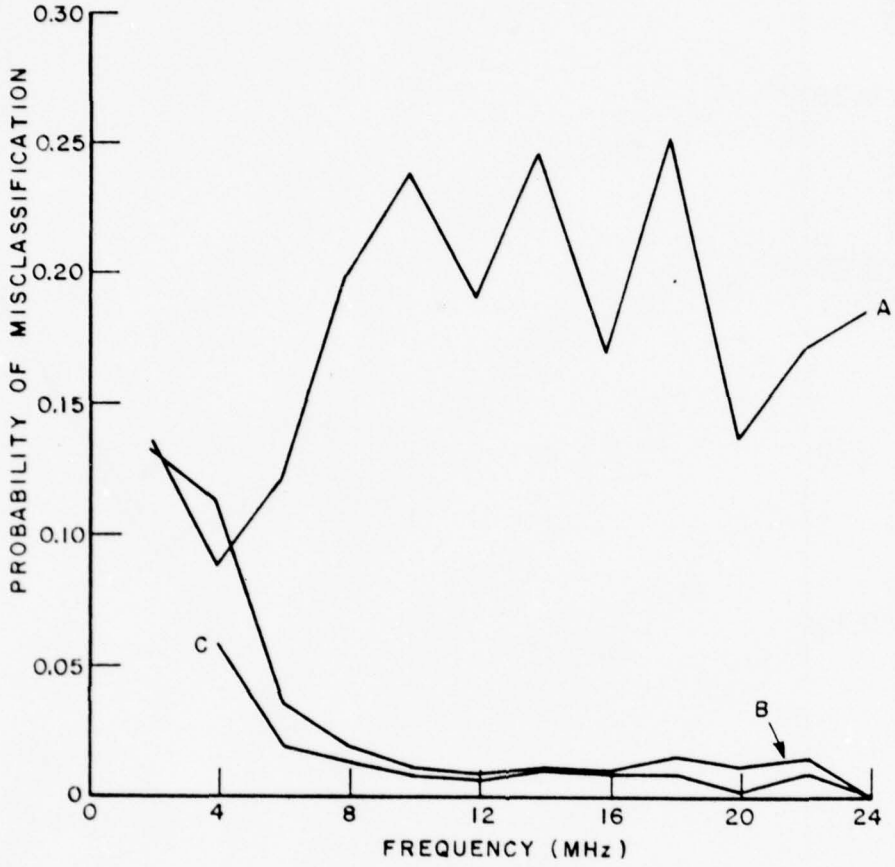

Figure 56. Comparison of average probability of misclassification, using 3 different sets of features for the eight aircraft at $\theta=0°$, $\phi=0°$. The noise added to each signal is 20% of the noise free signal.

A= single frequency amplitude returns

B= single frequency complex returns.

C= single frequency complex returns with the fundamental harmonic.

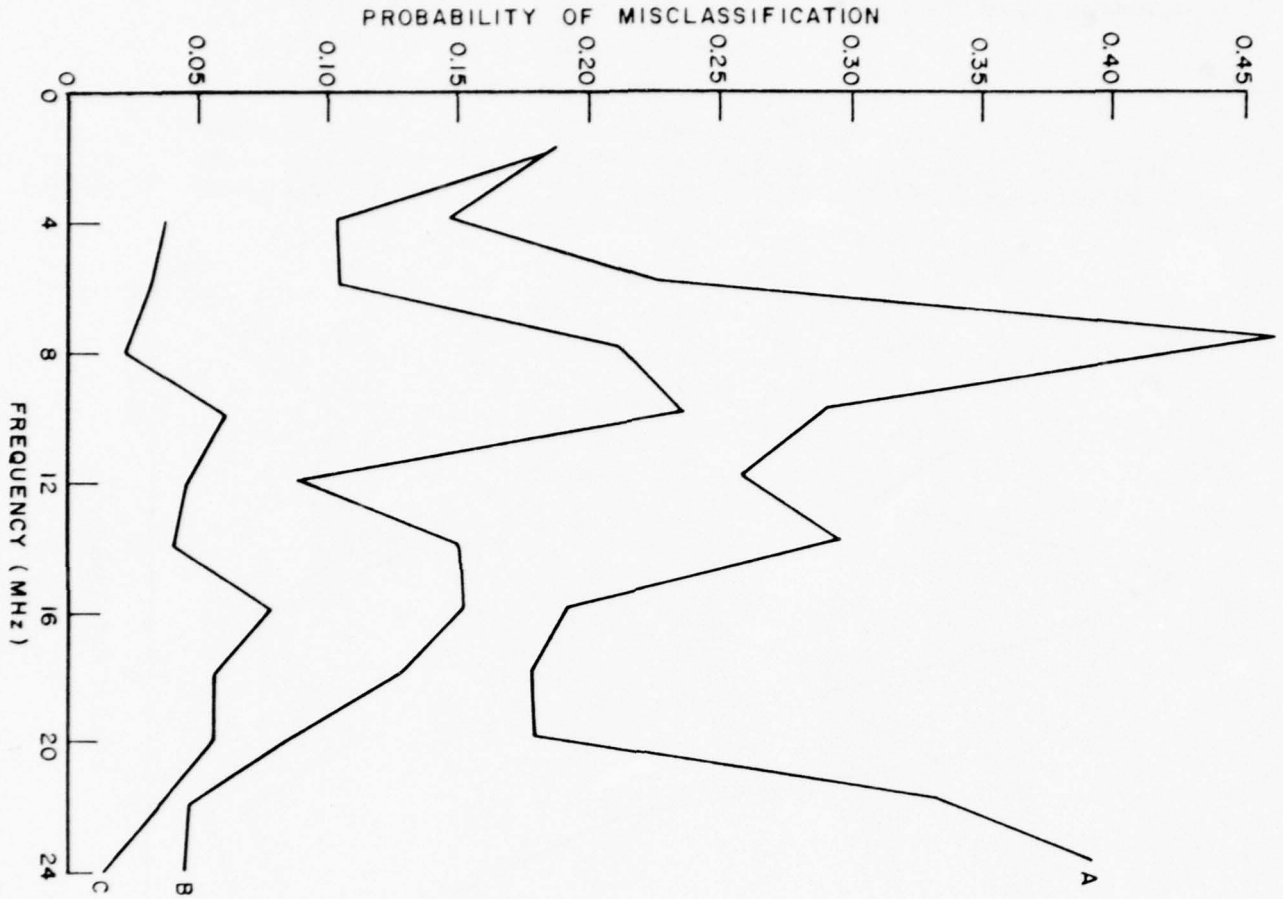

Figure 57. Comparison of probability of misclassification, using 3 different sets of features for the eight aircraft at $\theta=90°$, $\phi=0°$. The noise added to each signal is 20% of the noise free signal.

A=single frequency amplitude returns.

B=single frequency complex returns.

C=single frequency complex returns with the fundamental harmonic.

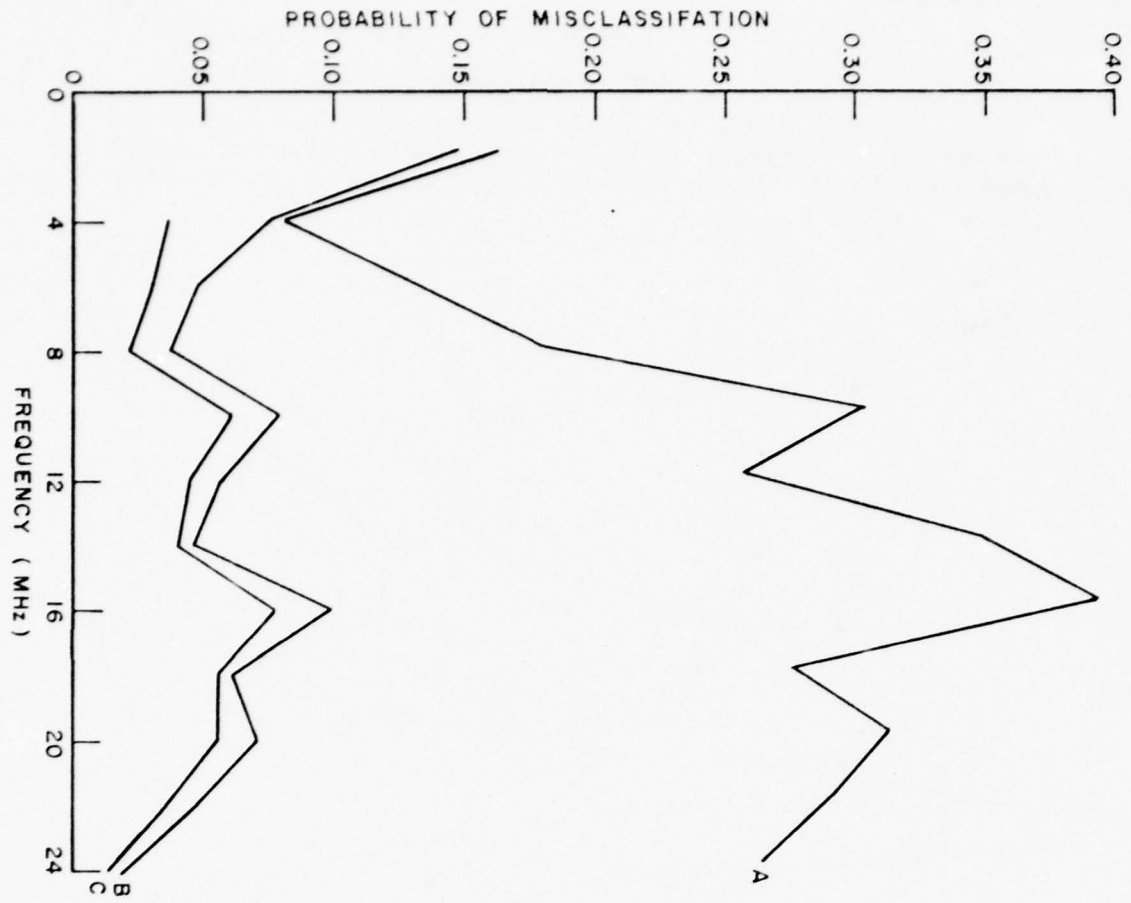

Figure 58. Comparison of probability of misclassification, using 3 different sets of features for the eight aircraft at $\theta=90°$, $\phi=90°$. The noise added to each signal is 20% of the noise free signal.

A=single frequency amplitude returns.

B=single frequency complex returns.

C=single frequency complex returns with the fundamental harmonic.

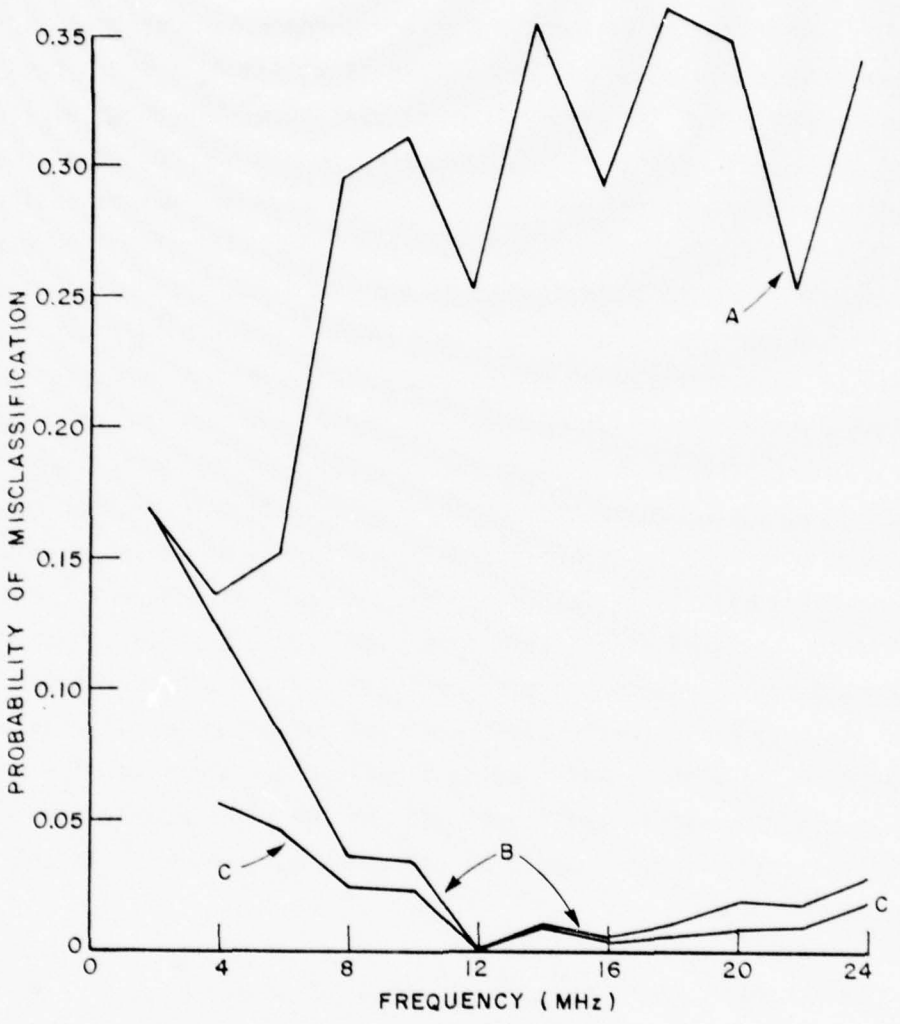

Figure 59. Comparison of probability of misclassification, using 3 different sets of features for the eight aircraft at θ=45°, ϕ=45°. The noise added to each signal is 20% of the noise free signal.

A=single frequency amplitude returns.

B=single frequency complex returns.

C=single frequency complex returns with the fundamental harmonic.

The use of the first harmonic as a reference is advantageous if the higher harmonic whose complex return is utilized is not a high multiple of the fundamental. For under these circumstances the phase $n\phi_o$ is indeed small. If, however n is large then $n\phi_o$ is not negligible and introduces a phase offset which prevents the accurate determination of ϕ_n the target phase at the nth harmonic. For classification purposes, however, the absolute target phase is not required, the relative phase $(\phi_n - n\phi_o)$ can serve as a modified phase feature which will yield in turn a modified complex return. If the phase at the lowest harmonic is not negligible there may be an advantage in using a higher harmonic than the fundamental for phase reference. The main advantage in using a higher frequency would be the resulting improvement in angular resolution, but additionally if n is large any error in measuring ϕ_o would get magnified by a large factor n. Thus picking an adjacent frequency say $(n-1)\omega_o$ would eliminate this effect and would provide a much more convenient implementation as a radar system. It would therefore be of interest to evaluate the classification performance utilizing various frequency pairs with one of them as a reference. Note that the measured net phase of the kth target illuminated by the nth harmonic with the mth harmonic as reference would be $(\phi_n^k - n/m\ \phi_m^k)$, where ϕ_n^k is the target's phase at frequency $n\omega_o$.

IX. CLASSIFICATION PERFORMANCE UTILIZING TWO FREQUENCIES

In previous discussions we have limited the number of frequencies used to one, except for the auxiliary amplitude of the fundamental. At present we introduce the simultaneous use of two frequencies picked from the set f_1=2 MHz through f_{12}=24 MHz. We will again consider first the use of amplitude alone, followed by the utilization of both phase and amplitude, that is two orthogonal components for each frequency, and in each case two orthogonal polarizations are employed. We have, therefore, a four feature vector for the amplitude case and an eight feature vector for the complex, or amplitude and phase, case.

The effort involved in choosing the optimum two frequencies is substantially greater than twice the effort of choosing one frequency because the two jointly optimum frequencies are not the best and second best single frequencies. This is true even in the case when all features are mutually independent and even more so when they are correlated as in the present case.[7,8] We were thus faced with a study involving all possible combinations of frequency pairs. Since no analytical method for optimum choices is available one must resort to an exhaustive search.[8] The classification results utilizing two frequency amplitude returns are shown in Figures 60-69. Figures 60-64 show the performance for each aircraft at the optimum frequency and the four chosen aspects. The performance is considerably better than in using only a single frequency amplitude return but worse than in using a single frequency complex return although the same number of features are used. The better performance of the single frequency may be due to the fact that in using two frequency amplitude returns, the returns are always positive, while in using one frequency complex returns, each component can be either positive or negative, increasing the range of the variable in feature space and consequently providing a better performance. This indicates that the phase information may be more effective than amplitude information in considering the use of additional features. Figure 63 shows that the amplitude features yield a peculiar response for some individual aircraft (C_4 here) as mentioned before, whereas in using one frequency complex returns this kind of odd response is essentially eliminated. Figures 65-69 show the average performance of the best five frequencies at the four chosen angles. As may be expected of amplitude returns, they are fairly orientation invariant.

The probability of misclassification for each individual aircraft using two frequency complex returns are shown in Figures 70-89. The performance curves for each aircraft for the best five frequencies at each of the four aspect angles are all listed here because they all did fairly well in terms of the overall average probability of error.

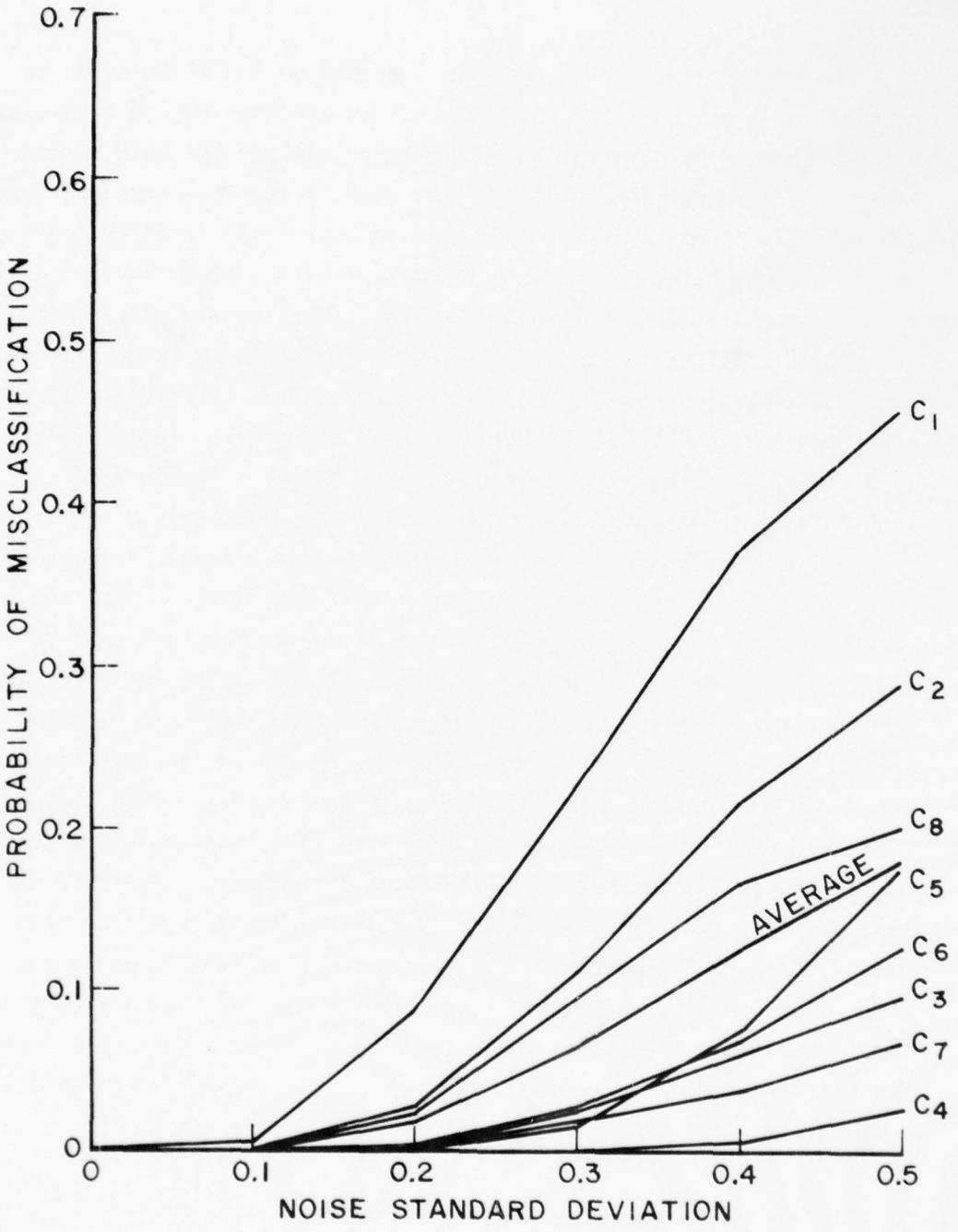

Figure 60. Probability of misclassification for individual aircratt, using amplitude returns of f_7, f_{11} at (0°,0°) aspect angle (nose on).

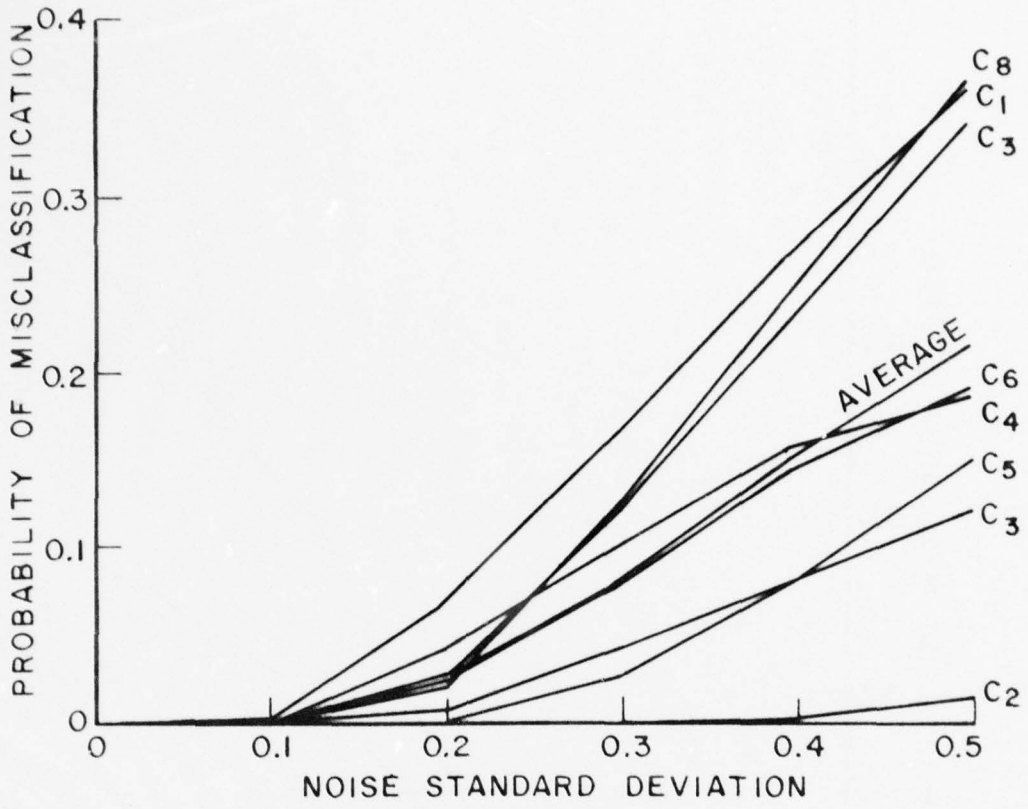

Figure 61. Probability of misclassification for individual aircraft, using amplitude returns of f_{11}, f_9 at (90°,0°) aspect angle (bottom view).

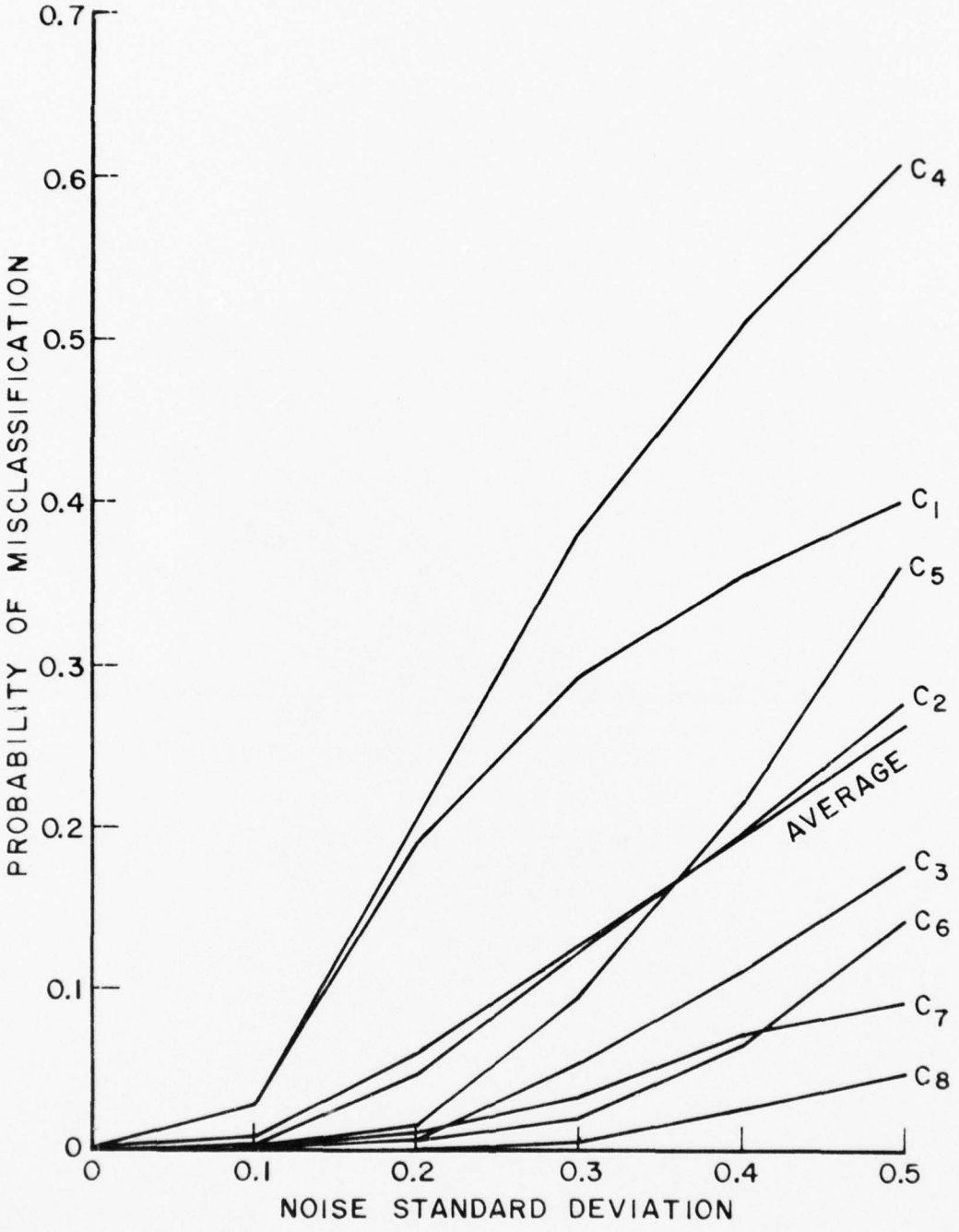

Figure 62. Probability of misclassification for individual aircraft, using amplitude returns of f_8, f_{11} at (90°,90°) aspect angle (side view).

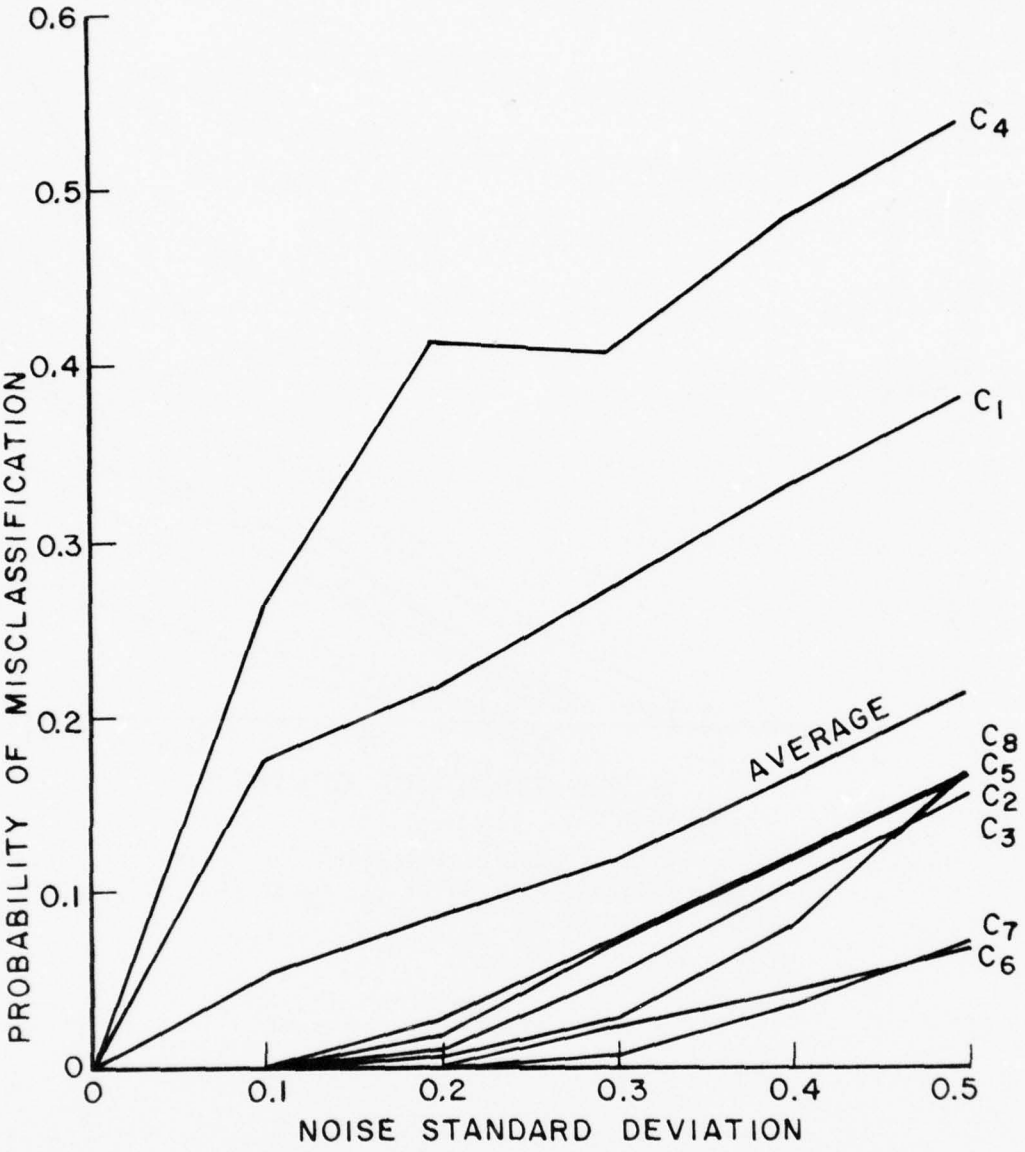

Figure 63. Probability of misclassification for individual aircraft, using amplitude returns of f_2, f_6 at (45°,45°) aspect angle.

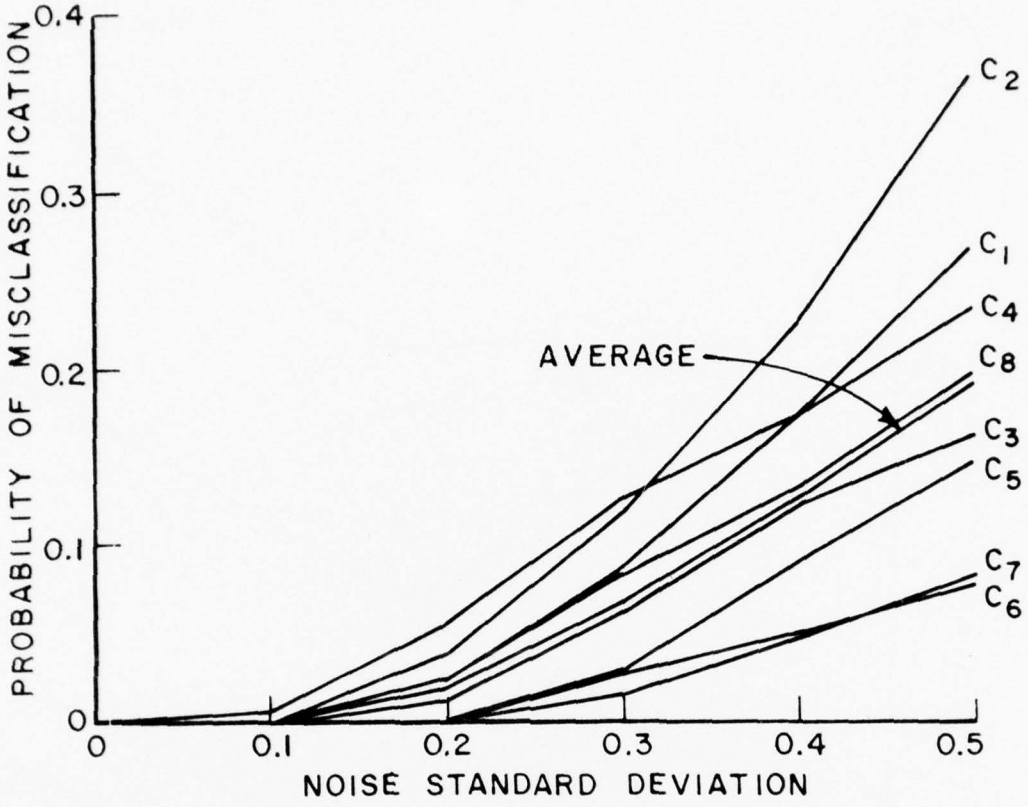

Figure 64. Probability of misclassification for individual aircraft, using amplitude returns of f_6, f_8 at (45°,45°) aspect angle.

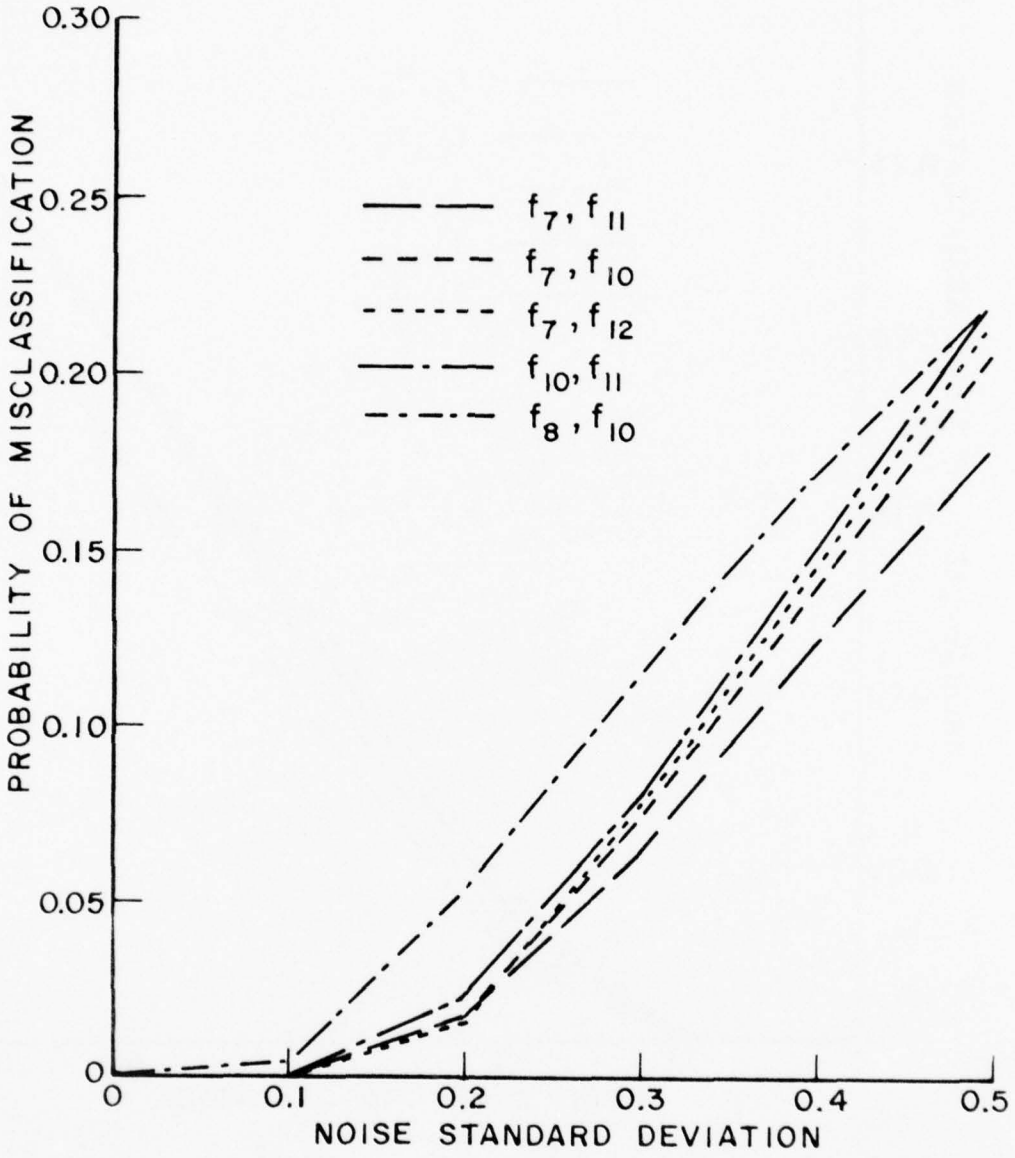

Figure 65. The average performance at different frequencies, using two frequency amplitude returns. The observation angle is $\theta=0°$, $\phi=0°$.

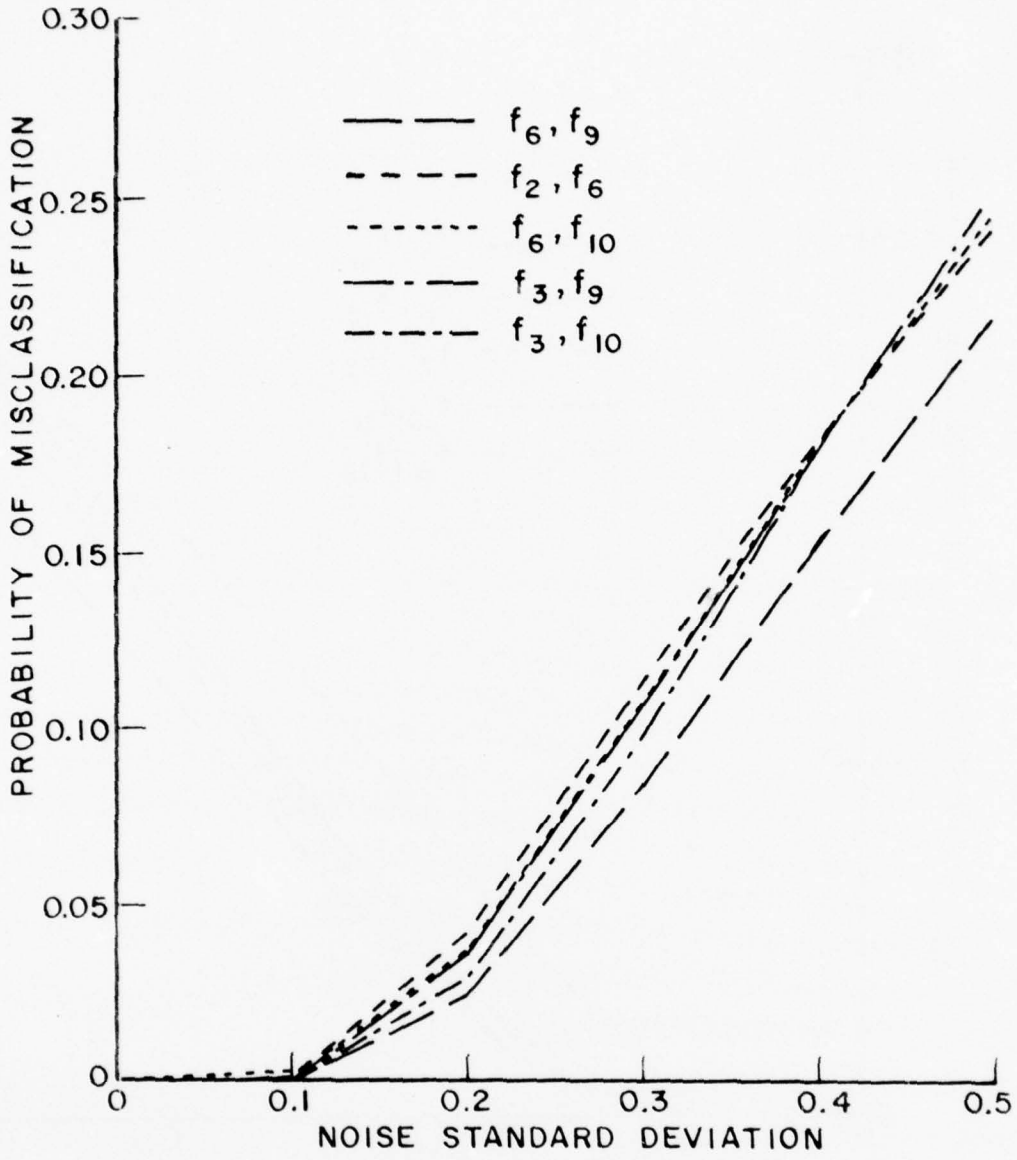

Figure 66. The average performance at different frequencies, using two frequency amplitude returns. The observation angle is $\theta=90°$, $\phi=0°$.

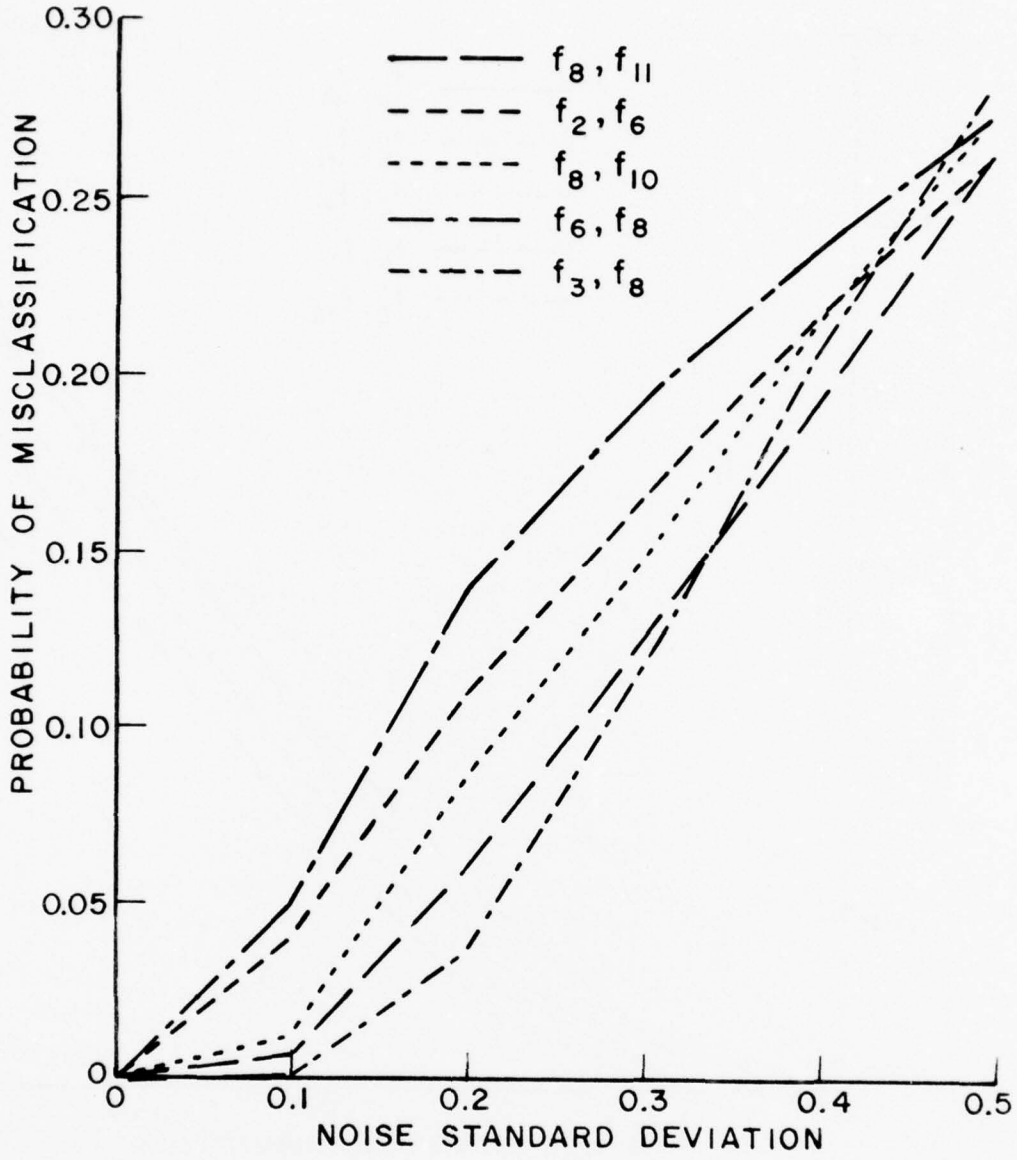

Figure 67. The average performance at different frequencies, using two frequency amplitude returns. The observation angle is $\theta=90°$, $\phi=90°$.

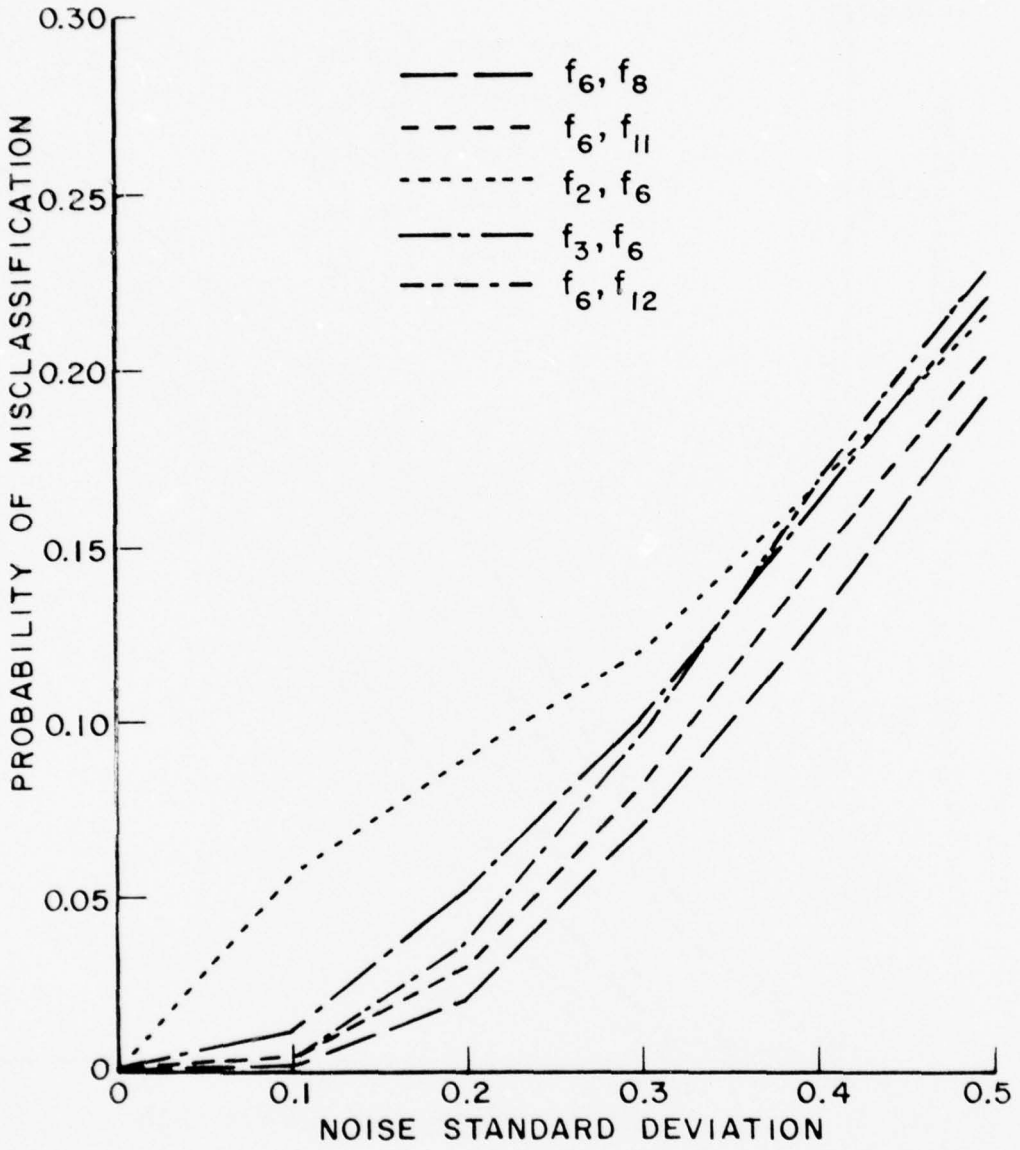

Figure 68. The average performance at different frequencies, using two frequency amplitude returns. The observation angle is $\theta=45°$, $\phi=45°$.

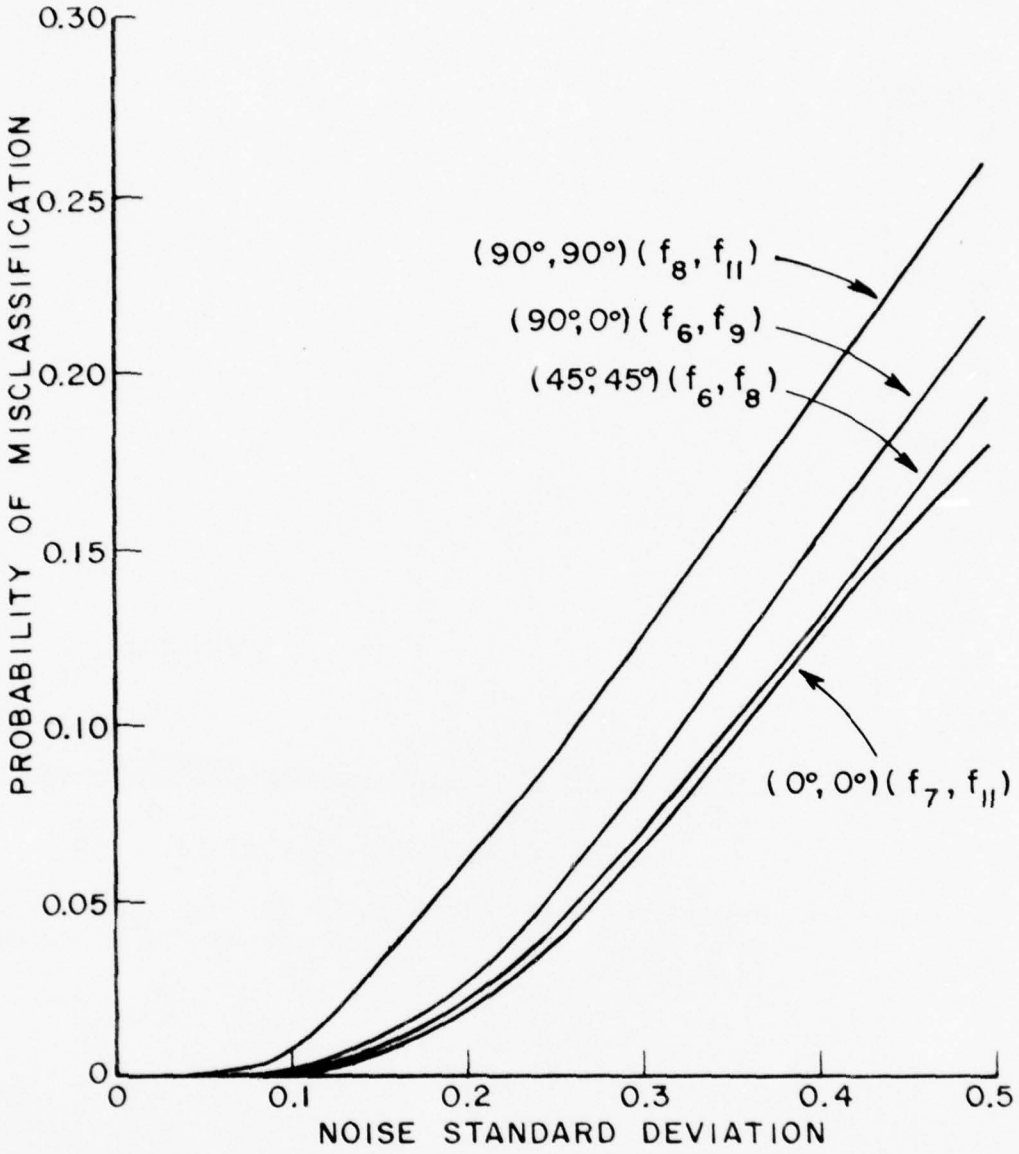

Figure 69. Performance comparison for different aspect angles employing optimum two frequency amplitude returns.

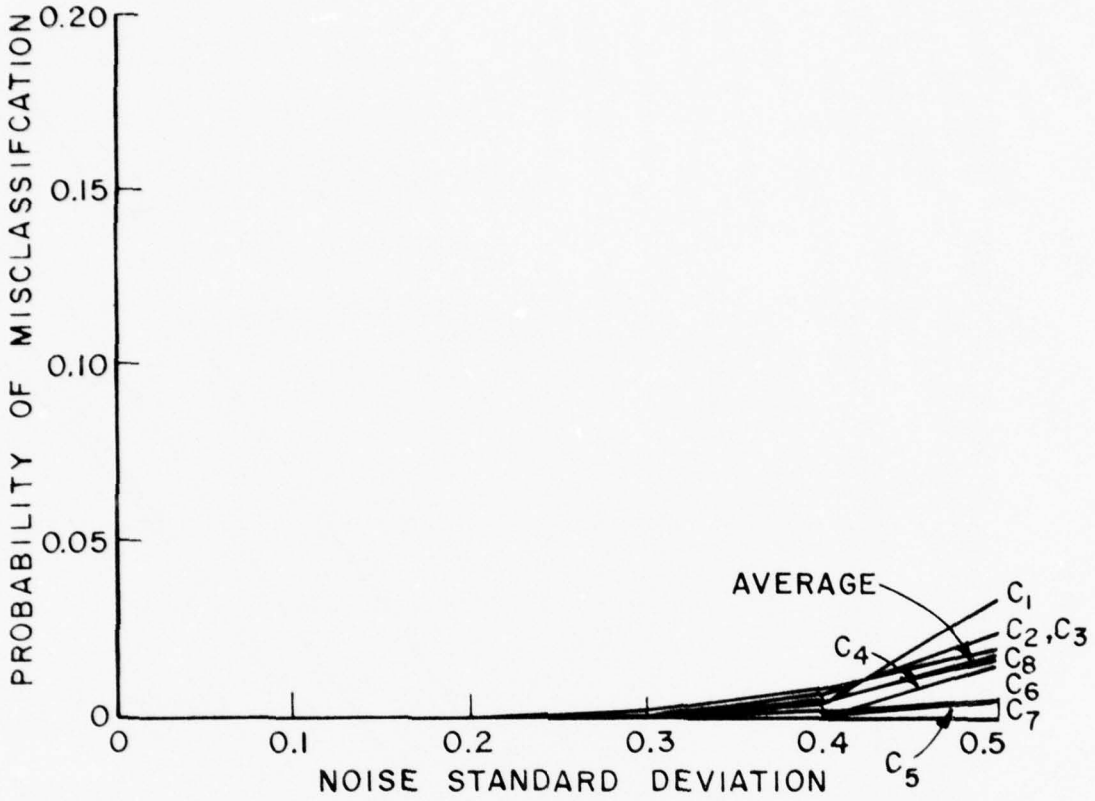

Figure 70. Probability of misclassification for individual aircraft, using complex returns of f_8, f_{12} at (0°, 0°) aspect angle (*nose on*).

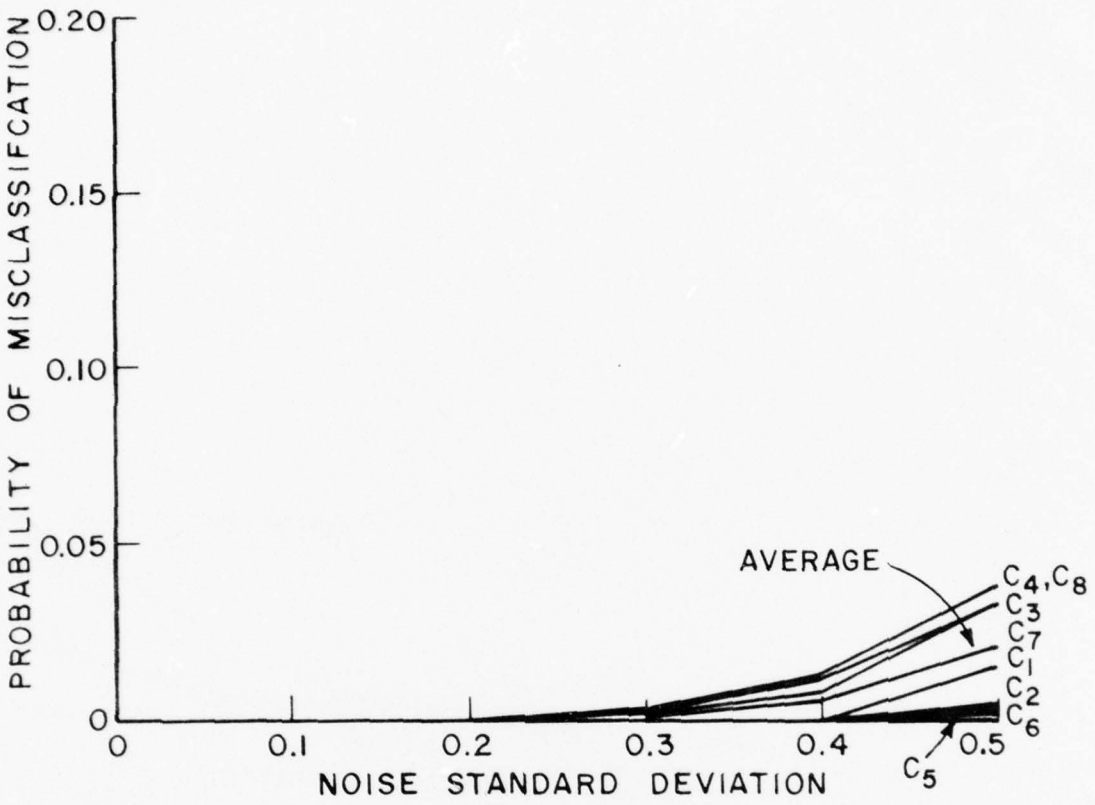

Figure 71. Probability of misclassification for individual aircraft, using complex returns of f_9, f_{12} at (0°,0°) aspect angle (nose on).

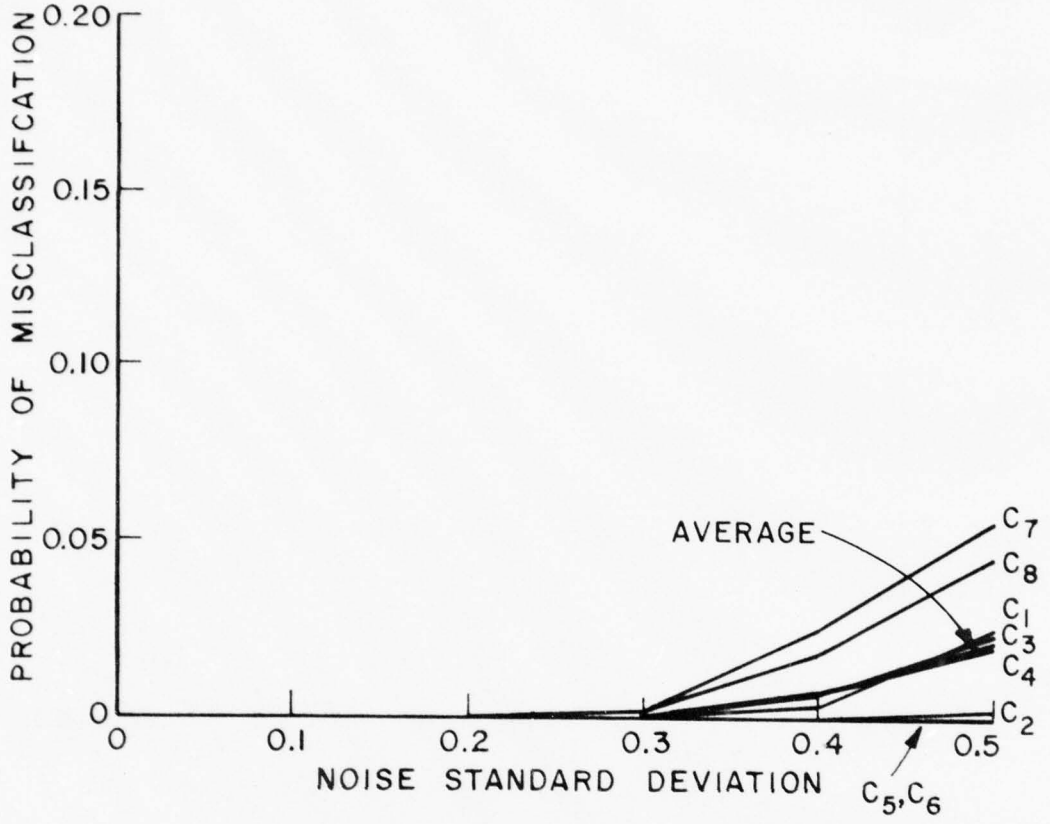

Figure 72. Probability of misclassification for individual aircraft, using complex returns of f_{10}, f_{11} at (0°,0°) aspect angle (nose on).

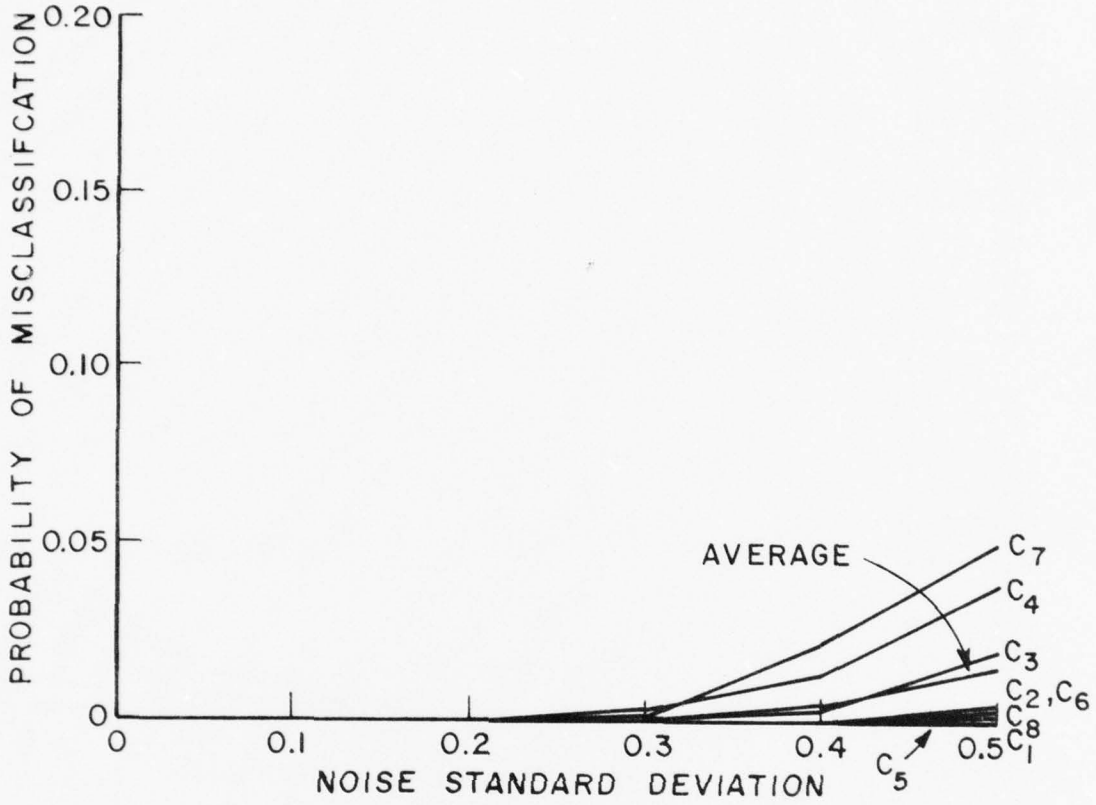

Figure 73. Probability of misclassification for individual aircraft, using complex returns of f_{10}, f_{12} at (0°,0°) aspect angle (nose on).

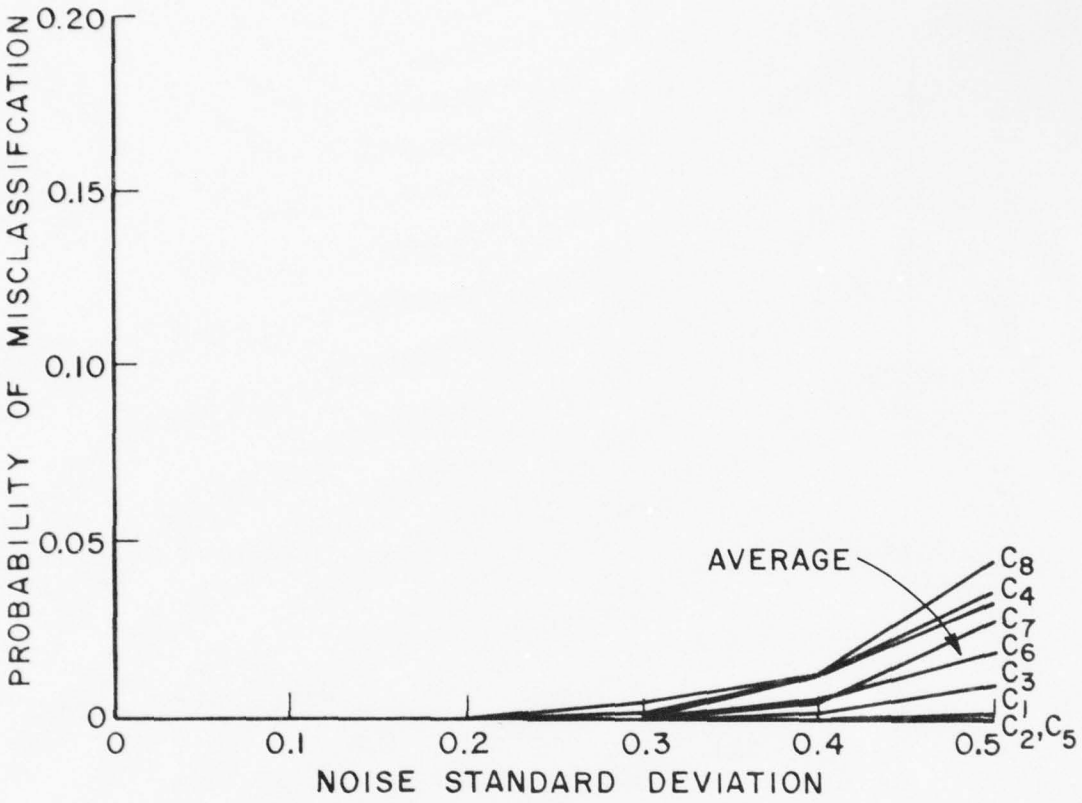

Figure 74. Probability of misclassification for individual aircraft, using complex returns of f_{11}, f_{12} at (0°,0°) aspect angle (nose on).

AD-A065 697 OHIO STATE UNIV COLUMBUS ELECTROSCIENCE LAB F/G 17/9
OPTIMUM FREQUENCIES FOR AIRCRAFT CLASSIFICATION.(U)
JAN 79 L HENG-CHENG , A A KSIENSKI AFOSR-74-2611
UNCLASSIFIED ESL-783815-6 AFOSR-TR-79-0255 NL

2 OF 2
ADA
065697

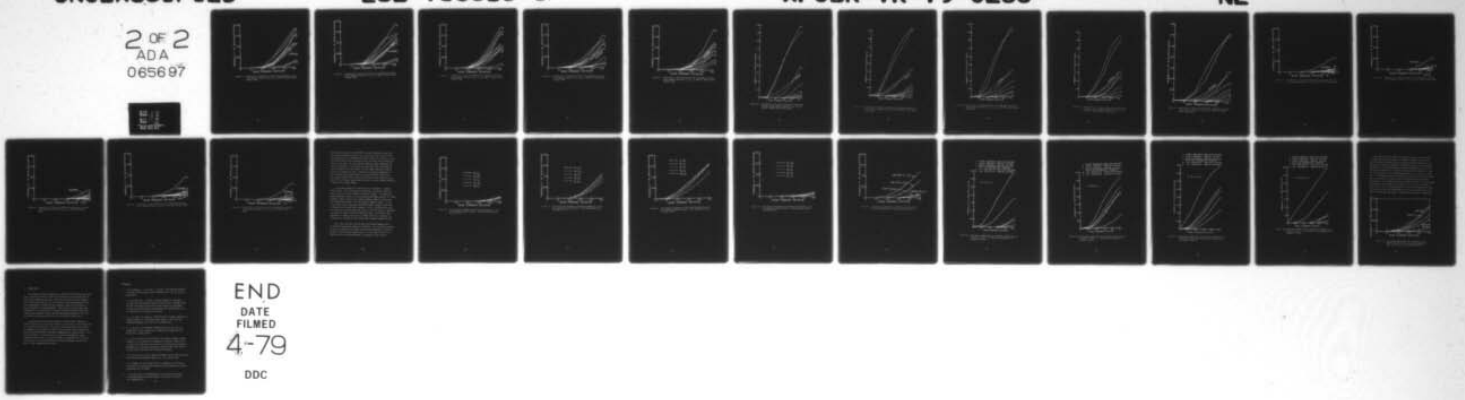

END
DATE
FILMED
4-79
DDC

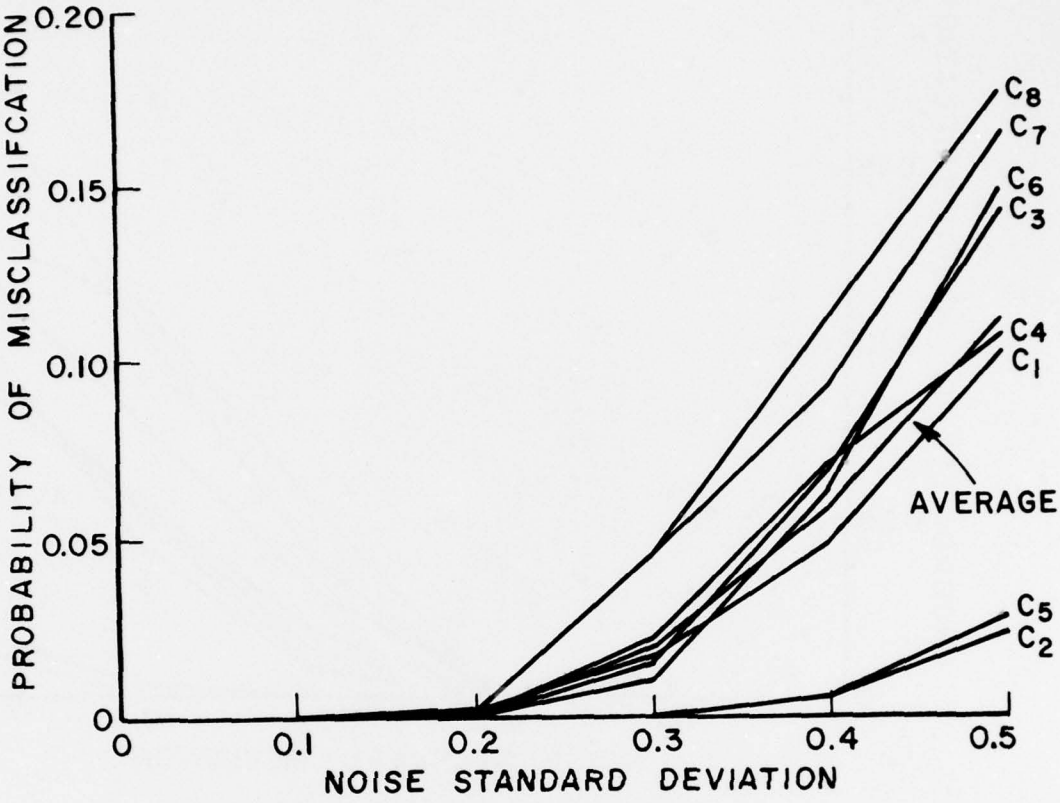

Figure 75. Probability of misclassification for individual aircraft, using complex returns of f_6, f_9 at (90°,0°) aspect angle (bottom view).

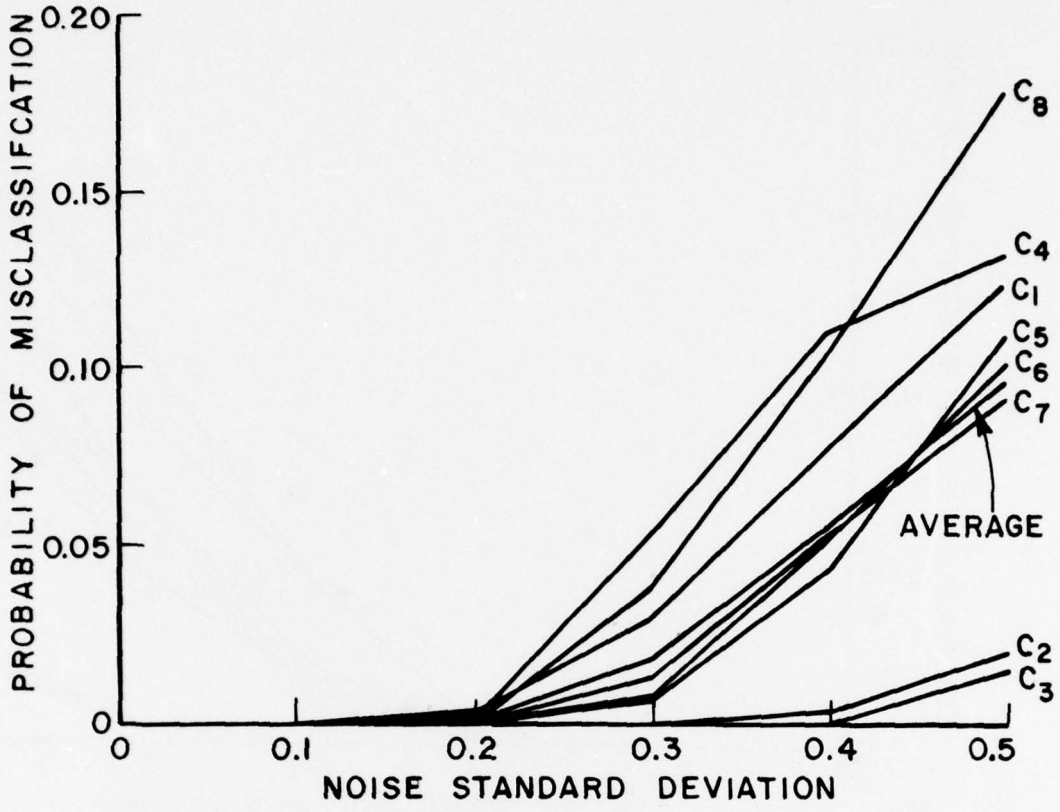

Figure 76. Probability of misclassification for individual aircraft, using complex returns of f_6, f_{11} at (90°, 0°) aspect angle (bottom view).

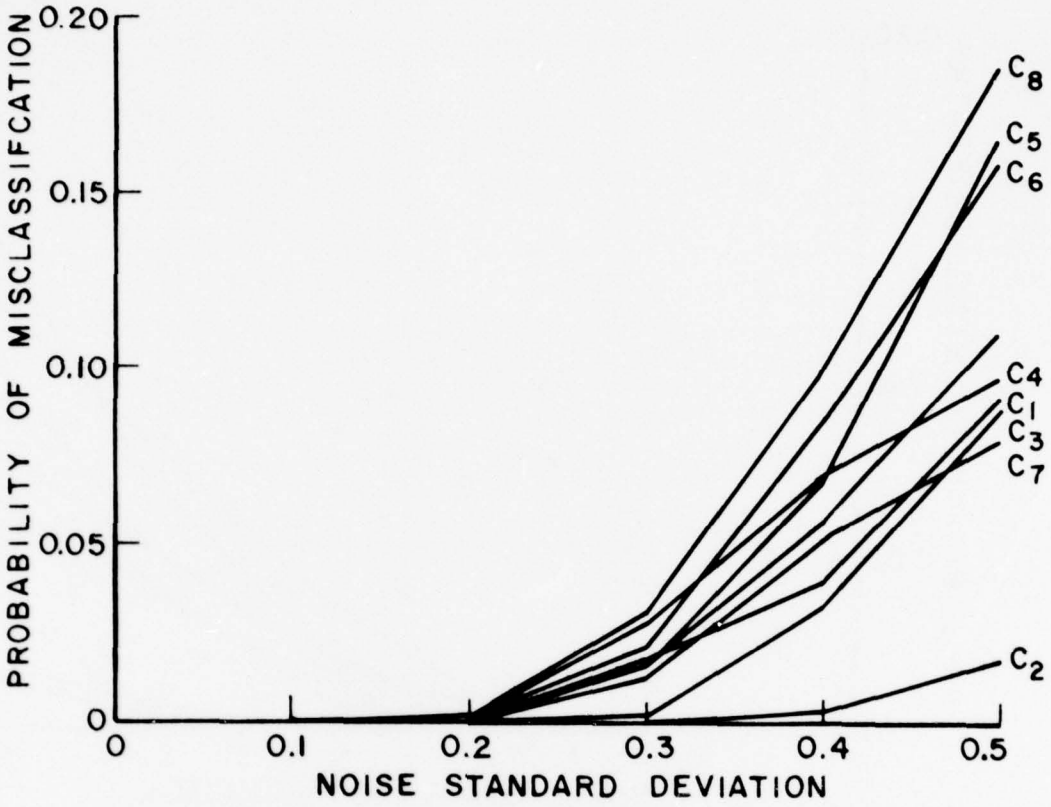

Figure 77. Probability of misclassification for individual aircraft, using complex returns of f_6, f_{12} at (90°,0°) aspect angle (bottom view).

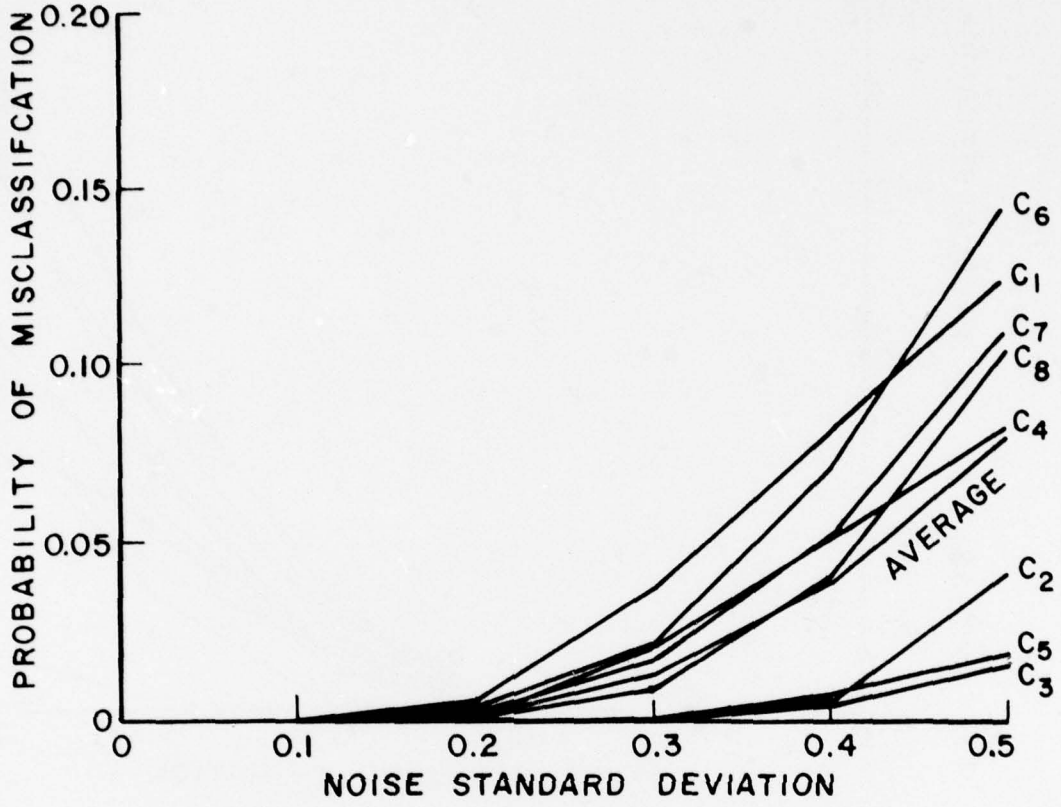

Figure 78. Probability of misclassification for individual aircraft, using complex returns of f_7, f_{11} at (90°,0°) aspect angle (bottom view).

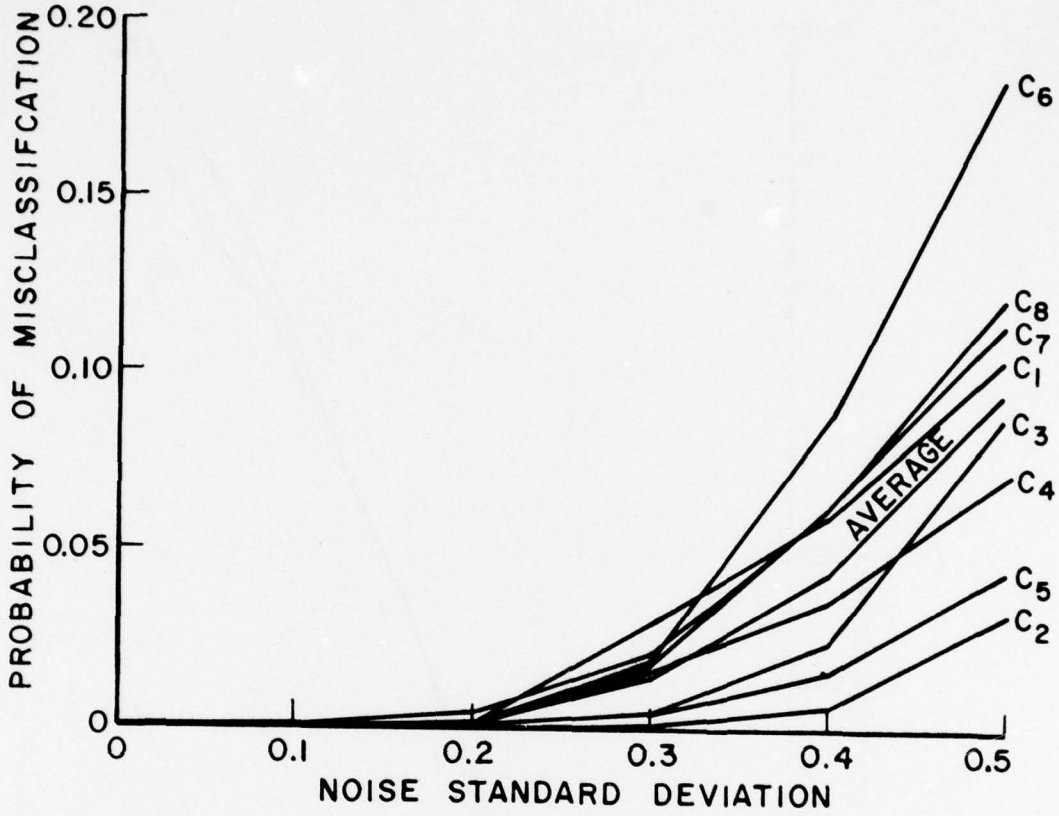

Figure 79. Probability of misclassification for individual aircraft, using complex returns of f_7, f_{12} at (90°,0°) aspect angle (bottom view).

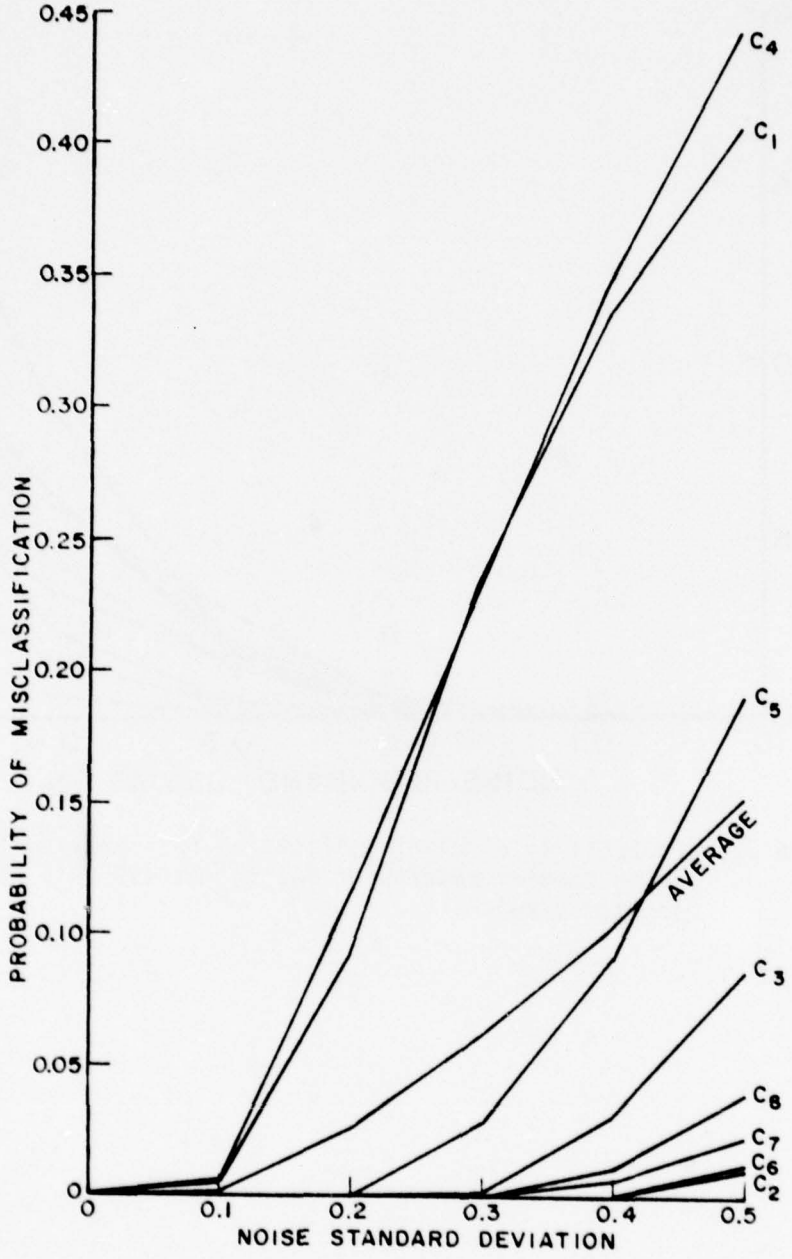

Figure 80. Probability of misclassification for individual aircraft using complex returns of f_6, f_{11} at (90°,90°) aspect angle (side view).

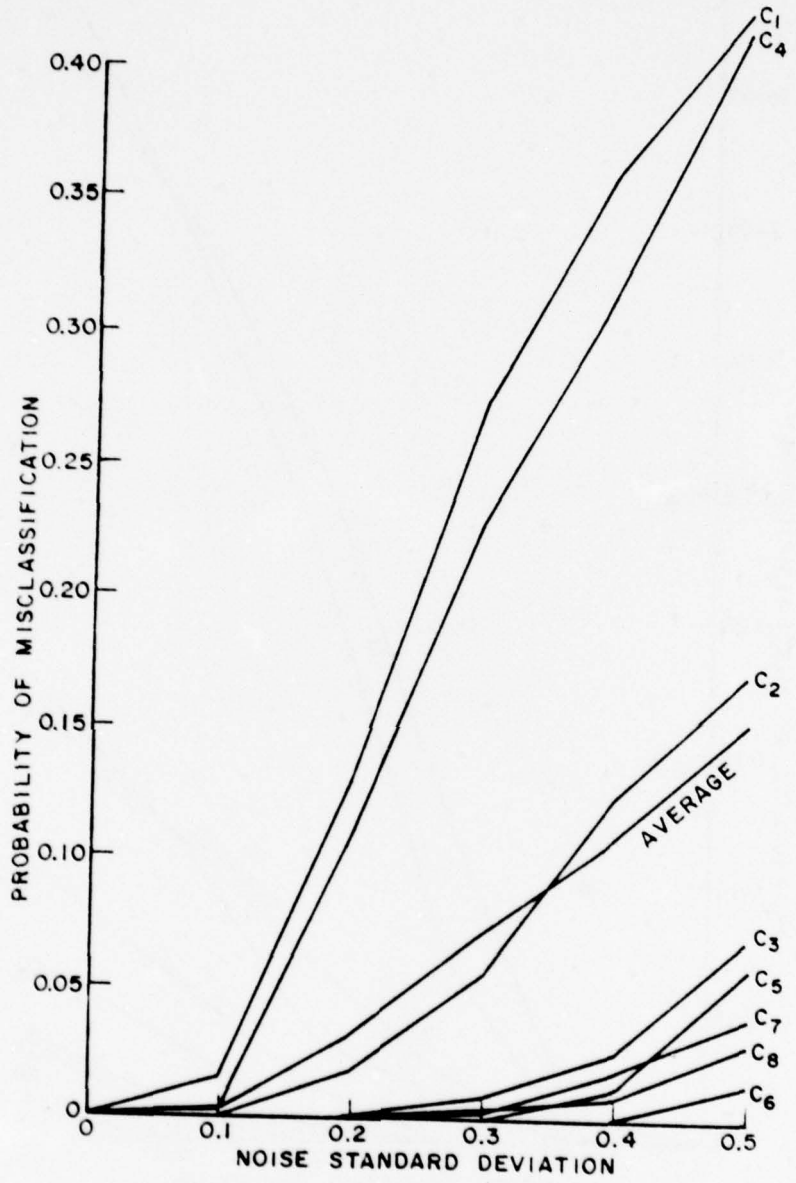

Figure 81. Probability of misclassification for individual aircraft, using complex returns of f_9, f_{11} at (90°,90°) aspect angle (side view).

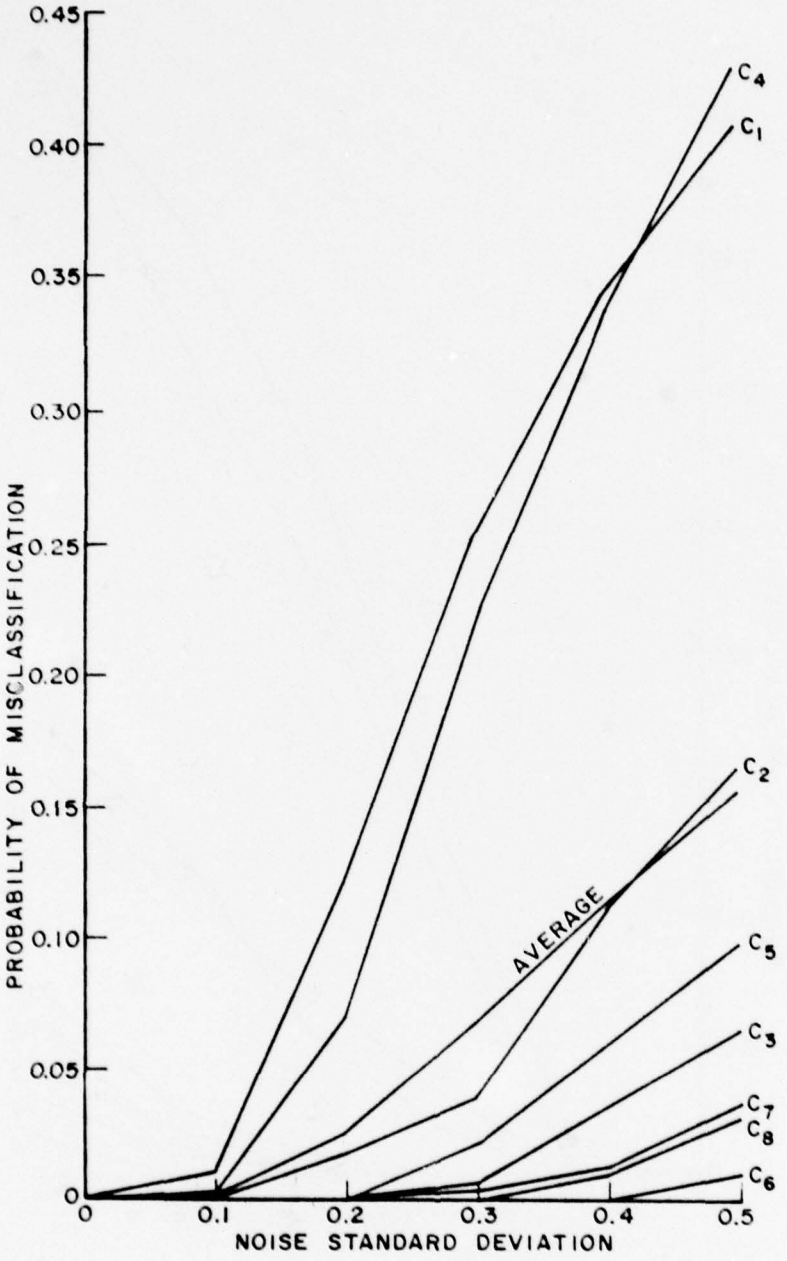

Figure 82. Probability of misclassification for individual aircraft, using complex returns of f_{10}, f_{11} at (90°,90°) aspect angle (side view).

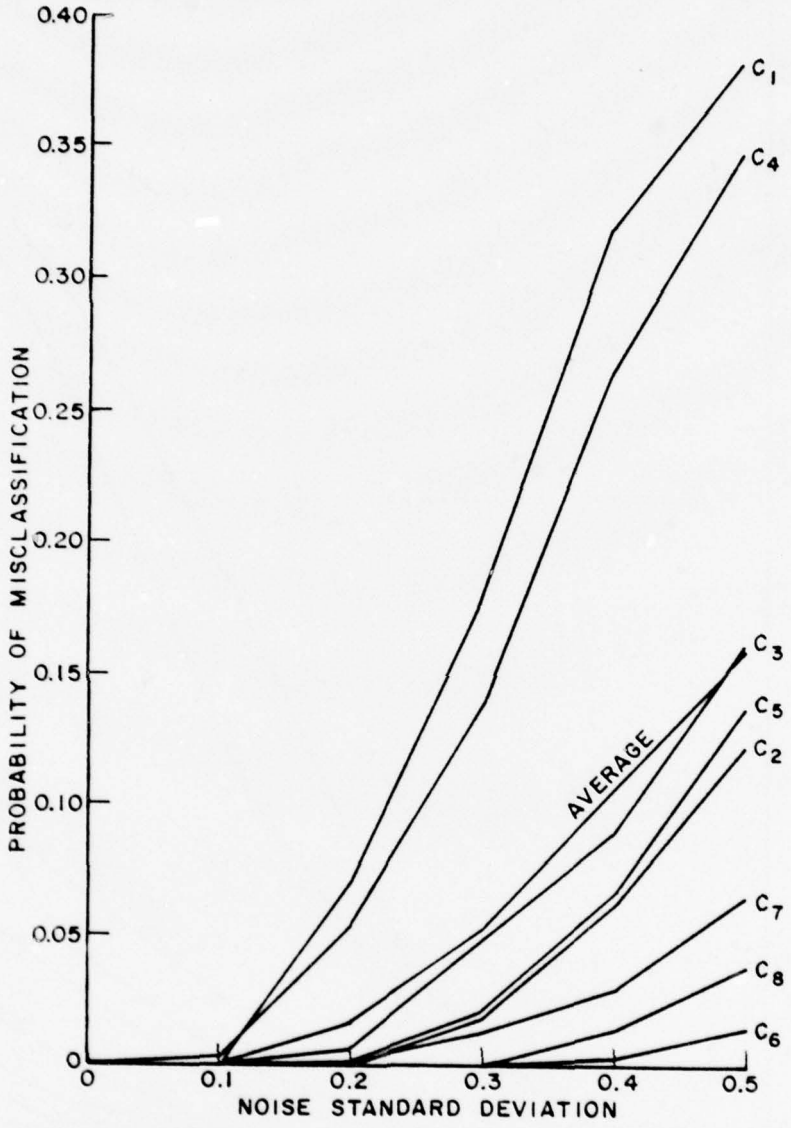

Figure 83. Probability of misclassification for individual aircraft, using complex returns of f_{10}, f_{11} at (90°,90°) aspect angle (side view).

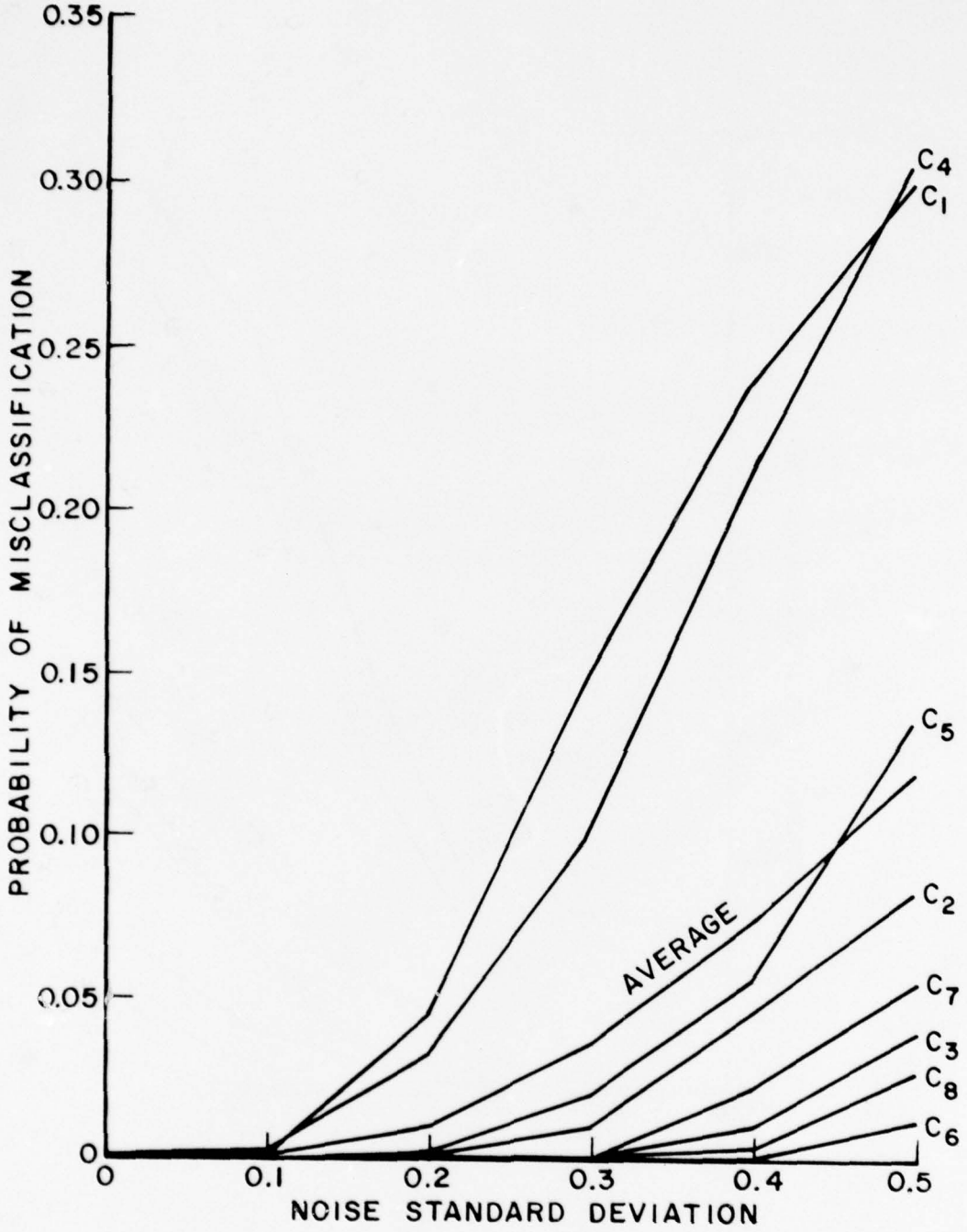

Figure 84. Probability of misclassification for individual aircraft, using complex returns of f_{11}, f_{12} at (90°,90°) aspect angle (side view).

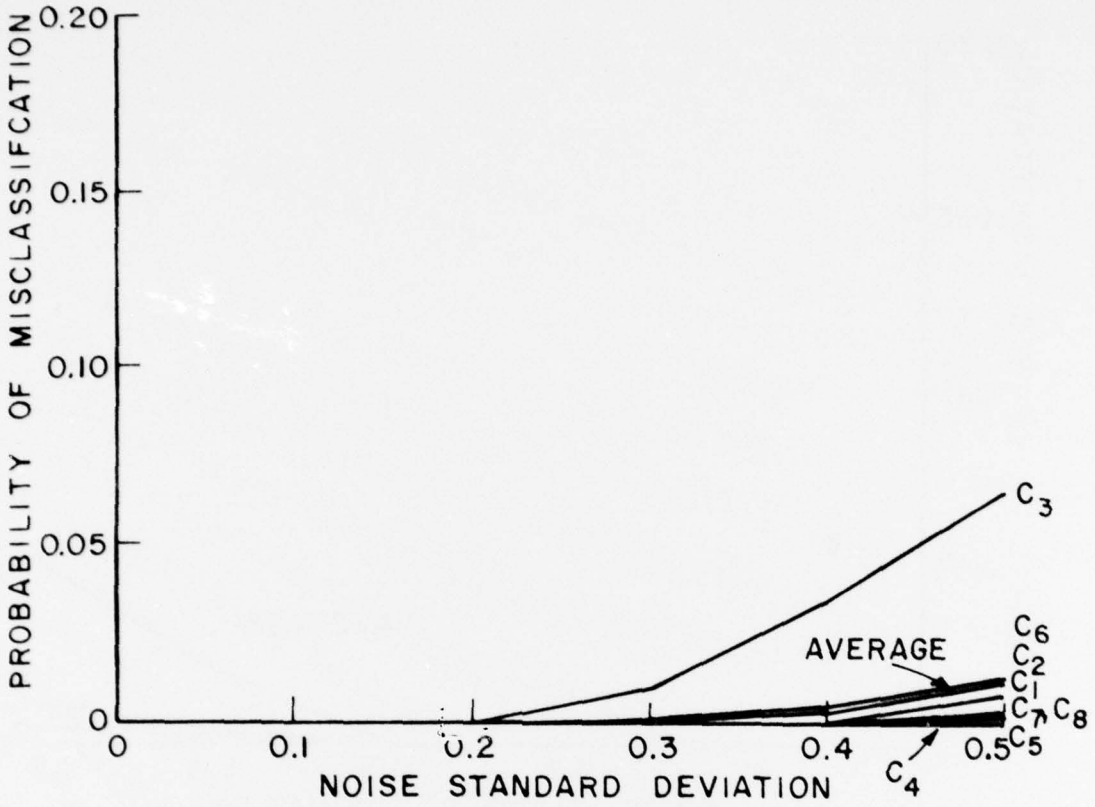

Figure 85. Probability of misclassification for individual aircratt, using complex returns of f_6, f_8 at (45°,45°) aspect angle.

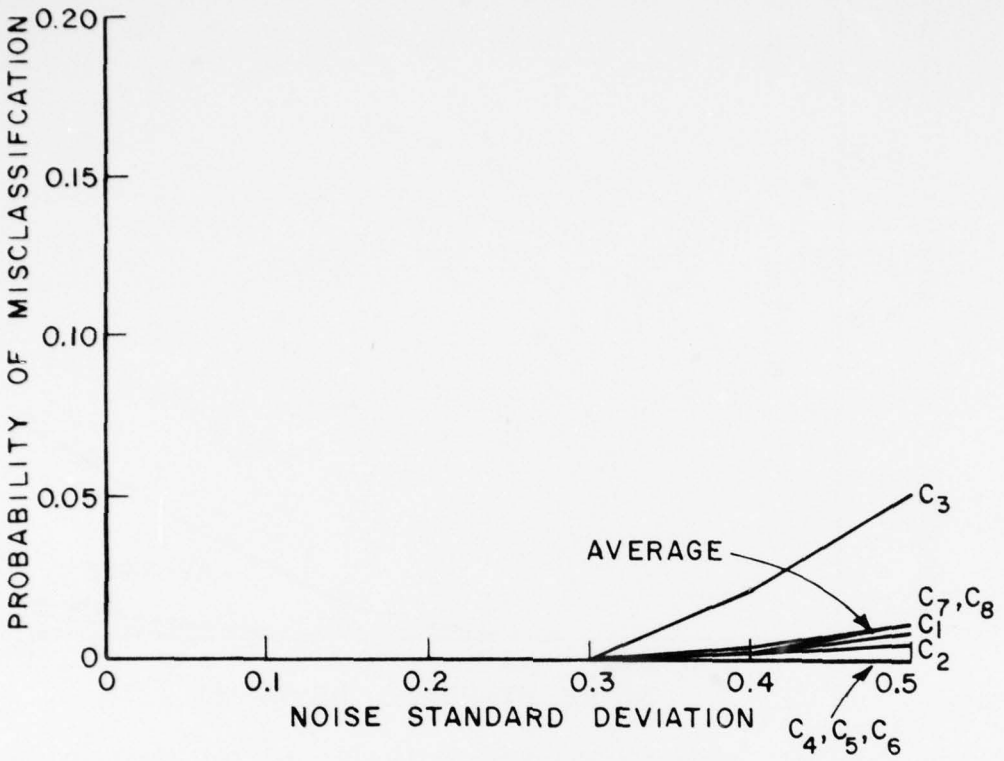

Figure 86. Probability of misclassification for individual aircraft, using complex returns of f_6, f_9 at (45°, 45°) aspect angle.

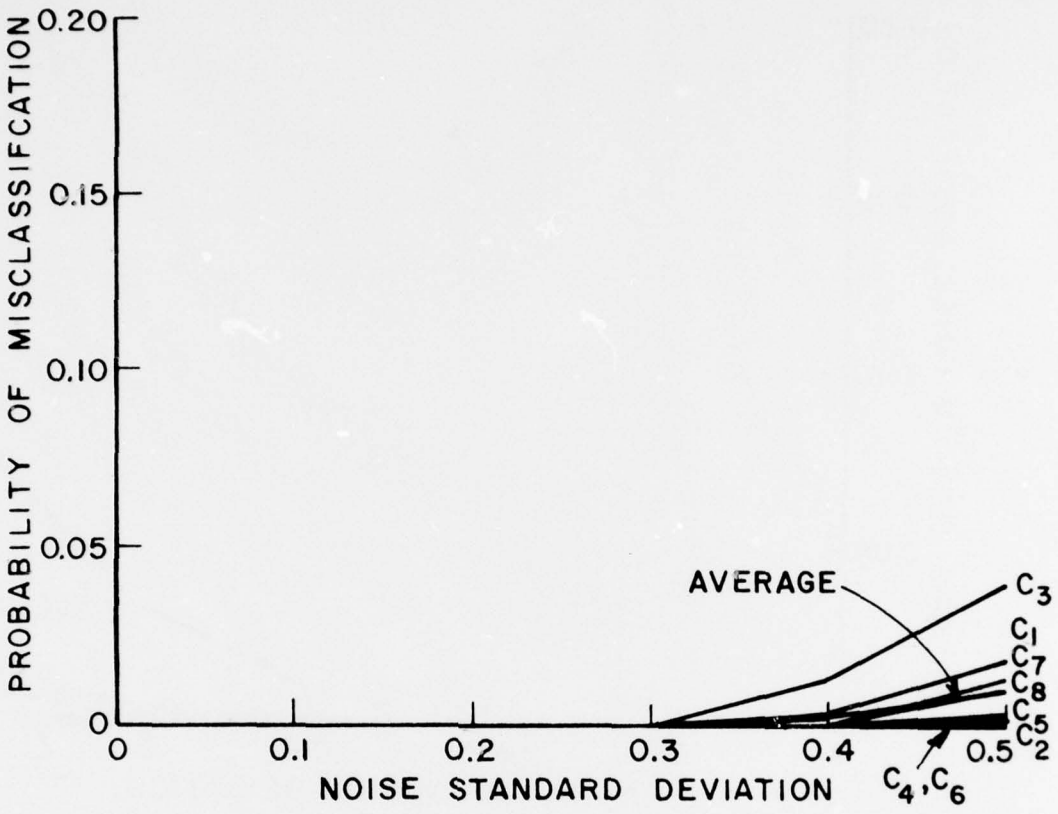

Figure 87. Probability of misclassification for individual aircraft, using complex returns of f_6, f_{10} at (45°,45°) aspect angle.

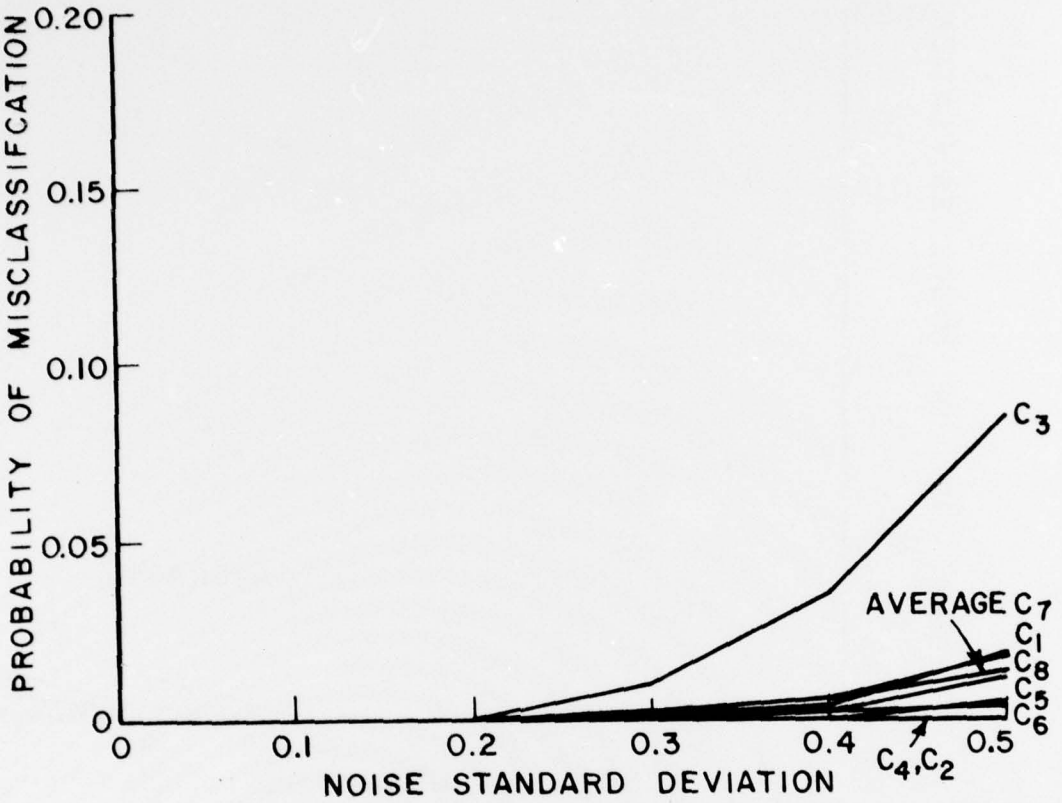

Figure 88. Probability of misclassification for individual aircraft, using complex returns of f_6, f_{11} at (45°,45°) aspect angle.

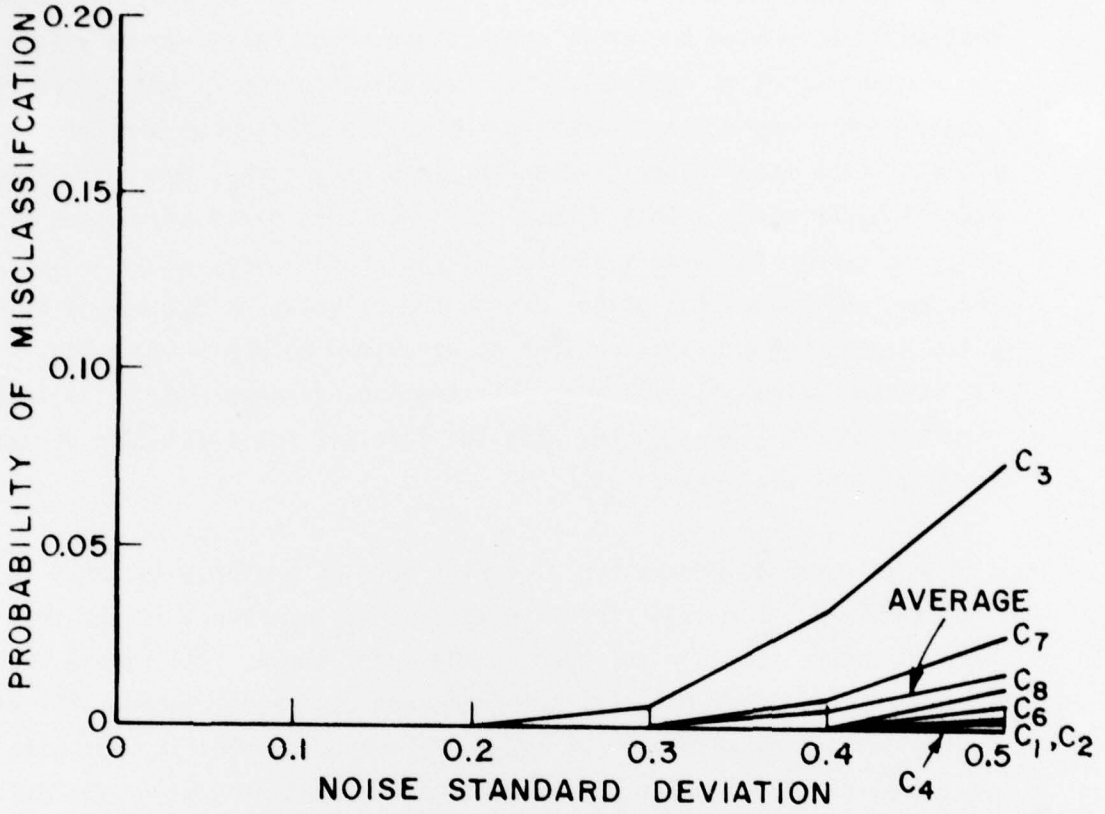

Figure 89. Probability of misclassification for individual aircraft, using complex returns of f_6, f_{12} at (45°,45°) aspect angle.

The performance curves for $(90^0,90^0)$ are worse than others, but note that we have doubled the error scale since error rates are very low. The probabilities of individual misclassification of C_1 and C_4 are relatively high because the scattering returns for those two airplanes are close to each other over the observed frequency range, degrading the overall performance. This occurs only when both sizes and shapes of aircraft appear to be very similar at the chosen observation angles, and does not happen too often. Again the orientation dependence is quite strong for the same reasons as discussed before (Figure 94). The average probability of misclassification has been reduced to less than 15% in all aspect angles when the level of noise standard deviation is 50 percent (Figures 90-94).

A performancesummary for different sets of features is shown in Figures 95-98. The classification reliability increases as the following feature sets are selected in the order shown: (1) single frequency amplitude returns, (2) two frequency amplitude returns, (3) single frequency complex returns, (4) single frequency complex returns with the fundamental harmonic, (5) two frequency complex returns. In utilizing two features, the phase information shows stronger effect than an amplitude at an additional frequency. This is caused by the closeness among two frequency amplitude returns since the system is operating at frequencies mostly within the Rayleigh range. On the other hand components of complex returns can go either positive or negative, increasing their variability and reducing the closeness among the data.

The results obtained indicate that the optimum frequency pairs at different observation angles are different. For a practical system, it may be inconvenient to change the operating frequencies as the orientation of the observed target varies. In this case a pair of frequencies must be chosen beforehand in designing a radar system.

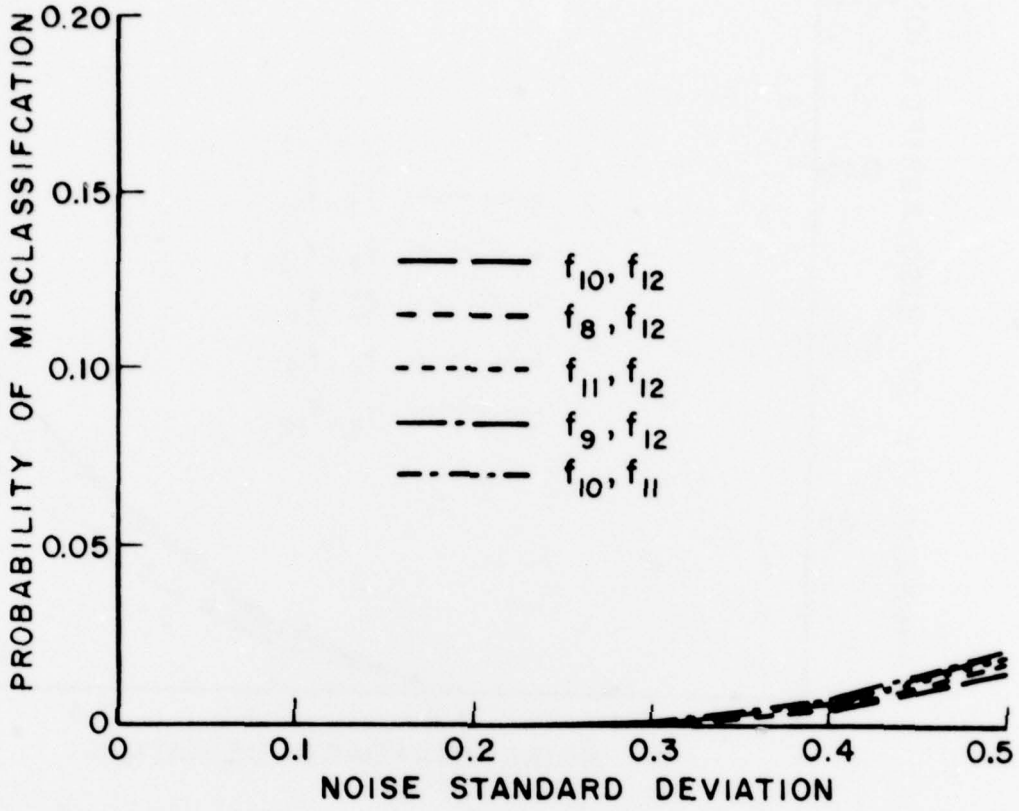

Figure 90. The average performance at different frequencies, using two frequency complex returns. The observation angle is $\theta=0°$, $\phi=0°$.

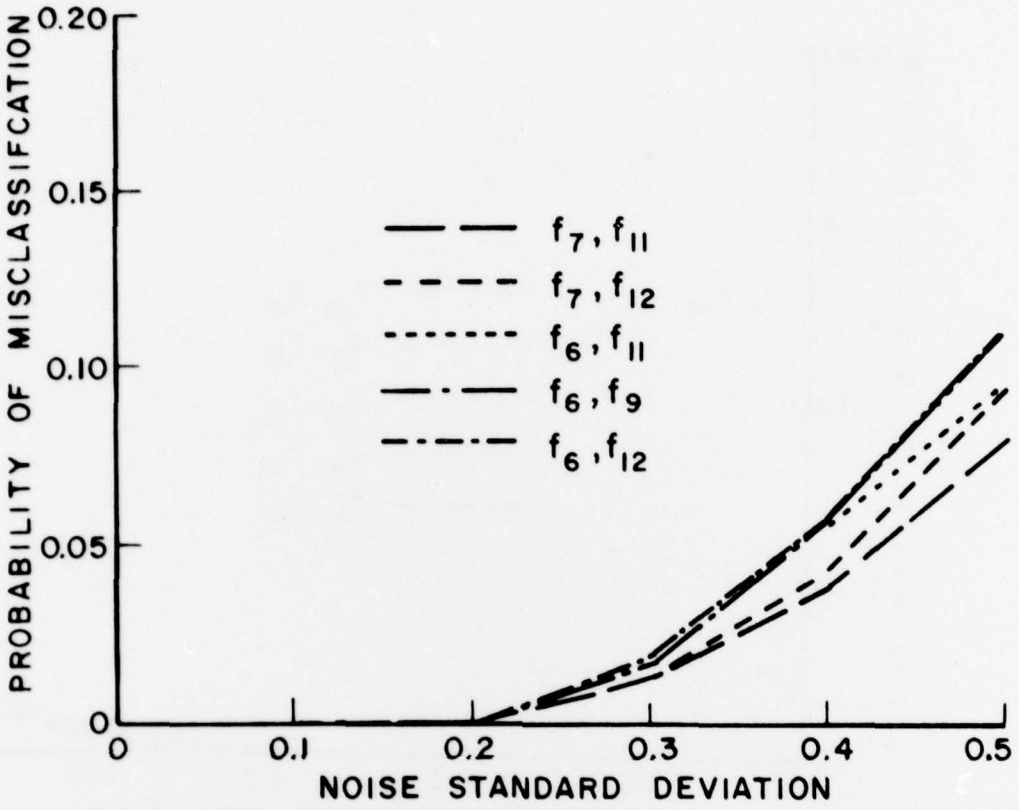

Figure 91. The average performance at different frequencies, using two frequency complex returns. The observation angle is $\theta=90^\circ$, $\phi=0^\circ$.

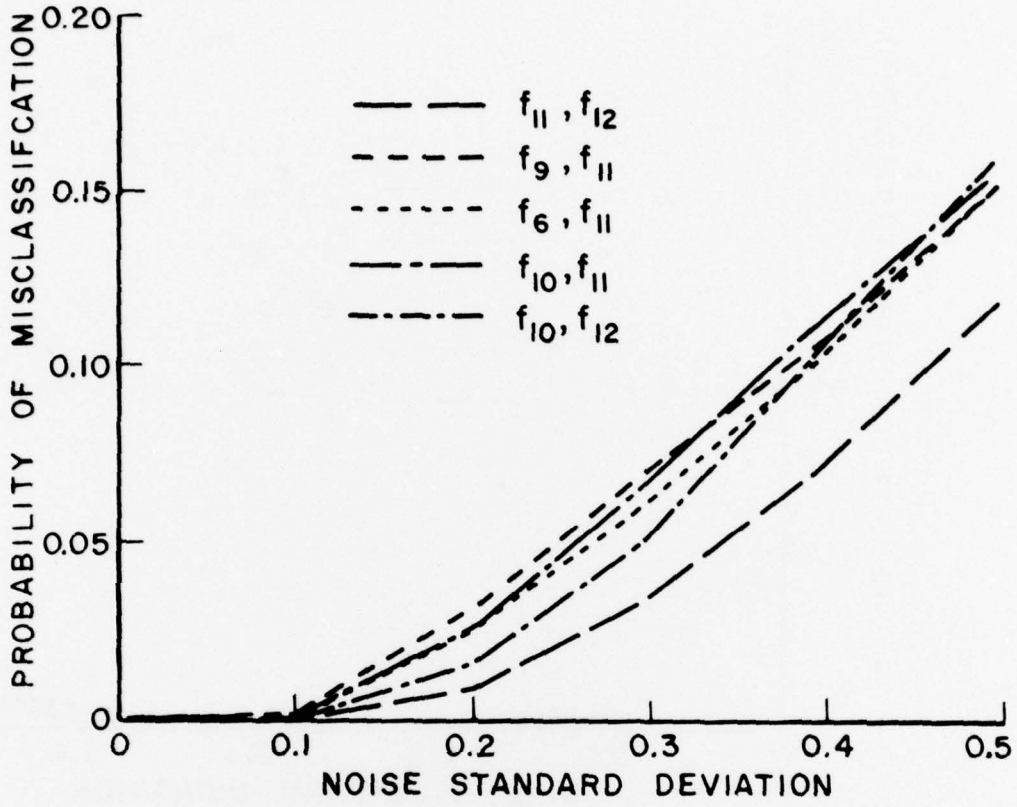

Figure 92. The average performance at different frequencies, using two frequency complex returns. The observation angle is $\theta=90^\circ$, $\phi=90^\circ$.

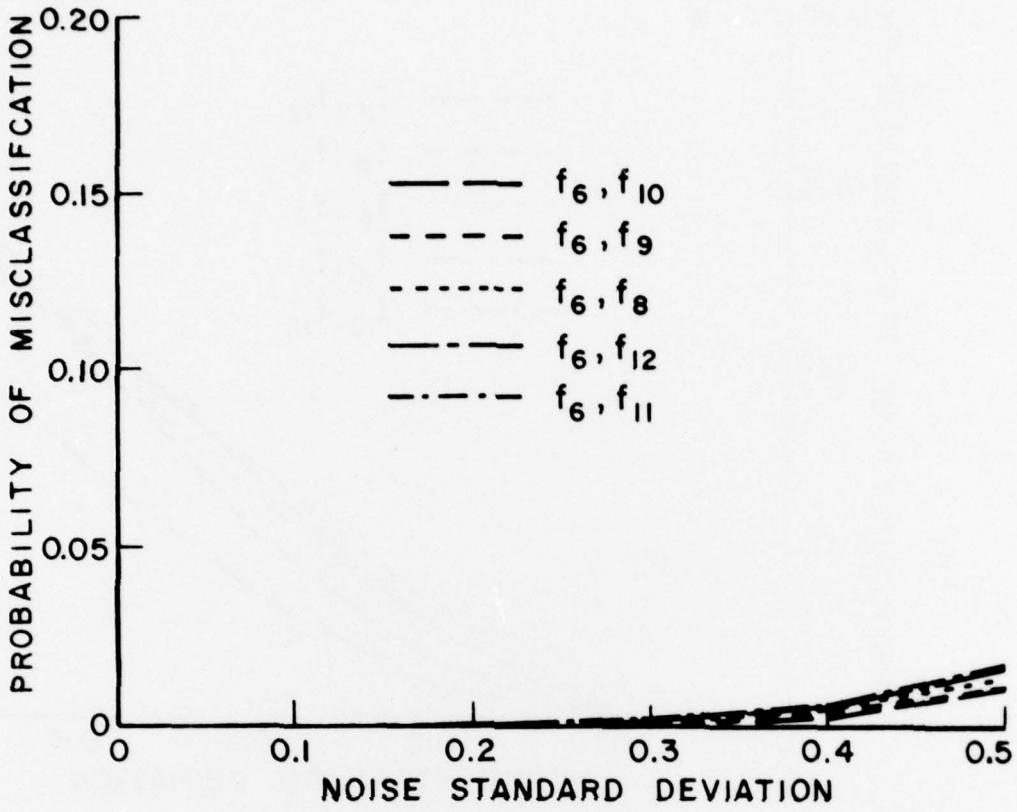

Figure 93. The average performance at different frequencies, using two frequency complex returns. The observation angle is $\theta=45°$, $\phi=45°$.

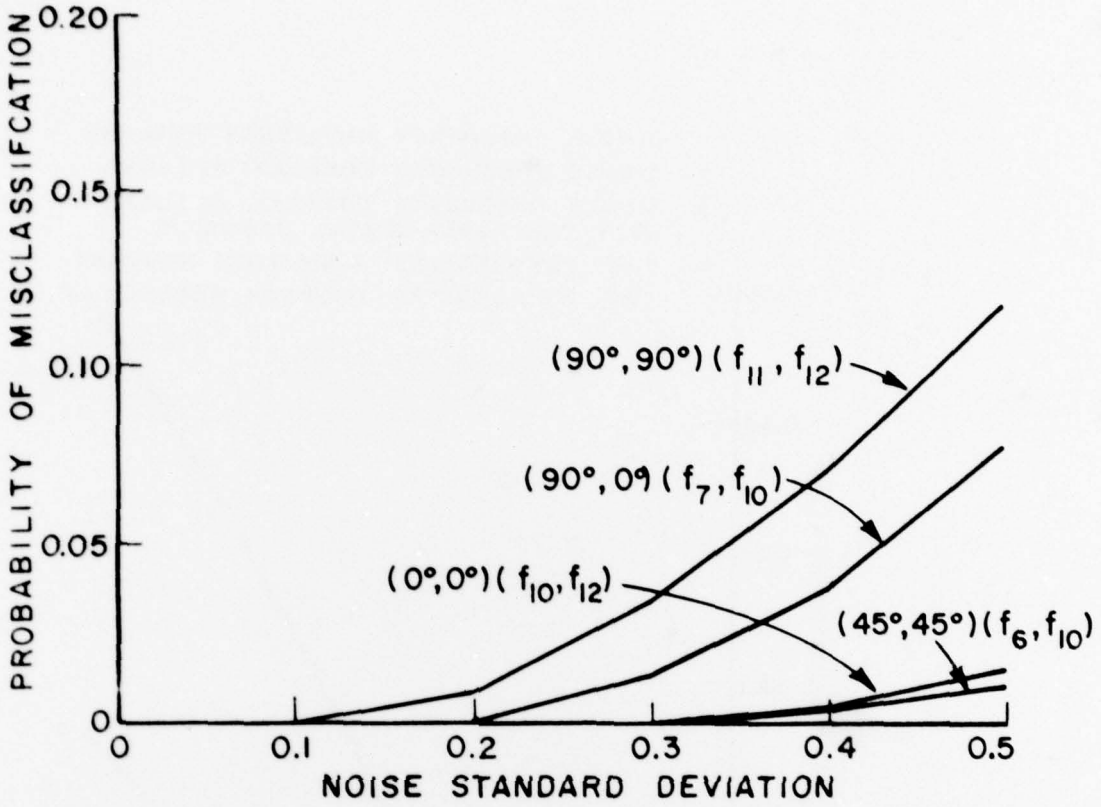

Figure 94. Performance comparison for different aspect angles employing optimum two frequency complex returns.

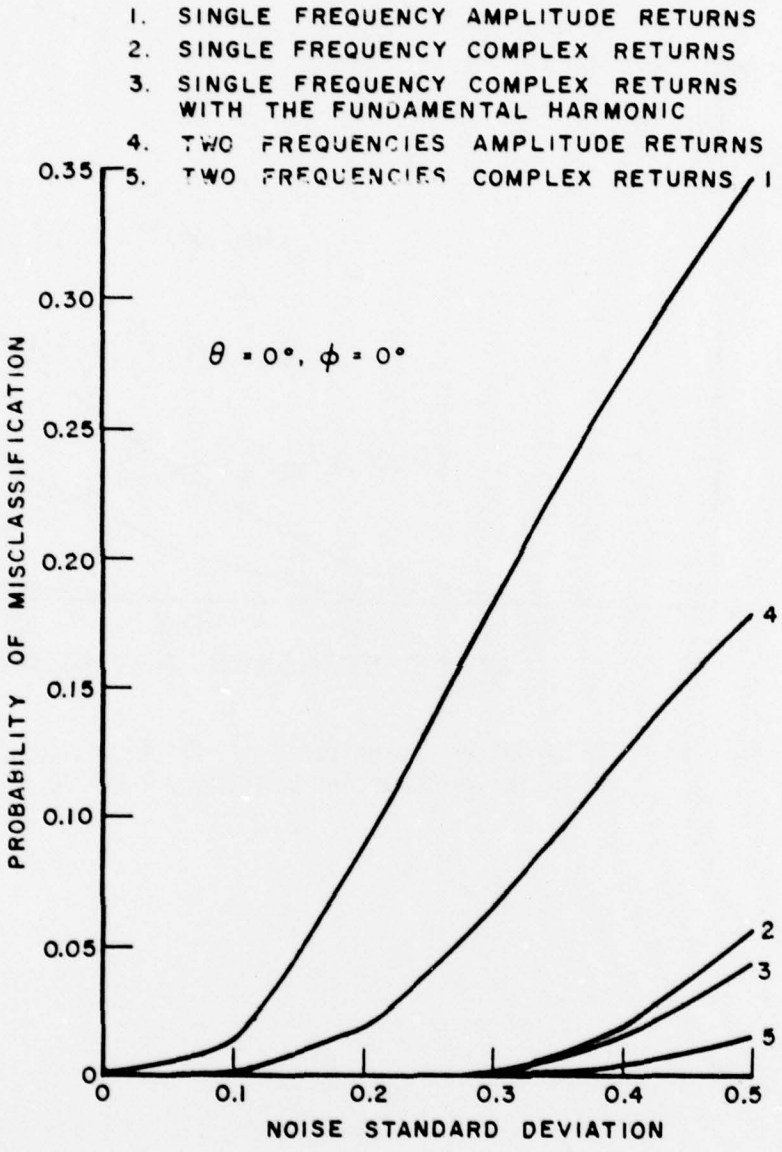

Figure 95. Performance comparison for different combinations of features at $\theta=0^0$, $\phi=0^0$ employing optimum set of frequency returns.

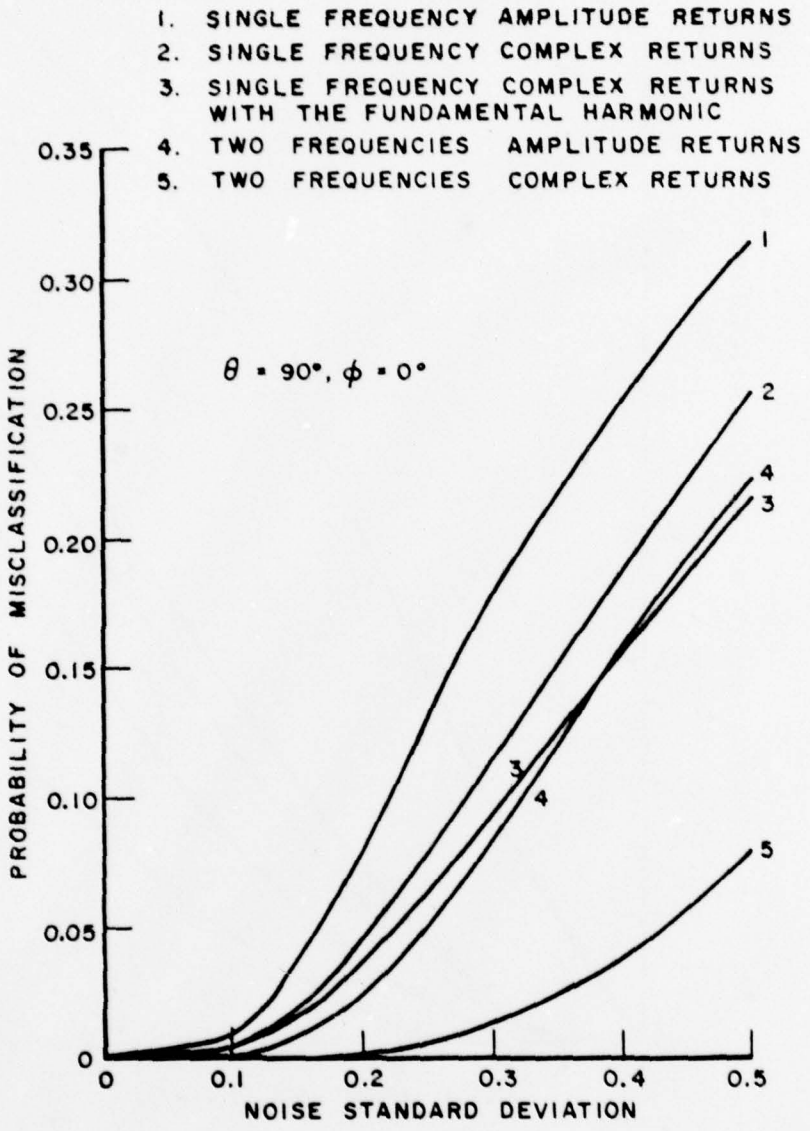

Figure 96 Performance comparison for different combinations of features at $\theta=90^\circ$, $\phi=0^\circ$ employing optimum set of frequency returns.

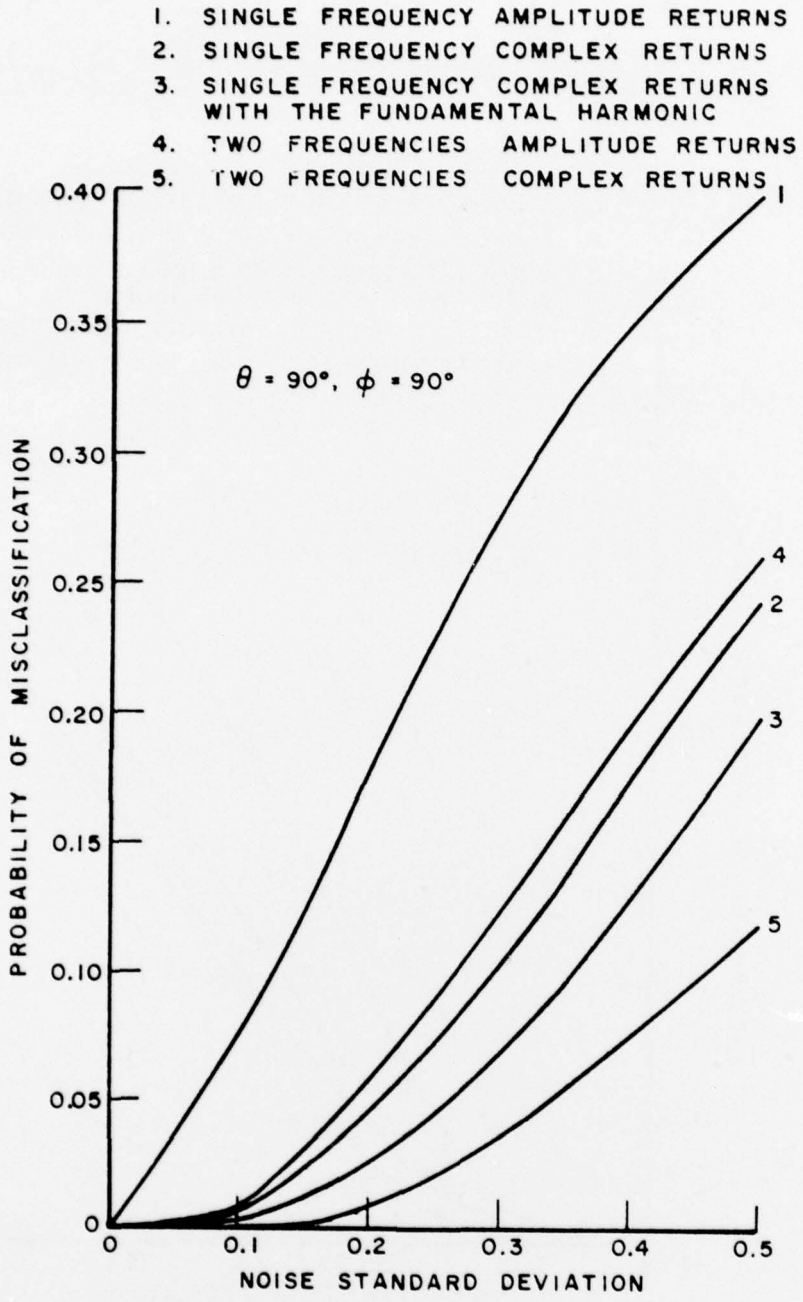

Figure 97. Performance comparison for different combinations of features at $\theta=90°, \phi=90°$ employing an optimum set of frequency returns.

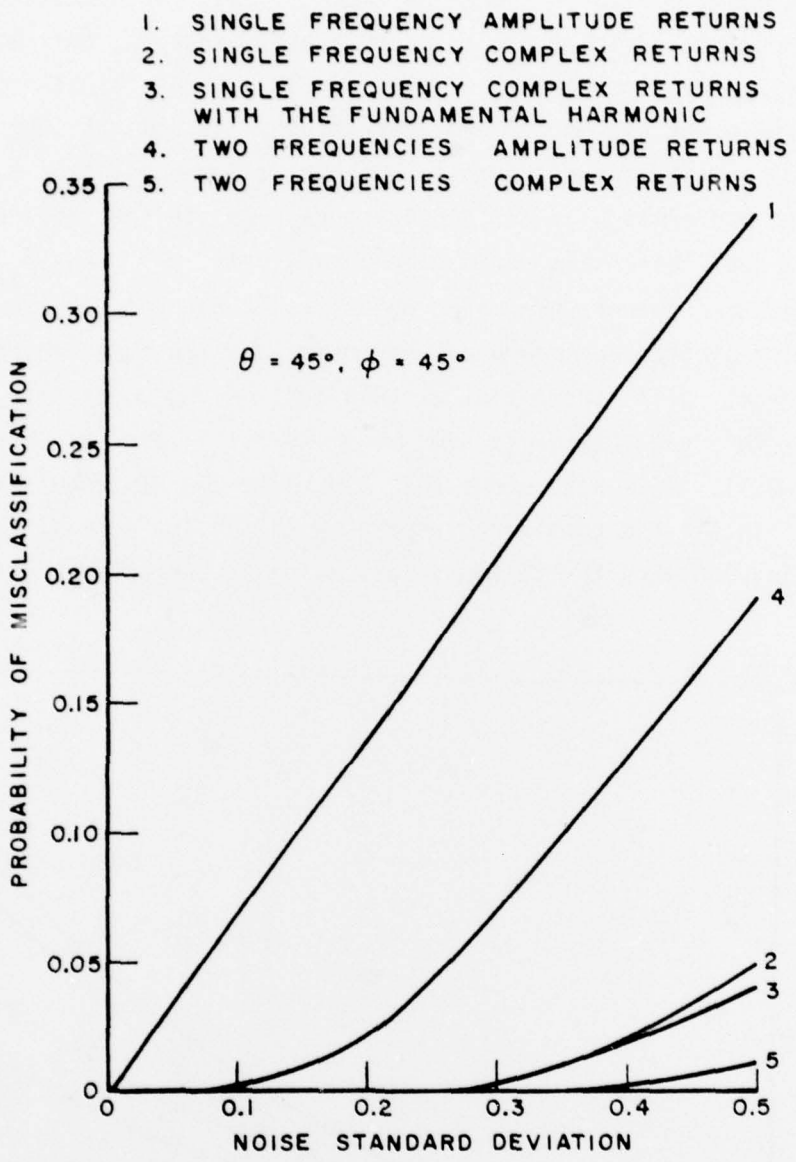

Figure 98 Performance comparison for different combinations of features at $\theta=45°$, $\phi=45°$ employing an optimum set of frequency returns.

One would be led to chose the frequency pair such that the error averaged over all aspect angles is smallest. However, this may not be satisfactory since the error at a specific aspect might not be tolerable while the system performs extraordinarily well at other aspects. Therefore, it it more reasonable to choose a frequency pair such that the worst performance at all aspects considered is the smallest. From the data available, this optimum frequency pair is f_{11} and f_{12} (Figure 99). The performance when using these two frequencies at the four aspect angles are plotted in Figure 99 and the unlabelled curve represents the average. It is shown that at this optimum frequency pair, the scheme performs very satisfactorily even when the noise level is extremely high (σ=0.5). This also shows that N.N. rule can distinguish the eight aircraft in all the considered aspects with the low probability of misclassification when the system is operating at the optimum frequencies.

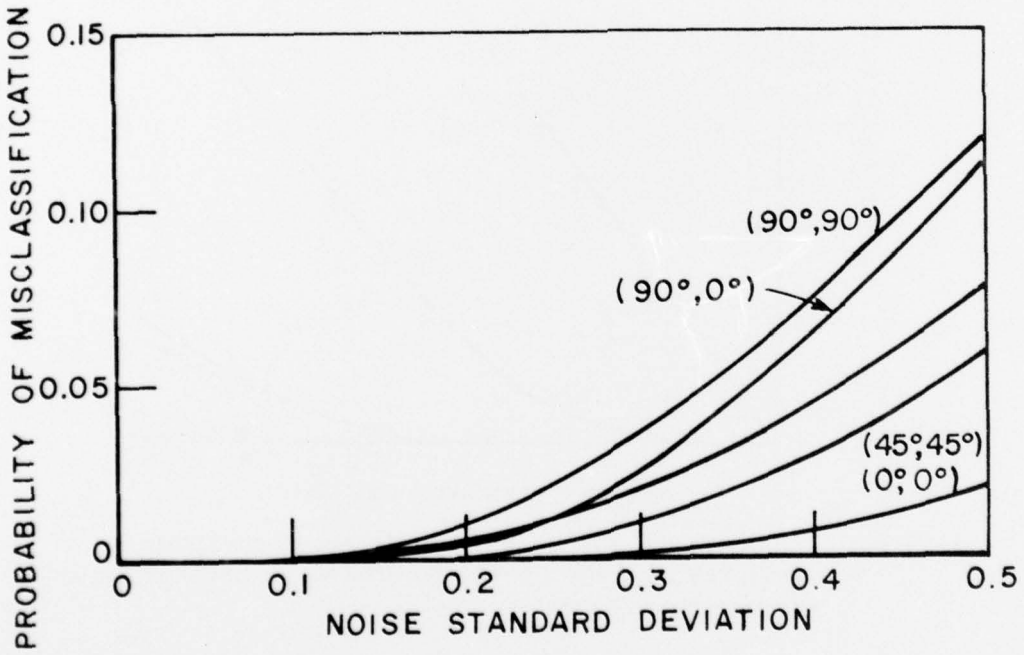

Figure 99. The average performance at 4 different aspect angles with the use of the optimum frequency pair (f_{11} and f_{12}), and complex returns.

X. CONCLUSIONS

The study of optimum frequencies for aircraft classification has shown that a high reliability of correct classification can be obtained when as few as two frequencies are used. This holds true for noise environments up to 30% of signal levels. A set of curves is provided showing the relative performances of single and two frequency returns and the effect of phase information on the performance. These results indicate that phase information is very effective in reducing misclassification probabilities. Indeed single frequency returns provide adequate performance of over 95% reliability in the presence of noise of up to 20% of signal level.

The eight aircraft that were chosen for classification represent a rather difficult set since some of them are very similar in size while others are substantially different. This puts a severe constraint on the choice of frequencies since the set of small similar objects require frequencies which are quite different from those accommodating the large objects. Since the total number is limited to one or at most two frequencies, severe comparisons are forced. It would, therefore, be expected that a less constraining set of aircraft may provide a better performance particularly when a single frequency must be used.

REFERENCES

1. A. A. Ksienski, Y. T. Lin and L. J. White, "Low Frequency Approach to Target Identification," IEEE Proceedings, Vol. 63, No. 12, December 1975.

2. S. N. Srihari and L. J. White, "Pattern Recognition Techniques for Radar Aircraft Indentification," Report 3815-2, September 1975, The Ohio State University ElectroScience Laboratory, Department of Electrical Engineering; prepared under Grant AFSOR-74-2611 for Air Force Office of Scientific Research.

3. Y. T. Lin and A. A. Ksienski, "Identification of Complex Geometrical Shapes by Means of Low Frequency Radar Returns," The Radio and Electronic Engineer, Vol. 46, No. 10, October 1976.

4. Y. T. Lin and J. H. Richmond, "EM Modeling of Aircraft and Low Frequencies," IEEE Transactions on Antenna and Propagation, Vol. AP-23, No. 1, January 1975.

5. Y. T. Lin, "Classification of Objects with Complex Geometric Shape by Means of Low Frequency Electromagnetic Responses," Report 3815-1, August 1974, The Ohio State University ElectroScience Laboratory, Department of Electrical Engineering; prepared under Grant AFOSR-74-2611 for Air Force Office of Scientific Research.

6. T. M. Cover and P. E. Hart, "Nearest Neighbor Pattern Classification," IEEE Trans. on Information Theory, Vol. 13-1, January 1967.

7. J. D. Elashoff, R. M, Elashoff and G. E. Goddman, "On the Choice of Variables in Classification Problems with Dichotomous Variables," Biometrika, Vol. 54, 1967.

8. T. M. Cover and J. M. VanCompenhout, "On the Possible Ordering in the Measurement Selection Problem," IEEE Trans. on SMC Vol. 7-9, September 1977.